Retargeting AAV Vectors via Cell-Specific Receptor Binding

Ning Meng

Inaugural dissertation

for

obtaining the doctoral degree

of the

Combined Faculty of Mathematics, Engineering and Natural Sciences

of the

Ruprecht - Karls - University

Heidelberg

Presented by

M. Sc. Ning Meng

born in: Jinan, China

Oral examination: 06.03.2025

Retargeting AAV Vectors via Cell-Specific Receptor Binding

Referees: Prof. Dr. Ursula Klingmüller

Prof. Dr. Dirk Grimm

Abstract

In recent years, the adeno-associated virus (AAV) has developed as the most widely-used vector for clinical gene therapy and basic biology research. AAV capsid has been extensively modified via different approaches to create the vectors with desired transduction efficiency and specificity in the target tissues. Nowadays, the majority of new capsids are developed from directed evolution in animal models because it does not require preliminary knowledge of the interaction between AAVs and target cells. However, in recent years, studies in different animal models have revealed that, variants selected in animals often fail to translate across species. One of the main reasons is the difference of receptors across species. Therefore, to develop AAV capsids that can be used in human for gene therapy, it is important to know the receptors that mediate the transduction.

In the study, I aimed to rationally design AAV vectors to transduce target cells by binding to cell-specific receptors. I worked on two major projects: (1) targeting to hACE2-expressing cells; and (2) penetration of the blood-brain-barrier (BBB) followed by targeting to glioblastoma (GBM). To achieve these goals, I displayed already known receptor-binding ligands (peptides and proteins) on the AAV capsid with three methods, namely, genetic insertion into the AAV capsid protein, chemical/covalent conjugation to the assembled AAV capsid, and non-covalent binding to the assembled AAV capsid. Here, I developed a site-specific chemical conjugation method, which allowed chemical conjugation of any kind of ligands on the desired site by introducing a cysteine residue. Furthermore, I adjusted the number of ligands displayed on the AAV capsid by producing mosaic capsids composed of wild-type VPs and ligand-displaying VPs. Thirdly, I displayed two ligands on the same capsid by producing mosaic capsids composed of two ligand-displaying subunits.

In the hACE2-targeting project, display of receptor binding domain of SARS-CoV-2 on the AAV capsid via non-covalent binding was successful and achieved the desired specific transduction of hACE2-expressing cells *in vitro*. In the BBB-penetration and GBM-targeting project, I identified two variants, AAV9-V4-FAL and AAV9-V8-FAL, displaying the EGFR and EGFRvIII binding peptide FALGEA, which transduced GBM efficiently in U87-transplanted nsg mice after intravenous administration and which were depleted from the major off-target tissue liver. Meanwhile, from the analysis of off-target tissues, I identified

another variant, AAV9-V8-RTD, displaying the integrin αvβ6/αvβ8 binding peptide RTDLDSLRT, which transduced heart and muscle with high efficiency.

Zusammenfassung

Bis heute wurde das Adeno-assoziierte Virus (AAV) als das am häufigsten verwendete Gentransfervehikel (Vektor) für die klinische Gentherapie und die biologische Grundlagenforschung entwickelt. Das AAV-Kapsid wurde auf verschiedene Weise umfassend modifiziert, wodurch AAV-Vektoren Zielgewebe mit der gewünschten Effizienz und Spezifität transduzieren können. Heutzutage wird die Mehrheit der neuen Kapside durch zielgerichtete Evolution in Tiermodellen entwickelt, da hierfür keine Vorkenntnisse über die Interaktion zwischen AAVs und Zielzellen erforderlich sind. In den letzten Jahren haben Studien an verschiedenen Tiermodellen jedoch gezeigt, dass in Tieren selektierte Varianten häufig nicht zwischen Arten übertragen werden. Ein Hauptgrund dafür sind die unterschiedlichen Rezeptoren zwischen den Arten. Um AAV-Kapside zu entwickeln, die bei Menschen für die Gentherapie verwendet werden können, ist es daher von entscheidender Bedeutung, die Rezeptoren zu kennen, welche die Transduktion einschließlich Zellanheftung und Virusaufnahme vermitteln.

In der Studie wollte ich AAV-Vektoren rational entwickeln, um Zielzellen durch Bindung an zellspezifische Rezeptoren zu transduzieren. Insbesondere verfolgte ich zwei Hauptprojekte: (1) Transduktion hACE2-exprimierender Zellen; und (2) Penetration der Blut-Hirn-Schranke (BHS) mit anschließender gezielter Ansteuerung des Glioblastoms (GBM). Um diese Ziele zu erreichen, habe ich bereits bekannte Rezeptorbindungsliganden (Peptide und Proteine) mit drei Methoden auf AAV-Kapside aufgebracht, nämlich genetische Insertion in das AAV-Kapsidprotein, chemische/kovalente Konjugation mit dem assemblierten AAV-Kapsid und nicht-kovalente Bindung mit dem AAV-Kapsid. Daher habe ich eine ortsspezifische chemische Konjugationsmethode entwickelt, die durch Einführung eines Cystein-Restes die chemische Konjugation beliebiger Liganden an der gewünschten Stelle ermöglicht. Darüber hinaus habe ich die Anzahl der auf AAV-Kapsiden dargestellten Liganden angepasst, indem ich Mosaik-Kapside hergestellt habe, die aus Wildtyp-VPs (virale Proteine) und Liganden-präsentierenden VPs bestehen. Drittens habe ich Mosaik-Kapside hergestellt, die aus zwei Arten von Liganden-präsentierenden Untereinheiten entstehen. Im hACE2- Projekt war die Darstellung der Rezeptorbindungsdomäne von SARS-CoV-2 auf AAV-Kapsiden über nicht-kovalente Bindung erfolgreich und erreichte die gewünschte spezifische Transduktion hACE2-exprimierender Zellen in vitro. Im BBB-Penetrations- und GBM- Projekt identifizierte ich zwei Varianten, AAV9-V4-FAL und AAV9-

V8-FAL, die das EGFR- und EGFRvIII-Bindungspeptid FALGEA aufweisen, die GBM in U87-transplantierten nsg-Mäusen nach intravenöser Verabreichung effizient transduzierten und die aus dem wichtigsten „Off-Target“-Gewebe Leber dezimiert waren. Zugleich identifizierte ich durch die Analyse von „Off-Target“-Geweben eine weitere Variante, AAV9-V8-RTD, die das Integrin αvβ6/αvβ8-Bindungspeptid RTDLDSLRT umfasst und die Herz und Muskel mit hoher Effizienz transduzierte.

Table of Contents

List of Abbreviations

AAV	Adeno-associated virus
AAVR	Adeno-associated virus receptor
ACE2	Angiotensin-converting enzyme 2
AdH	Adenoviral helper plasmid
ANOVA	Analysis of variance
BBB	Blood-brain-barrier
BZM	Bortezomib
Cas	CRISPR-associated protein
cDNA	Complementary DNA (i.e., reversely transcribed RNA)
CNS	Central nervous system
COVID-19	Coronavirus disease 2019
CMV	Cytomegalovirus
CPP	Cell penetrating peptide
CRISPR	Clustered regularly interspaced short palindromic repeats
Da	Dalton
DARPin	Designed ankyrin repeat protein
ddPCR	Droplet digital PCR
DLS	Dynamic Light Scattering
dsDNA	double-stranded DNA
DTT	Dithiothreitol
EGFR	Epidermal growth factor receptor
EM	Electron Microscopy
EMA	European Medicines Agency
eYFP	Enhanced Yellow Fluorescent Protein
FDA	U.S. Food and Drug Administration
GBM	Glioblastoma multiforme
GCE	Genetic codon expansion
gDNA	Genomic DNA
gRNA	guide RNA
HER2	Human epidermal growth factor receptor 2
HSPG	Heparan sulfate proteoglycan
ITR	Inverted terminal repeat
MOI	Multiplicity of infection
mRNA	Messenger RNA
NAb	Neutralizing antibody
ncAA	Non-canonical amino acid
NGS	Next generation sequencing
NLS	Nuclear localization signal
PBS	Phosphate buffered saline

PCR	Polymerase Chain Reaction
PEG	Polyethylene glycol
PLA2	Phospholipase A2
polyA	Polyadenylation signal
qPCR	Quantitative PCR
rAAV	Recombinant AAV
RBD	Receptor binding domain
RBM	Receptor binding motif
RNAi	RNA interference
rpm	Revolutions per minute
RT	Room temperature
SARS-CoV-2	Severe acute respiratory syndrome coronavirus 2
SDS	Sodium Dodecylsulfate
scAAV	Self-complementary AAV
scFv	Single-chain variable fragment
ssDNA	Single-stranded DNA
TCEP	Tris(2-carboxyethyl) phosphine
TfR	Transferrin receptor
TRS	Terminal resolution site
vg	virus genome
VP	Capsid protein/Virion protein
VR	Variable region

List of Tables

List of Figures

1 Introduction

Gene therapy is defined as a treatment of diseases by modifying gene expression in the target cells. Common strategies for gene therapy include: (1) gene replacement, where a functional copy of the faulty gene is introduced to express the normal protein; (2) gene addition, where an therapeutic gene is supplied to mediate a specific aspect of the disease; (3) gene silencing, which aims to silence a mutated gene that results in the expression of toxic proteins; (4) gene editing, which enables direct modification of the somatic genome with the aid of nucleases such as the clustered regulatory interspaced short palindromic repeat (CRISPR)/Cas system. One of the major challenges for gene therapy is to efficiently deliver the therapeutic genetic materials to the cells. Delivery vectors include viral and non-viral vectors. Several viral vectors have been studied and developed, including adenovirus, retrovirus, lentivirus, herpes simplex virus and Adeno-associated virus (AAV). In recent years, AAV vector has become the most attractive option, because it exhibits a relatively safe profile, is able to transduce numerous cell types, and sustains long-term expression of the transgene.

1.1 Adeno-associated Virus (AAV)

AAV was first discovered as a contaminant in adenovirus laboratory preparations in the 1960s[1,2]. Its replication is dependent on co-infection of one of the helper viruses, which include adenovirus, herpes simplex virus[3,4] and human papilloma virus[5]. Therefore, AAV was classified as a new genus named *Dependoparvovirus* within the *Parvoviridae* family. Since then, distinct serotypes of AAV have been isolated from humans, non-human primates and other animals. AAV was defined as a “defective” virus, but has been developed as an efficient viral vector for gene delivery and gene therapy.

1.1.1 Genome

Similar to other parvoviruses, AAV is a small, non-enveloped, single-stranded DNA (ssDNA) virus[6,7]. The AAV genome is ~4.7 kb in length. The sense or anti-sense strand is encapsidated in an icosahedral capsid of ~25 nm with equal proportions[8]. The genome comprises two major genes, *rep* and *cap*, which are flanked by T-shaped inverted terminal

repeats (ITRs)[9,10] (Figure 1). The ITR contains *cis*-elements required for genome replication and packaging[11]. The *rep* gene encodes four nonstructural Rep proteins. The transcript driven by the p5 promoter expresses two large Rep proteins, Rep78 and Rep68, and the transcript driven by the p19 promoter expresses two small Rep proteins, Rep52 and Rep40. The *cap* gene encodes three structural capsid proteins (VPs), VP1, VP2 and VP3, whose expression is driven by the p40 promoter[12]. The use of a splice donor and two splice acceptors, major splice acceptor SA_M and minor splice acceptors SA_m, leads to the alternative splicing of Rep proteins and VPs. Rep78 and Rep52 are expressed from the unspliced p5-driven or p19-driven transcript, respectively, while Rep68 and Rep40 are expressed from spliced p5-driven and p19-driven transcripts, respectively. VP1 is produced by minor splicing of the p40-driven transcript and an AUG start codon; and VP2 and VP3 are produced by major splicing of the p40-driven transcript[13]. VP2 starts with a non-canonical weak ACG start codon while VP3 starts with an AUG start codon. Taken together, the expression levels of VP1, VP2 and VP3 are at an approximate ratio of 1:1:10. VP1, VP2 and VP3 assemble stoichiometrically, resulting in a 1:1:10 ratio in the capsid[14].

Rep proteins play key roles in AAV genome replication, encapsidation and integration[16,17,18]. The DNA-binding domain in the N-terminus of Rep78 and Rep68 can site-specifically bind to the *rep* binding element (RBE) located within the ITR, and the site-specific endonuclease domain can nick the AAV genome at the terminal resolution site (TRS) within ITRs, initiating replication of the AAV genome. All Rep proteins have DNA helicase and ATPase activities to unwind the double-stranded DNA (dsDNA) during replication and packaging. In the absence of a helper virus, Rep78 and Rep68 also mediate the integration of the AAV genome into the host genome[19]. In recent years, two additional proteins, the assembly-activating protein (AAP) and the membrane-associated accessory protein (MAAP), were discovered, which are expressed from a +1 frameshifted open reading frame within the *cap* gene. AAP is required for capsid assembly of most serotypes[20-22]. The function of MAAP is still unclear, but it can facilitate cellular egress of AAV capsids[23-25].

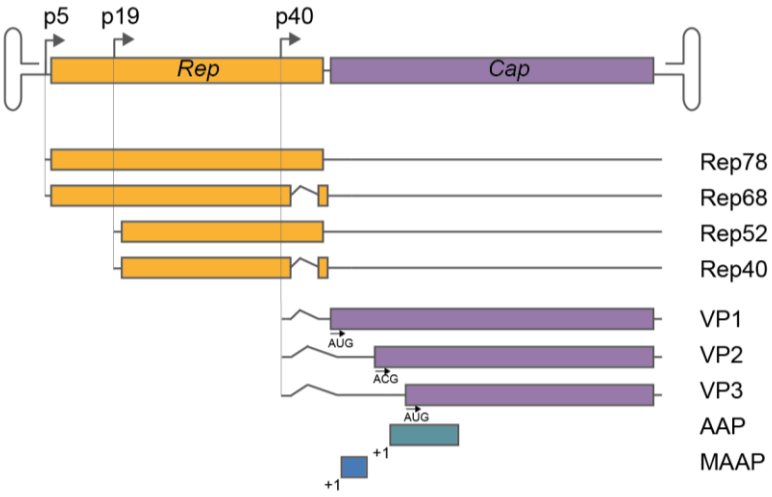

Figure 1. Structure of the AAV genome and transcriptome.
The AAV genome contains *rep* and *cap* genes flanked by inverted terminal repeats (ITRs). The *rep* gene expresses four non-structural *Rep* proteins, and the *cap* gene expresses three structural capsid proteins VP1-VP3. Two additional proteins AAP and MAAP are encoded in a +1 frameshifted open reading frame within *cap*.

1.1.2 Capsid Structure

Cryogenic electron microscopy (Cryo-EM) or X-ray crystallography have been used to solve the structures of AAV1-9, 11-13. Similar to other members in the *Parvoviridae* family, the AAV capsid is composed of 60 monomeric VPs arranged with a T=1 icosahedral symmetry. The icosahedral capsid has a depression at the 2-fold axis, three protrusions surrounding the 3-fold axis, and a moat-like depression surrounding a central channel at the 5-fold protrusion[26-30].

The three capsid proteins VP1, VP2 and VP3 form the capsid in an approximate 1:1:10 ratio. VP1-3 share the same C-terminal sequence of 533 amino acid residues. The N-terminal VP1 unique (VP1u) region, the VP1/VP2 common region and the first 15 residues of VP3 region are disordered and thus cannot be observed. The N-terminus of VP1 and VP2 is hidden inside the capsid and becomes externalized during intracellular trafficking. VP1u contains a phospholipase A2 (PLA_2) domain, which is important for AAV endosome escape, and a nuclear localization signal (NLS), which is important for nucleus entry[31,32].

A comparison of available AAV structures shows that the core of each VP has a conserved β-barrel motif consisting of eight β-strands βA-I and an α-helix αA, which constitutes the inner face of the capsid[33,34]. Mutations in this region impede capsid assembly[35]. The DE loops (connecting βD and βE) form the channel at the 5-fold axis, through which the genome is encapsidated into the capsid and the N-terminus of VP1 and VP2 is externalized[36]. Nine variable regions (VRs) I-IX connect the β-strands and form the surface of the capsid. Differences in the VRs result in the diversity of binding to receptors and antibodies, which in turn results in the diversity of cellular tropisms and antigenicities.

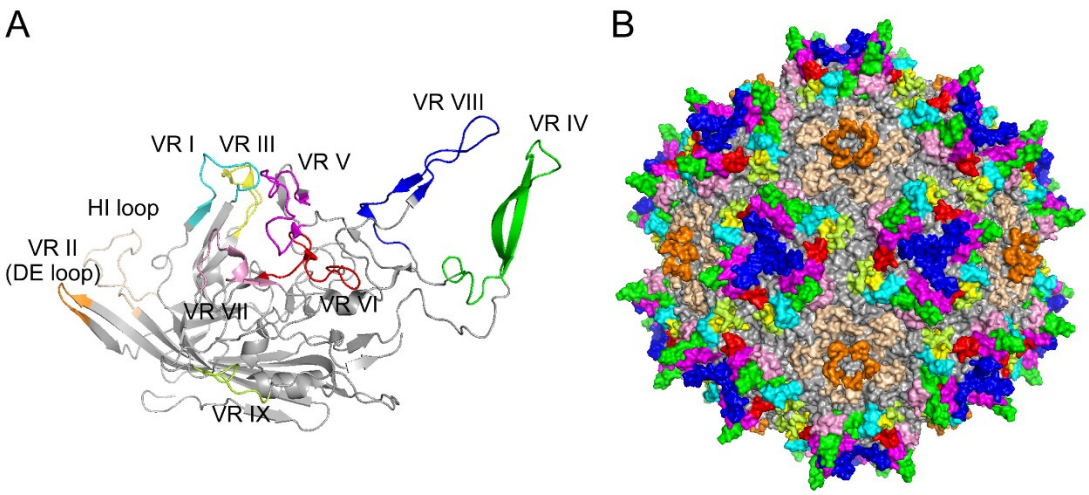

Figure 2. Structure of AAV VP and capsid.
(**A**) Ribbon diagram representation of the VP of AAV2 (amino acid residues 219-735, PDB ID: 6IH9). The β-barrel motif (eight β-strands βA-I) and an α-helix αA constitute the inner face of the capsid. (**B**) Assembled icosahedral AAV2 capsid. Figures were generated with PyMOL. VR I: cyan, VR II (DE loop): orange, VR III: yellow, VR IV: green, VR V: magenta, VR VI: red, VR VII: pink, VR VIII: blue, VR IX: lemon (green-yellow), HI loop: wheat (light orange).

1.1.3 Infection Pathway

The infection of AAV begins with attachment and binding to cell membrane receptors, followed by internalization, intracellular trafficking to the nucleus, genome release, gene expression and genome replication (Figure 3).

AAV first attaches to primary receptors at the cell surface, which then facilitates the sequential interaction with secondary receptors for particle internalization. Different AAV serotypes use different glycan receptors and proteinaceous receptors (Table 1) as primary and secondary receptors, respectively, which is the major reason for their different

tropisms[37,38]. For example, AAV2, the best-studied serotype, binds to heparan sulfate proteoglycan (HSPG)[39] as its primary receptor and can use fibroblast growth factor receptor (FGFR)[40], hepatocyte growth factor receptor (HGFR)[41], laminin receptor (LamR)[42], integrin αvβ5[43] or integrin αvβ1[44] as secondary receptor. Notably, later studies reported that these co-receptors are not necessary for infection. In 2016, by using genome-wide CRISPR screening, the transmembrane glycoprotein KIAA0319L was identified as a common receptor that is required for the transduction of most AAV isolates, except AAV4 and rh32.33[45]. It was then named AAV receptor (AAVR). In 2019, another universal receptor for AAV transduction, GPR108, was identified[46,47]. GPR108 is required for most AAV isolates, except AAV5. AAVR and GPR108 are mainly expressed on the Golgi membrane but not the cell membrane. They affect neither attachment nor binding of AAV, but are essential for intracellular trafficking and successful transduction.

Table 1. AAV Receptors.

	Glycan receptors	**Co-receptors**	**Entry factors**
AAV1	N-linked sialic acid[48]		AAVR, GPR108
AAV2	HSPG	α5β1 integrin, αVβ5 integrin, FGFR1, HGFR, LamR	AAVR, GPR108
AAV3B	HSPG[49]	FGFR, HGFR[50], LamR[51]	AAVR, GPR108
AAV4	O-linked sialic acid[52]		GPR108
AAV5	O-linked sialic acid[52]	PDGFR[53]	AAVR
AAV6	HSPG[54], N-linked sialic acid[48]	EGFR[55]	AAVR, GPR108
AAV7	Unknown		AAVR, GPR108
AAV8	Unknown	LamR[51]	AAVR, GPR108
AAV9	Galactose[56]	LamR[51]	AAVR, GPR108

After binding to the cell surface, AAV is internalized into cells via endocytosis. AAV can be efficiently internalized via different pathways, including clathrin-mediated, caveolin-mediated, clathrin- and caveolae-independent endocytosis and micropinocytosis[57-59]. After endocytosis, the endosome carries AAV virions towards the *trans*-Golgi network[60,61]. The acidic environment in early to late endosomes triggers a conformational change of the VP that exposes the hidden N-terminus of VP1/VP2. For successful infection, AAV needs to escape to the cytosol and translocate into the nucleus. The PLA_2 domain in VP1u helps with the escape to the cytosol, and NLS regions (basic cluster 1-3) in VP1u mediate

transport into the nucleus[31,62-64]. However, most virions are trapped in the endosome or the *trans*-Golgi network. Furthermore, many virions that successfully escape to the cytosol are degraded by the proteasome[65,66]. As a result, only less than 1% of all incoming viruses reach the nucleus via microtubules. AAV is imported into the nucleus intact through the nuclear pour complex (NPC)[59,67,68]. Then, the AAV capsid transits to the nucleolus where the genome can be released from the capsid[69,70], albeit the exact mechanism(s) how the viral genome is released from the capsid is poorly understood.

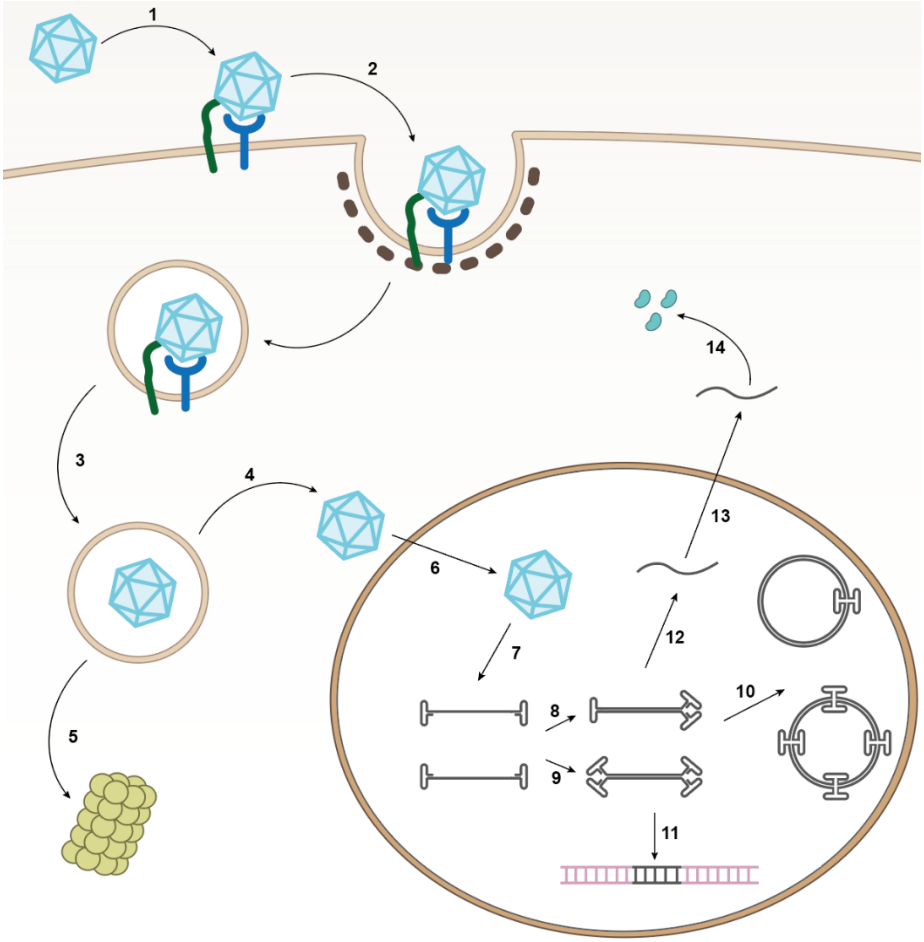

Figure 3. AAV infection pathway.
AAVs bind to receptors and co-receptors on the cell membrane (step 1) and enters cells via endocytosis (step 2). The acidic environment in early-to-late endosomes triggers a conformational change of VP that exposes the hidden N-terminus comprising VP1u and VP1/VP2 regions (step 3). The PLA2 domain in VP1u enables AAVs to escape into the cytosol (step 4). Within the cytosol, AAV virions are either ubiquitylated and degraded by the proteasome (step 5), or they traffic to the nucleus and enter it through the NPC (step 6). In the nucleus, the AAV genome is released (step 7). The single-stranded DNA (ssDNA) genome is converted to dsDNA via second-strand synthesis (step 8) or strand annealing (step 9). In the absence of helper viruses, AAV enters a latent phase. Genomes stay episomally as monomer or concatemer (step 10), or they are integrated into the

cellular genome including into the AAVS1 locus on chromosome 19 (step 11). In the presence of a helper virus, AAVs enter a lytic phase in which genome replication is activated. Subsequently, viral messenger RNA (mRNA) is transcribed (step 12) and exported into the cytosol (step13) for translation of viral proteins (step 14).

After release from the capsid, the ssDNA genome is converted to dsDNA via second-strand synthesis or annealing of sense and anti-sense strands[71,72]. Second-strand synthesis is primed by the 5' ITR and requires a host DNA polymerase. In the absence of helper viruses, AAVs enter a latent phase in which most of the AAV genomes persist episomally as monomer or concatemer[73]. A fraction of genomes is integrated into the AAVS1 locus on chromosome 19, which is mediated by Rep78 and Rep68[73-75]. In the presence of a helper virus, AAV enters a lytic phase, in which genome replication is activated[76]. All three AAV promoters are activated by helper viruses, and expression of Rep proteins and capsid proteins is induced. Large Rep proteins can bind to the RBE located within the ITR and their endonuclease activity can nick the dsDNA at the TRS, which generates a new 3' hydroxyl group at the TRS as primer for DNA replication[77]. In parallel, mRNAs are transcribed and translocated to the cytosol for expression of Rep and capsid proteins; the latter then assemble to icosahedral capsids. Rep proteins facilitate encapsidation of ssDNA genomes though the pore at the five-fold axis[78,79].

1.2 Recombinant AAV (rAAV) for gene therapy

AAV vectors have become the most commonly used viral vector for gene therapy in clinical trials because they can transduce a broad spectrum of tissues and cells, have a relatively good safety profile (they are less immunogenic than other viral vectors, are non-pathogenic, and rarely integrate), mediate long-term transgene expression and benefit from a versatile portfolio of engineering and manufacturing methods.

ITRs are the only *cis*-elements required for genome replication and packaging during virus production, as well as for gene expression during transduction (next to regulatory elements such as promoters). Therefore, recombinant AAVs (rAAVs) used for gene delivery are generated by replacing the viral genome between the ITRs with the transgene cassette[80]. The complete removal of viral gene cassettes maximizes the packaging capacity of rAAVs and contributes to their low immunogenicity and cytotoxicity. Even in

the presence of helper viruses, rAAVs are completely replication-deficient due to the lack of *rep* and *cap* genes. To produce rAAV, *rep/cap* and helper genes are supplied *in trans.* A standard method to produce rAAV vectors involves triple-transfection of HEK293 cells with an AAV helper plasmid that expresses *rep* and *cap* genes, a transgene plasmid that bears two ITRs and can be packaged into the capsid, as well as an adenoviral helper plasmid that expresses E2A, E4 and VA genes that are essential for AAV genome replication and gene expression (HEK293 cells already express the adenoviral E1A and E1B genes that are also required for rAAV prodcution)[81].

Nowadays, most of the AAV gene therapy clinical trials are for monogenic diseases, which are caused by deficiency in a single gene, including hemophilia, ocular diseases, neurological diseases, muscular diseases, and other disorders. For diseases caused by loss-of-function mutations, such as hemophilia A and B, Leber congenital amaurosis type 2 (LCA2), X-linked retinitis pigmentosa, spinal muscular atrophy (SMA) or Duchenne muscular dystrophy (DMD), the most straightforward method is gene replacement. For gain-of-toxicity mutations that lead to expression of toxic gene products, such as retinitis pigmentosa, RNA interference or knock-out strategies are used. Seven AAV gene therapy products have achieved approval by the U.S. Food and Drug Administration (FDA), the European Medicines Agency (EMA) or both. In 2012, Glybera was approved as the first AAV-based gene therapy product in the Western world by the EMA[82]. It delivers a functional copy of the gene encoding lipoprotein lipase (LPL) to muscle cells by AAV1 to treat lipoprotein lipase deficiency (LPLD). In 2017, the FDA approved Luxturna, which delivers a functional copy of the *RPE65* gene to retina cells by AAV2 LCA2[83]. Seven additional AAV-based gene therapy products have been approved until now: Zolgensma (2019) for SMA[84], Upstaza (2022) for Aromatic L-amino acid decarboxylase deficiency (AADC)[85], Roctavian (2022)[86] for hemophilia A, Hemgenix (2022) for Hemophilia B[87], Elevidys (2023) for DMD[88] and Beqvez for Hemophilia[89] (Table 2). Notably, a rapidly increasing number of preclinical studies on AAV-mediated gene therapy for other diseases, including cancer and infectious diseases, is also showing promise.

However, tragically, some patients died after receiving high-dose rAAV treatment. The deaths were mainly caused by liver dysfunctions and immune responses[90-92]. Naturally occurring AAV serotypes that have been mainly used in clinical trials exhibit low transduction efficiency and specificity, and neutralizing antibodies against natural AAV serotypes are prevalent in humans. Innate and adaptive immune responses to the vector

play a critical role in the observed toxicity. Hepatotoxicity was caused by the inherent liver tropism of most natural AAV serotypes upon entering the circulation after intravenous administration. Therefore, there is an urgent demand to develop AAV vectors that can transduce target cells with high efficiency and specificity while escaping from neutralizing antibodies, in order to reduce vector doses and ameliorate immune responses.

Table 2. Approved AAV-mediated gene therapy products.

Product	Approval Time	AAV serotype	Transgene	Administration	Disease
Glybera	2012	AAV1	LPLS477X	Intramuscular	LPLD
Luxturna	2017	AAV2	RPE65	Subretinal	LCA2
Zolgensma	2019	AAV9	SMN1	Intravenous	SMA
Upstaza	2022	AAV2	AADC	Intraputaminal	AADC
Roctavian	2022	AAV5	Factor VIII	Intravenous	Hemophilia A
Hemgenix	2022	AAV5	Factor IX	Intravenous	Hemophilia B
Elevidys	2023	AAVrh74	Micro-dystrophin	Intravenous	DMD
Beqvez	2024	AAVrh74var	Factor IX	Intravenous	Hemophilia B

1.3 Capsid Engineering of AAV Vectors

Although AAV has many advantages as a vector for gene therapy, it also has limitations including low transduction efficiency, transduction of off-target tissues (especially the liver), triggering of immune responses, clearance by the immune system and limited packaging capacity, which impede its therapeutic application. Consequently, many approaches have been studied to overcome these limitations.

To deliver large genes that exceed the packaging capacity, different dual-vector delivery systems were developed, which split a transgene over two vectors. In transduced cells, the full-length protein is reconstituted by either DNA recombination[93-97] or intein-mediated protein ligation[98,99]. Inclusion of strong, tissue-specific and short promoters improves AAV transduction efficiency, specificity and packaging space for transgenes, respectively[100-102]. Several post-transcriptional regulatory *cis* elements such as the woodchuck hepatitis virus post-transcriptional regulatory element (WPRE)[103], which can promote mRNA export to the cytoplasm, or short UC-rich elements[104], which can improve mRNA stability, can be used to further enhance gene expression. Notably, the invention of self-complementary

AAV (scAAV) vector genomes significantly enhanced AAV transduction efficiency[105-107]. Traditional AAV vectors carry a ssDNA genome. Transformation to dsDNA is a rate-limiting step during transduction. A scAAV genome is generated by introducing a mutation in the *trs* within the ITR, which prevents Rep from nicking the DNA and results in a scDNA genotype. In transduced cells, the scDNA genome forms a dsDNA by means of self-annealing, which can the directly serve as a template for transcription. The drawback of scAAV is that the packing capacity is also halved.

Because transduction tropism and antigenicity are primarily dependent on the AAV capsid, capsid engineering has become the principal strategy to create AAV vectors with desired transduction efficiency and specificity in target tissues, combined with the ability to evade from the immune system. Common approaches include genetic engineering, covalent conjugation, non-covalent binding, and formation of mosaic capsids (Figure 4).

1.3.1 Genetic Engineering

1.3.1.1 Rational design

Rational design comprises the introduction of specific modifications in selected sites on AAV capsids, which is based on the understanding of rAAV structure and biology. Typical methods include peptide or protein insertion, chimeric capsid formation and site-specific mutation.

Peptide and protein insertion

Peptide insertion was among the earliest reported approaches for capsid engineering. The goal is to change the tropism of AAV by grafting peptides or proteins that bind to cell-specific receptors onto the AAV capsid. The first engineered AAV capsid variant with peptide insertion was published in 1999, when Girod *et al*. inserted the integrin-binding peptide QAGTFALRGDNPQG into the AAV2 capsid and found that it increases transduction efficiency in cells that were resistant to wild-type AAV2[108]. Importantly, Girod *et al.* screened several peptide insertion sites and identified residue 587 as the best position. Nowadays, identification of AAV capsid structures by cryo-EM and X-ray diffraction provides better insights into suitable insertion sites (Figure 2). VR-VIII (around residues 586-589) and VR-IV (around residues 454-457), which forms the protrusions surrounding the 3-fold axis, have become the first and second most widely used sites for

peptide insertion, respectively. Since then, many different peptides have been inserted to VP of different AAV serotypes and were shown to mediate transduction of different cells and tissues. For example, insertion of the CD13-binding peptide NGRAHA at VR-VIII of AAV2 enhanced the transduction in CD13-positive tumor cells *in vitro*[109]; insertion of the integrin αvβ3/αvβ3 binding peptide CDCRGDCFC at VR-VIII of AAV2 enhanced the transduction in integrin-overexpressing tumor cells *in vitro* and *in vivo* after local injection[110]; insertion of the muscle-targeting peptide ASSLNIA at residue 587 retargeted AAV2 to myoblasts *in vitro* and to various muscles (particularly to heart) in mice after intramuscular and intravenous injection[111]; insertion of the cell-penetrating peptides (CPPs) TVSALK and TVSALFK, which were derived from the Ku60 protein, at residue 588 of AAV9 enhanced penetration of the blood-brain-barrier (BBB) in mice and cynomolgus macaques after intravenous injection[112].

Other than peptides, receptor-binding proteins like single-chain variable fragment (scFv)[113], designed ankyrin repeat proteins (DARPins)[114] and nanobodies[115] have also been inserted. Proteins were first fused to the N-terminus of VP2, which can tolerate insertion of large fragments[113,114,116]. By inserting mCherry randomly throughout the AAV2 VP, Judd *et al.* identified VR-IV as a site that can tolerate the insertion of large proteins[117]. Afterwards, nanobodies[115] and DARPins[118] were also successfully inserted into this site. Notably, due to the large size, proteins were only inserted to the N-terminus of VP2 or VR-IV of VP1, which leads to the display of approximately 1-5 copies of proteins per capsid.

Chimeric capsid

As different AAV variants bind to different receptors, instead of grafting a receptor-binding peptide or protein from somewhere else, chimeric capsids were built by grafting binding motifs from one AAV serotype to another. Asokan *et al*. generated a panel of chimeric vectors by replacing a hexapeptide HSPG binding motif (residues 585-588) of AAV2 with corresponding residues from other serotypes, and identified AAV2i8 (AAV2/AAV8 chimera) that selectively transduced cardiac and skeletal muscle with high efficiency and that showed an altered antigenic profile[119]. Later studies generated AAV2G9 by grafting a galactose-binding footprint from AAV9 onto AAV2, and then AAV2i8G9 by grafting the galactose-binding footprint from AAV9 onto AAV2i8[120]. This AAV2/AAV8/AAV9 chimera remains liver-detargeted like AAV2i8 while selectively transducing muscle with high efficiency.

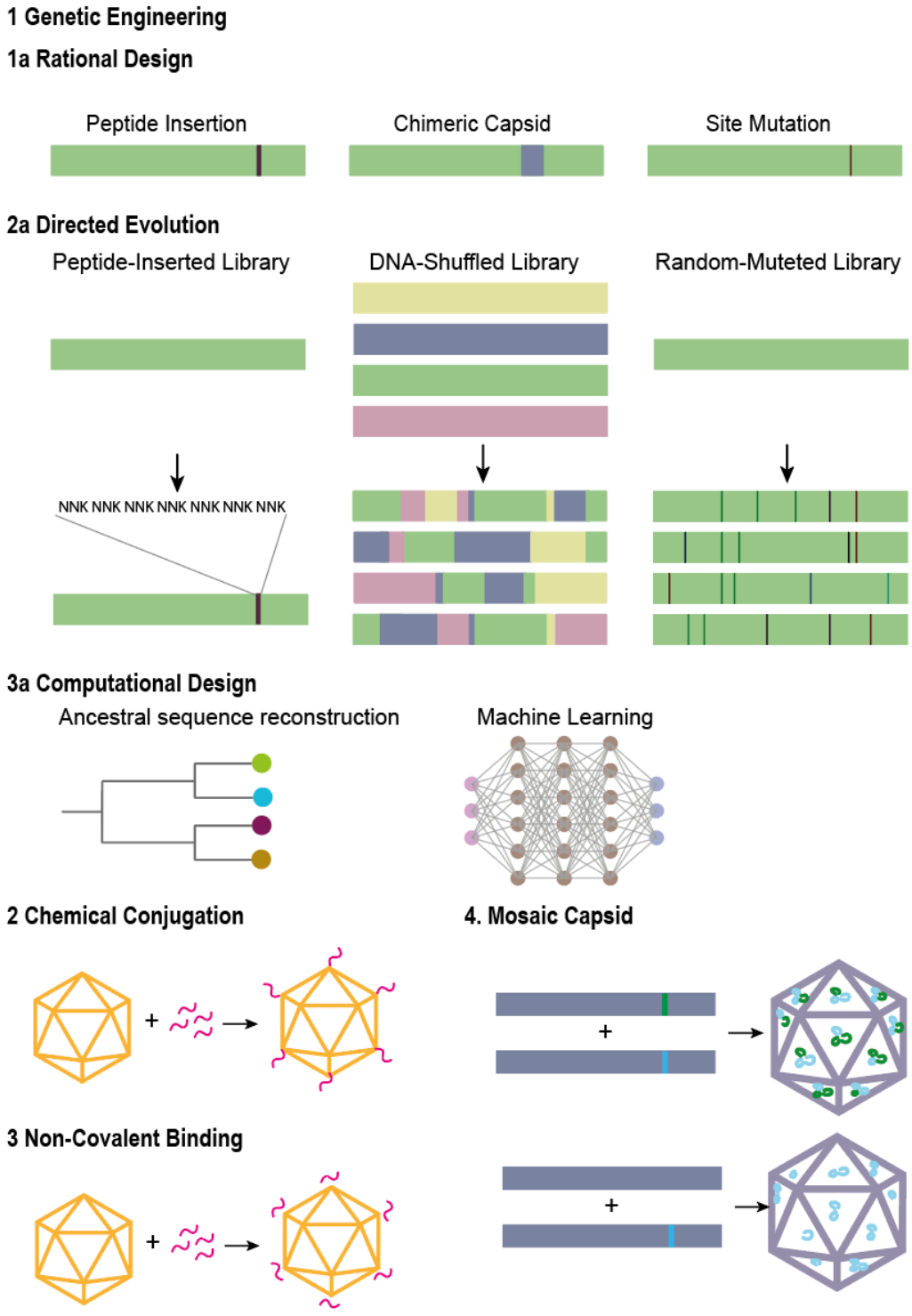

Figure 4. Capsid engineering approaches.
Common AAV capsid engineering approaches include: (1) Genetic engineering, which includes rational design (peptide insertion, chimeric capsid formation, site-directed mutation), directed evolution (peptide-displaying library, DNA-shuffled library, randomly mutated library), and computational design; (2) covalent/chemical conjugation; (3) non-covalent binding; and (4) production of mosaic capsids composed of two types of capsid proteins (VPs).

Site-specific mutation

Several studies have exemplified that a change of a single amino acid in the AAV capsid can change its transduction properties. For instance, substitution of surface-exposed tyrosine residues of AAV2 to phenylalanine (Y444F, Y730F and triple-mutation of Y444F+Y500F+Y730F) helps AAV to evade proteasome-mediated degradation, which leads to an improvement of AAV transduction efficiency by facilitating intracellular trafficking to the nucleus[121-123]. Furthermore, site-directed mutagenesis of key residues for receptor binding can deplete AAV transduction in off-target tissues. For example, substitution of R585 and R588 of AAV2 impeded its binding with HSPG[124], and substitution of W503 of AAV9 impeded its binding with galactose[125,126]. This is often combined with gain-of-function modifications like peptide insertion[115,127,128]. Thirdly, mutation of epitopes can facilitate evasion from pre-existing neutralizing antibodies (NAbs). For example, insertion of threonine at position 265 of AAV2 reduced binding with NAbs and enhanced transduction in muscle[129]. By predicting immunogenic epitopes, a single S671A mutation was introduced to AAVrh10, and the variant showed a higher Nab-evading rate in pre-immunized mice[130].

1.3.1.2 Directed evolution

Nowadays, directed evolution has become the most widely used method to develop new capsids, because it does not require prior knowledge of how AAV vectors transduce target cells. The principle of directed evolution is to identify AAV capsid variants with specific properties under selective pressure. In brief, the procedure requires to first generate a library of diverse AAV capsids, followed by several rounds of selection either *in vitro* or *in vivo* to identify variants that are enriched in the target cells or tissues. Next-generation sequencing (NGS) enables the high-throughput analysis of enriched clones. Strategies to generate a library include random peptide insertion, DNA shuffling and *de novo* mutation, which correspond to the rational design methods peptide insertion, chimeric capsid formation and site-directed mutation.

Random Peptide Display

A random peptide displaying AAV library is generated by means of insertion of random short peptides (mostly 7-9 amino acid residues) into AAV VP. Similar to single peptide insertion, VR-VIII (VP1 residues 587 or 588 of AAV2 and the equivalents in other serotypes) is the most commonly used insertion site for the random peptides. Perabo *et al.* and Müller

et al. published the first two reports on peptide display library technology in 2003[131,132]. Since then, many variants have been identified from peptide display libraries with outstanding transduction efficiency in different cell lines *in vitro*. In 2009, Michelfelder *et al.* conducted the first *in vivo* selection using murine breast cancer and lung tissue as prototype targets[133]. In their study, they found that vectors selected *in vitro* were not suitable for transduction of the same target cells under *in vivo* conditions. Nowadays, the selections are mainly conducted *in vivo*. For instance, screening of an AAV2 peptide display library in mice identified a variant AAV2_L1 that transduces lung endothelial cells with high efficiency and specificity[134]; screening of an AAV9 peptide display library in C57BL/6 mice identified a variant PHP.B that penetrates the BBB and transduces central nervous system (CNS) efficiently[135]; and screening of an AAV9 peptide display library in mice and macaques identified a set of muscle-targeted variants (myoAAVs)[136].

DNA Shuffling

DNA family shuffling technology can generate a complex library of chimeric capsids from different serotypes by recombination of homologous DNA fragments *in vitro*. In brief, *cap* genes of different parental serotypes are fragmented to pieces with a length of a few hundred base pairs by DNase digestion, then the DNA fragments undergo recombination and primer-free PCR elongation. Grimm *et al*. published the first AAV shuffling library in 2008. The liver-targeted AAV-DJ, a AAV2/8/9 chimeric capsid, was evolved via selection on human hepatocytes from a shuffled library comprising eight AAV variants[137]. In contrast to peptide display that introduces novel motifs restricted at the specific sites, DNA shuffling can engineer the whole VP; however, the diversity of each residue is limited within the parental natural serotypes. Therefore, combining these two methods can create AAV variants with more diverse properties. For instance, El Andari *et al.* identified the muscle-tropic and liver-depleted variants AAVMYO2 and AAVMYO3 by inserting the peptide RGDLGLS in two shuffled variants[140]. Furthermore, our group is currently working on peptide-displaying shuffled library, generated by first inserting random short peptides into the VP of several natural serotypes followed by DNA shuffling.

Random mutations

Error-prone PCR can generate a capsid library with random mutations. In 2005, Perabo *et al.* generated an AAV2 error-prone PCR library for the first time, from which they identified variants that can escape from NAbs[141]. Qian *et al.* selected two AAV5 variants,

MV50 and MV53, by screening an AAV5 error-prone PCR library in Huh7 cells, which mediated increased transduction in Huh7 cells and primary human hepatocytes while maintaining the low antigenic property of AAV5[142].

1.3.1.3 Computational Design

Due to the labor-intensive and time-consuming process of rational design and directed evolution, in recent years, computer-based approaches are emerging as alternative novel means for capsid engineering. Two studies used *in silico* ancestral sequence reconstruction algorithms to predict putative ancestral AAV capsid sequences[143,144]. One of the variants, Anc80, the predicted ancestor of the AAV serotypes 1, 2, 8, and 9, emerged as a promising vector for targeting liver, muscle, retina, inner ear hair cells and kidney mesenchymal cells.

Machine learning (ML) has emerged as a groundbreaking computational approach in biology and biomedical research, including protein engineering. The initial AAV capsid libraries for directed evolution often contain a high proportion of defective variants that are unable to assemble or package their genomes. Several pioneering studies have applied ML to AAV capsid design, in which they used previously collected high-throughput NGS data from capsid library screens to train ML models, in order to predict variants that can assemble and package their genomes[145-147]. Using these variants as initial libraries, directed evolution can be accelerated and reinforced.

1.3.2 Chemical Conjugation

Chemical conjugation is an alternative method to display or mask functional motifs on AAV capsids. Genetic engineering may have unpredicted impacts on the structure of the capsid protein and the complex assembled particle. Chemical conjugation introduces modifications on already assembled and packaged capsids, which minimizes the impact on capsid assembly, capsid structure and genome encapsidation. Besides, the modification is not limited to amino acid residues; instead, chemical conjugation can introduce any kind of molecules with novel properties. For instance, PEGylation by conjugating PEG to lysine residues yielded a moderate protection of AAV2 from NAbs[148,149]. Conjugation of N-acetylgalactosamine (GalNAc) to lysine residues enhanced asialoglycoprotein receptor-mediated AAV transduction in hepatocytes[150].

Conventional modification mainly relies on the primary amine group (-NH2) of lysine residues, which can react with N-hydroxysuccinimide (NHS) ester or isothiocyanates[148-153]. Several studies also reported modification on arginine[154] and tyrosine[155] residues. In recent years, a site-specific modification method has been developed that utilizes genetic code expansion technology (GCE). It requires the expression of an orthogonal aminoacyl-tRNA synthetase (aaRS)/tRNA pair, which can incorporate non-canonical amino acids (ncAAs) to the introduced UAG stop codon at the desired site on VP. The functional group on the ncAA enables subsequent biorthogonal conjugation. In 2016, two pioneering studies screened potential ncAA-incorporating sites and then conjugated cyclic-RGD peptides to the AAV capsid, which resulted in retargeting of AAV vectors to integrin-overexpressing cell lines[156,157]. In the last two years, folic acid[158], tumor-targeting aptamer[158], HER2-binding nanobody and antibody[159] have been conjugated to AAV capsids via GCE, and the modified AAVs showed specific transduction in the target cells. Interestingly, ncAA Nε-2-azideoethyloxycarbonyl-L-lysine (Azk or NAEK) itself also confers novel properties to AAV capsids. One NAEK-AAV5 vector showed lung-specific transduction after systemic or intranasal delivery in mice[160].

1.3.3 Non-covalent Binding

Other than genetic engineering and chemical conjugation, functional molecules can be non-covalently bound to AAV capsids. In 1999, Bartlett *et al*. retargeted AAV to human megakaryocytes by using a bispecific $F(ab')_2$ antibody, which binds to AAV on one side and to the cell-surface receptor αIIbβ3 integrin on the other side[161]. Incubation of CPPs and BBB shuttle peptides with AAV showed that the THR peptide enhances CNS transduction of AAV8[162], and that the LAH peptide enhanced CNS transduction of AAV9[163].

1.3.4 Mosaic Capsid

A mosaic capsid, also named a haploid capsid, is a capsid that consists of VPs of different serotypes. Because VPs assemble stoichiometrically, mosaic rAAV vectors can be produced by mixing AAV helper plasmids from different viral isolates during transfection[164,165]. The ratio of VPs can be adjusted by changing the ratio of the corresponding plasmids. Ideally, mosaic capsids combine the properties of their parental

serotypes. For instance, the AAV1/2 mosaic vector exhibited muscle tropism similar to AAV1 and liver tropism similar to AAV2, yet it was also inhibited by both anti-AAV1 and anti-AAV2 antiserum[164]. Morover, mosaic capsids might also aid the evasion from NAbs. For example, an AAV2/8/9 mosaic capsid can escape Nab activity from mouse sera immunized with parental serotypes[166]. Another approach to produce mosaic capsid is to separate the expression of VP1, VP2 and VP3. This method is often used to reduce the number of proteins or large peptides displayed on AAV capsids (see section 1.3.1.1 “Peptide and protein insertion”).

1.3.5 Barcoded Library

In 2014, Adachi and colleagues established a barcode-based method which allows the characterization and comparison of hundreds of different AAV variants in a high-throughput manner[167]. They generated DNA barcode-tagged AAV libraries in which a unique DNA barcode was inserted into the genome of each AAV variant after the *cap* gene, and determined the phenotype of each AAV variant by Illumina sequencing of the barcodes. By applying this method, they drew a high-resolution map of AAV capsid amino acids important for the structural integrity, receptor binding, tropism, neutralization and blood clearance. Using barcoded AAV libraries can dramatically reduce the number of animals and enable a direct comparison of all AAV variants in the same organism. Also in 2014, Marsic *et al.* generated barcoded luciferase-expressing rAAVs, in which barcodes are incorporated in the 3’UTR of the transgene cassette between transgene and polyA[168]. Jonas Weinmann from our group has further optimized and validated a barcode-based AAV capsid screening pipeline to enable the simultaneous validation and comparison of different capsid variants *in vivo*. The barcode was integrated into the 3’UTR of a CMV promoter-driven eYFP transgene cassette between eYFP and polyA, and the abundance of each barcode was analyzed on the DNA and RNA level[169].

1.4 Sars-CoV-2

After its first emergence in December 2019, Severe Acute Respiratory Syndrome Coronavirus (SARS-CoV-2) spread worldwide rapidly. It was declared as a COVID-19 pandemic by the world health organization in March 2020. By August 2024, over 775

million cases and 7 million deaths caused by SARS-CoV-2 have been reported (https://data.who.int/dashboards/covid19).

SARS-CoV-2 belongs to β coronaviruses. It is an enveloped, positive-sense, single-stranded RNA virus. The spike protein (S protein) embedded on the surface of the membrane mediates the entry of SARS-CoV-2 to the target cells. The receptor-binding domain (RBD) in the S protein binds to the host entry receptor angiotensin-converting enzyme 2 (ACE2), which initiates virus entry[170-173]. In addition, the cellular transmembrane serine protease 2 is required for priming of the S protein[173,174]. Distribution of ACE2 is the primary determinant of infection tropism of SARS-CoV-2. ACE2 is highly expressed on epithelial cells of the respiratory tract (such as tracheal and bronchial epithelial cells, or alveolar type II epithelial cells), but it is also widely expressed on cells in many other organs including the cardiovascular system, gastrointestinal tract, urogenital system as well as liver and nervous systems[174,175].

Prophylactic vaccination has become the most effective strategy to combat COVID-19, and multiple vaccines have been approved. Significantly, novel mRNA vaccines from Pfizer/BioNTech[176] and Moderna[177] emerged as a groundbreaking vaccination technology. Unlike traditional vaccines, mRNA vaccines can be designed and produced rapidly, offering unprecedented flexibility and speed in response to emerging infectious diseases. Concurrently, numerous studies focused on exploring therapeutic methods for treatment of infected patients. Antiviral drugs were developed, mainly by screening drugs that have been used to suppress related RNA viruses. However, only a few drugs, including Remdesivir[178], Molnupiravir[179] and Paxlovid (Nirmatrelvir-ritonavir)[180], have been approved. They inhibit the enzymes that are required for replication and transcription of the viral genome: Remdesivir and Molnupiravir target the RNA-dependent RNA-Polymerase (RdRp) and Paxlovid targets the 3CLpro enzyme. One of the main drawbacks of conventional drugs is the lack of specificity, which leads to their low efficiency and toxic side effects. Neutralizing monoclonal antibodies (mAbs) have also been developed, which can target the S protein with high specificity[181]. Neutralizing mAbs can prevent SARS-CoV-2 from binding to the ACE2 receptor and enhance the immune response. However, neutralizing mAbs, as well as vaccines, utilize the S protein as the antigenic target, which mutates and evolves rapidly. Accordingly, the emergence of new variants affects the effectiveness of vaccines and neutralizing mAbs[182].

RNA interference (RNAi) is a promising alternative therapeutic approach. RNAi is mediated by small interfering RNAs (siRNAs) or short-hairpin RNAs (shRNAs), which can block or degrade viral genome RNA and mRNA with high specificity and flexibility[183,184]. Theoretically, siRNA or shRNA can be designed to silence almost any gene. Therefore, the RNAi strategy covers a wide antiviral target range and enables quick adaptation to emerging mutations. Many groups have published databases of predicted RNAi targets in SARS-CoV-2 and the corresponding siRNA sequences[185-187]. The CRISPR/Cas13 system has also been developed as another method to inhibit SARS-CoV-2 expression and replication on the RNA level[188,189].

One of the challenges for the clinical application of RNAi- and CRISPR/Cas13-meditated therapies is to deliver the therapeutic RNA or DNA to the infected cells. The delivery of siRNAs against SARS-CoV-2 has been achieved with lipid nanoparticles (LNPs)[190,191], peptide dendrimers[192], or VIPER (virus-inspired polymer for endosomal release) polyplexes[193] *in vivo*. Also Cas13a mRNAs and guide RNAs (gRNAs) against SARS-CoV-2 have been delivered with polymers *in vivo*. Due to the short half-time of RNA (siRNA, mRNA and gRNA), the effect was transient and multiple doses are required. Delivery of DNA encoding shRNA or Cas13a and gRNA with AAV vectors is more likely to mediate long-lasting antiviral effects. Our group has developed an AAV/RNAi expression vector, AAV-SAVIOR, which co-expresses a cocktail of three shRNAs against the SARS-CoV-2 RdRp and N genes as versatile and effective antiviral agents[194]. AAV-SAVIOR suppressed SARS-CoV-2 infection to background levels *in vitro*, and single intranasal administration of AAV-SAVIOR showed moderate diminishment of viral loads and alleviation of symptoms in mice. Furthermore, use of a triple-shRNA variant prevented viral escape efficiently. One can expect that the therapeutic effects can be improved in the future by exploring other shRNA targets and developing AAV vectors with higher delivery efficiency and specificity to the infected cells.

1.5 Glioblastoma and Cancer Therapy

Glioblastoma, also called glioblastoma multiforme (GBM), is the most common and most aggressive type of malignant primary tumor in the CNS. It is characterized by its infiltrative nature, impairment of the blood-brain-barrier, aberrant vascularization and high resistance to multimodal treatment[195,196]. Current therapeutic modalities include surgical resection,

radiotherapy, chemotherapy and combinations thereof. However, GBM is highly resistant to these conventional treatments[197]. GBM is fast-growing and highly invasive so that it infiltrates into the nearby brain tissues before any symptoms occur. Therefore, it is difficult to be eliminated completely and the recurrence rate is high. Furthermore, the BBB limits the immune cells and most therapeutic agents to reach their target. Even with treatment, the typical survival time is between 12 and 15 months. The 3-year survival rate is less than 16% and the 5-year survival rate is less than 5%[198]. Thus, there is an urgent need to develop novel and effective therapeutic strategies.

Gene therapy has been developed for cancer therapy. In fact, more than 60% of all clinical trials for gene therapy were conducted to treat cancer, although AAV-mediated cancer therapy is still at the preclinical study stage[199]. Strategies in AAV-mediated cancer gene therapy include: (1) Induction of cytotoxic killing of tumor cells by delivery of suicide genes that can convert non-toxic compounds into cytotoxic compounds inside tumor cells (e.g., Herpes Simplex Virus thymidine kinase (HSV-TK), which convents the non-toxic prodrug ganciclovir to toxic ganciclovir monophosphate); (2) Induction of tumor cell apoptosis by over-expressing tumor suppressors (e.g., TNF-related apoptosis-inducing ligand (TRAIL)); (3) Suppression of tumor angiogenesis by over-expressing anti-angiogenic factors (e.g., endostatin, angiostatin and vastatin) or blocking the VEGF pathway; as well as (4) Immunotherapy, which includes modification of CAR-T cells, cancer vaccination, and induction of immunosuppressive cytokines[200,201].

Due to the presence of the BBB, in early studies, AAV vectors were administered to GBM animal models by intracranial local injection or intracerebroventricular (ICV) injection[202-206]. However, AAV vectors administered by local injection or ICV injection cannot reach the GBM cells that migrated away from the tumor bulk. Furthermore, both methods invoke surgical risks. The discovery of the BBB-penetrating ability of AAV9 promoted the concept of non-invasive systematic delivery of AAV for CNS transduction[207,208]. Systematic injection (e.g., intravenous injection) of AAV vectors enables widespread transduction in the CNS and avoids invasive surgery, which would be ideal for treating CNS diseases including GBM.

The BBB regulates homeostasis of the CNS by forming a tightly regulated neurovascular unit, which is composed of endothelial cells, basal lamina, pericytes, and astrocytic endfeet. The endothelial cells are associated with each other by tight junctions[209,210]. The BBB protects the brain from detrimental components, while at the same time also rejecting

approximately 98% of small-molecule drugs and almost all macromolecular drugs[211]. Some small molecules can passively cross the BBB via transcellular diffusion or paracellular diffusion, while the only non-invasive way for large molecules to cross is transcytosis[212]. Using primary human brain microvascular endothelial cells as a model of the human BBB, Merkel *et al.* proved that AAV9 penetrates the brain endothelial cell barrier through an active, cell-mediated process without disruption of BBB integrity[213].

As the BBB-penetrating efficiencies of AAV9 or other natural serotypes (e.g., AAVrh.8 and AAVrh.10[214]) are limited, studies have focused on engineering AAV capsids to enhance the BBB-penetrating and CNS transduction efficiency, mainly by directed evolution[215]. PHP.B and the optimized PHP.eB variant have become the most famous variants, which exhibit a striking BBB-penetrating ability and CNS tropism in C57BL/6 mice. However, later studies discovered that these capsids can only cross the BBB of selected mouse strains such as C57BL/6 but not other animals, because the receptor of these two variants, Ly6a, is specifically expressed in these mouse strains[217-219]. Therefore, to develop AAV capsids with enhanced BBB-penetrating efficiency that can be used in patients, it is important to characterize the receptors that mediate transcytosis in humans.

1.6 Aim

In this study, I aimed to rationally design AAV vectors to transduce target cells by binding cell-specific receptors. Therefore, I pursued two major projects: (1) AAV targeting to cells expressing the SARS-CoV-2 receptor hACE2 (section 3.1); and (2) penetration of the BBB and targeting to GBM (section 3.2). To achieve these goals, I displayed known receptor-binding ligands (peptides and proteins) on AAV capsids. More specifically, I used and compared three different methods: genetic insertion into the AAV capsid protein (VP), chemical/covalent conjugation to the assembled AAV capsid, and non-covalent binding to the assembled AAV capsid. Furthermore, I adjusted the number of ligands displayed on the AAV capsid by producing mosaic capsids composed of wild-type and ligand-displaying VP. Thirdly, I displayed two ligands on the same capsid by producing mosaic capsids of two different ligand-displayed VPs.

2 Materials and Methods

2.1 Materials

2.1.1 Devices

Table 3. Devices used in this study.

Application	Device	Provider
pipetting	2, 10, 20, 200, 1000 µL pipette	Eppendorf
	2, 10, 20, 200, 1000 µL pipette	Gilson
	10, 100 µL 12-well multichannel pipette	Eppendorf
	200 µL 12-well multichannel pipette	Brand GmbH
	accu-jet pro	Brand GmbH
PCR, qPCR, and ddPCR	Mastercycler pro S	Eppendorf
	Corbett Roter-Gene 6000	QIAGEN
	StepOnePlus Real-Time PCR	Applied Biosystems
	C1000 Touch Thermal Cycler	Bio-Rad
	QX200™ Droplet Generator	Bio-Rad
	PX1 PCR Plate Sealer	Bio-Rad
	QX200™ Droplet Reader	Bio-Rad
Hood and incubator	Captair Bio Smart PCR-Hood	Erlab
	Heraus function line incubator	Thermo Fisher Scientific
	Multitron Shaking Incubator	INFORS HT
	HERA cell 150 incubator	Thermo Fisher Scientific
	HERA safe sterile work bench	Thermo Fisher Scientific
Centrifugation	Benchtop Centrifuge 5415R	Eppendorf
	Benchtop Centrifuge 5417R	Eppendorf
	Allegra X-12 Centrifuge	Beckman Coulter
	Avanti J-26 XP Centrifuge	Beckman Coulter
	Avanti J-25 Centrifuge	Beckman Coulter
	JA-10 rotor	Beckman Coulter
	OptimaTM L-90K Ultracentrifuge	Beckman Coulter
	Fixed angle type 70 Ti rotor	Beckman Coulter
	Fixed angle type 70.1 Ti rotor	Beckman Coulter
	Tube Sealer	Beckman Coulter
Agarose gel electrophoresis	EasyPhor	Biozym Scientific
	CONSORT E835 power supply	Nexigen GmbH
	UV-Transilluminator	Biostep GmbH
	Gel Doc XR	Bio-Rad
	Mitsubishi P93D Printer	Mitsubishi Electric

SDS-PAGE and Westernblot	mini-PROTEAN Tetra Cell	Bio-Rad
	PowerPac HV	Bio-Rad
	Mini Trans-Blot Electrophoretic Transfer	Bio-Rad
	Bio-Dot Apparatus	Bio-Rad
	Azure 300 Visible Fluorescent imager	Azure Biosystems
Flow cytometry	BD FACS Celesta Cell Analyzer	BD Biosciences
	BD High Throughput Sampler (HTS)	BD Biosciences
Microscopy	Olympus microscopy CKX41	Olympus
	Olympus laser U-RPL-T	Olympus
	Olympus microscopy IX81	Olympus
	JEM1400 electron microscope	JEOL
DNA assessment	2100 Bioanalyzer	Agilent Technologies
	Qubit 2.0 Fluorometer	Thermo Fisher Scientific
	NanoDrop 2000 Spectrophotometer	Thermo Fisher Scientific
Incubation and mixing	Mixing Block MB 102	Bioer Technology
	TW12 Water Bath	Julabo
	Lauda Aqualine AL5	DJB Labcare
	Vortex Genie 2	neoLab
	Magnetic stirrer	Thermo Fisher Scientific
	Tube roller TRM-V	neoLab
	Rocking Shaker	neoLab
	Rotator	VWR
	MagnaBot 96	Promega
Sonication	Sonorex Super	Allpax
Cell counter	Countess	Thermo Fisher Scientific
Cell freezing	Mr.Frosty Frozen Container	Thermo Fisher Scientific
Tissue lysis	TissueLyser LT	Qiagen

2.1.2 Consumables

Table 4. Consumables used in this study.

Product	Provider
Tubes (0.5, 1.5, 2 mL)	Eppendorf
Falcon tubes (15, 50 mL)	Greiner bio-one
DNA LoBind Tubes (1.5 mL)	Eppendorf
Glass bottles	DWK Life Sciences
Glass flasks	DWK Life Sciences
Pipet Tips (10, 200, 1000 µL)	

Filtered pipet Tips (10, 20, 100, 1000 µL)	Biozym Scientific
Serological pipettes (2, 5, 10, 25, 50 mL)	Greiner Bio-One
25 mL Clear Advantage Reagent Reservoirs	Integra Biosciences
8-strip PCR tubes, 0.2 mL	Biozym Scientific
qPCR 4-Tube & 4-Cap Strips	Biozym Scientific
96-well qPCR plates, semi skirted	Biozym Scientific
96-well qPCR plates, semi skirted	Biozym Scientific
96-well ddPCR plates, semi skirted	Bio-Rad
MicroAmp optical adhesive films	Thermo Fisher Scientific
Pierceable foil heat seals	Bio-Rad
DG8 Cartridges	Bio-Rad
DG8 gaskets	Bio-Rad
Centrifuge Bottles, 500ml	Beckmann
Centrifuge Bottles (for virus)	Corning
Quick-Seal centrifuge tubes, 25 x 89 mm	Beckman Coulter
Re-seal polyallomer centrifuge tubes, 16 x 76 mm	Seton Scientific
Pasteur capillary pipettes	Corning
Inoculation loops	Greiner bio-one
Petri dishes	Greiner Bio-One
Cell lifters	Corning
Countess cell counting chamber slides	Thermo Fisher Scientific
Millipore membrane filters, 0.22 µm	Merck
Millipore steritop filter, 0.22 µm	Merck
Cell culture flasks (75, 175 mL)	Greiner Bio-One
Cell culture dishes, 150 x20 mm	Sarstedt
Cell culture plates, 6 / 12 / 24 / 48 / 96 - well	Greiner Bio-One
96-Well plates, flat clear bottom, black wall	Corning
96-Well plates, V-bottom	Corning
Amicon Ultra-15 Centrifugal Filters, 100,000 MWCO	Merck
Amicon Ultra-4 Centrifugal Filters, 100,000 MWCO	Merck
Mini-PROTEAN TGX Precast protein Gels 7.5%	Bio-Rad
Mini-PROTEAN TGX Precast protein Gels 8-15%	Bio-Rad
Blotting Membranes, CN 0.45um	NeoLab
Whatman paper 3mm	Whatman
Dynabeads Protein A	Thermo Fisher Scientific
Formvar/Carbon Thin Bar Square Mesh (Cu, 200 Mesh, SB)	Electron Microscopy Sciences
Stainless steel beads, 3 mm	Qiagen
Microlance 3 needles	BD
Microlance 3 canules, 19G / 21G	BD

Syringes (3, 5 mL)	BD
Scalpel blades	Heniz Herenz
DNA chip	Agilent Technologies

2.1.3 Chemicals

Table 5. Chemicals used in this study.

Product	Provider
Nuclease-free H_2O	Qiagen
Aqua B. Braun	B. Braun Avitum Saxonia GmbH
Deoxynucleotide (dNTP) Solution Mix, 10mM	NEB
1 kb Plus DNA ladder	Thermo Fisher Scientific
Ethidium Bromide	Roth
Droplet Generation Oil for Probes	Bio-Rad
Biozym LE Agarose	Biozym Scientific
PageRuler Plus Prestained Protein Ladder	Thermo Fisher Scientific
Sodium Dodecylsulfate (SDS)	Serva
Rotiphorese Gel 40 (19:1)	Roth
Ammonium Persulfate (APS)	Thermo Fisher Scientific
UltraPure TEMED	Thermo Fisher Scientific
Ampicillin	Roth
Bacto agar	BD
Bacto tryptone	BD
Bacto yeast extract	BD
DMEM GlutaMAX	Gibco
1× Dulbecco's phosphate buffered saline (DPBS)	Gibco
Penicillin / Streptomycin (P/S)	Gibco
Fetal bovine serum (FBS)	Capricorn Scientific
MEM Non-Essential Amino Acids Solution	Gibco
0.25% Trypsin / EDTA	Gibco
Polyethyleneimine (PEI MAX)	Polysciences Europe GmbH
Lipofectamine 2000	Invitrogen
Paraformaldehyde (PFA)	Merck
OptiPrep (Iodixanol)	Progen
Phenol red	Merck
Acetic acid	VWR chemicals
Potassium chloride (KCl)	GRÜSSING GmbH
Potassium acetate (KAc)	GRÜSSING GmbH

Sodium chloride (NaCl)	GRÜSSING GmbH
Sodium deoxycholate (DOC)	Merck
Sodium hydroxide (NaOH)	Merck
Magnesium chloride (MgCl2)	Applichem
Magnesium sulfate (MgSO4)	
Hydrochloric acid (HCl)	VWR chemicals
TRIS	Roth
TRIS-HCl	Roth
Triton X-100	Merck
Tween20	Roth
Ethylendiamintetraacetate (EDTA)	GRÜSSING GmbH
Ethanol absolute	Merck
Isopropanol	Merck
Methanol	
Glycerol	VWR chemicals
Pluronic F-68	Gibco
β-Mercaptoethanol (BME)	Roth
Dithiothreitol (DTT)	Thermo Fisher Scientific
Tris(2-carboxyethyl)phosphine (TCEP)	Merck
Biotin-PEG3-Maleimide	TCI Chemicals
Albumin fraction V (BSA)	Roth
Bortezomib	Merck
Hoechst 3000	Dianova
Trypan Blue	Thermo Fisher Scientific
Milk powder	Roth

2.1.4 Buffers and Solutions

Table 6. Commercial buffers used in this study.

Product	Provider
Gel Loading Dye, Purple (6×)	NEB
TE Buffer	Thermo Fisher Scientific
5× HF Buffer	Thermo Fisher Scientific
5× GC Buffer	Thermo Fisher Scientific
NEBuffer 1.1 buffer	NEB
NEBuffer 2.1 buffer	NEB
NEBuffer 3.1 buffer	NEB
CutSmart buffer	NEB

Tango Buffer	Thermo Fisher Scientific
T4 DNA Ligase Buffer	NEB
T4 DNA Ligase Buffer	Thermo Fisher Scientific
Diluent B	NEB
4× Laemmli Sample Buffer	Bio-Rad
10× Tris/Glycine/SDS (TGS) Buffer	Bio-Rad
10× TBS Buffer	Bio-Rad
HEPES Buffer	Gibco
1M TRIS-HCL (pH=8.0) Buffer	Gibco
1M TRIS-HCL (pH=7.5) Buffer	Gibco
RNAlater	Thermo Fisher Scientific

Table 7. Self-made buffers used in this study.

Buffer	Composition
PBS-MK	PBS (1×), 2.5 mM KCl, 1 mM MgCl2
PBS-MK-NaCl	1M NaCl in PBS-MK
15% iodixanol	75.00% PBS-MK-NaCl, 25.00% OptiPrep
25% iodixanol	58.19% PBS-MK, 41.56% OptiPrep, 0.25% Phenol red stock
40% iodixanol	66.67% OptiPrep, 33.33% PBS-MK
60% iodixanol	99.75% OptiPrep, 0.25% Phenol red stock
Benzonase buffer	150 mM NaCl, 50 mM TRIS-HCl (pH 8.0), 2 mM MgCl2
Phenol red stock	Nuclease-free H_2O, 0.5% Phenol red
LB medium	1.0% Bacto tryptone, 1.0% NaCl, 0.5% Bacto yeast extract
LB agar	1.5% Bacto agar, 1.0% NaCl, 1% Bacto tryptone, 0.5% Bacto yeast extract
SOB medium	2% Bacto Tryptone, 0.5% (w/v) Bacto Yeast Extract, 10 mM NaCl, 2.5 mM KCl, 10 mM MgSO4 (add after autoclaving), 10 mM MgCl2 (add after autoclaving)
miniprep P1 buffer	50 mM Tris-HCl (pH 8.0), 10 mM EDTA, 100 µg/mL RNase A
miniprep P2 buffer	200 mM NaOH, 1% SDS
miniprep P3 buffer	2.8 M KAc (pH 5.1)
50× TAE buffer	2 M Tris, 1 M acetic acid, 50 mM EDTA
RIPA buffer	50 mM Tris/HCl pH 8.0, 150 mM NaCl, 1mM EDTA, 1% Triton, 0.1% SDS, 0.5% DOC, 1x Protease Inhibitor
TBST	1x TBS, 0.05% Tween20
Transfer buffer	1x TGS, 20% Methanol

2.1.5 Enzymes

Table 8. Enzymes used in this study.

Enzyme	Provider
Restriction Enzymes:	
AscI	NEB
AgeI	NEB
BamHI-HF	NEB
BbsI-HF	NEB
BglII	NEB
BsmBI v2	NEB
BsaI-HF v2	NEB
BspEI	NEB
BsiWI-HF	NEB
ClaI	NEB
EcoRI-HF	NEB
Esp3iI (BsmBI)	Thermo Fisher Scientific
HindIII-HF	NEB
NotI-HF	NEB
PacI	NEB
SpeI-HF	NEB
SfiI	NEB
XmaI	NEB
Other Enzymes:	
Antarctic Phosphatase	NEB
Benzonase	Merck
DNase I (RNase-free)	NEB
ezDNase enzyme	Thermo Fisher Scientific
Phusion Flash High-Fidelity PCR Master Mix	Thermo Fisher Scientific
Phusion HS II	Thermo Fisher Scientific
Proteinase K	Qiagen
Q5 Hot Start High-Fidelity 2X Master Mix	Thermo Fisher Scientific
Quick CIP	NEB
T4 DNA ligase	NEB
T4 DNA ligase	Thermo Fisher Scientific
T4 Polynucleotide Kinase	NEB
RNase A	Qiagen

2.1.6 Kits

Table 9. Kits used in this study.

Kit	Provider	Application
QIAprep Spin Miniprep Kit	Qiagen	Plasmid miniprep
PureYield Plasmid Midiprep System	Promega	Plasmid midiprep
NucleoBond PC 500 Maxi Kit	Macherey-Nagel	Plasmid maxiprep
QIAquick Gel Extraction Kit	Qiagen	DNA gel extraction
Allprep DNA/RNA mini Kit	Qiagen	DNA and RNA extraction
DNeasy Blood & Tissue mini Kit	Qiagen	DNA extraction
RNeasy mini Kit	Qiagen	RNA extraction
DNA clean & concentrator-5	Biozol	DNA purification
ProNex Size-Selective Purification	Promega	DNA purification
RNase-Free DNase Set	Qiagen	DNA digestion
High-Capacity cDNA Reverse Transcription Kit	Thermo Fisher Scientific	cDNA synthesis
SuperScript IV VILO Master-Mix with ezDNase Enzyme	Thermo Fisher Scientific	cDNA synthesis
KAPA HiFi HotStart ReadyMix PCR Kit	Roche	NGS index PCR
Nextera XT Index Kit v2 (Set A and Set D)	illumina	NGS index PCR
DNA 1000 Kit	Agilent Technologies	Bioanalyzer 2100
Qubit dsDNA HS Assay Kit	Thermo Fisher Scientific	Qubit
Sensimix II Probe Kit	Bioline	qPCR
iTaq Universal SYBR Green Supermix	Bio-Rad	qPCR
ddPCR Supermix for Probes (No dUTP)	Bio-Rad	ddPCR
SignalFire Elite ECL Reagent	Cell Signaling Technology	Western Blot
WesternBright Quantum Western blotting detection Kit	Biozym Scientific	Western Blot
SilverQuest Silver Staining Kit	Invitrogen	Silverstaining

2.1.7 Oligonucleotides

DNA oligonucleotides used as primers were ordered from Merck or Integrated DNA Technologies (IDT). The primers used for sanger sequencing are listed in Table 10. The primers used for cloning are listed in section 2.2. DNA oligonucleotides with fluorophores and quenchers used as probes for qPCR and ddPCR were ordered from IDT. The primers and probes used for qPCR and ddPCR are listed in Table 11. DNA oligonucleotides with 5'- maleimide used as aptamers were ordered from biomers and are listed in section 3.1.2.2 Table 32.

Table 10. Oligonucleotides used for sanger sequencing.

Name	Sequence
LSeqFor	GATCTGGTCAATGTGGATTTG
Pos680For	GAAATTGGCATTGCGATTCC
SeqFor39	GCAGCTACGCTCACAGCCA
DJrev (real)	GTCGCAAAACACTCACGTGACCTC

Table 11. Oligonucleotide used for qPCR and ddPCR.

Name	Sequence
eGFP_fr	GAGCGCACCATCTTCTTCAAG
eGFP_rv	TGTCGCCCTCGAACTTCAC
eGFP_probe	FAM-ACGACGGCAACTACA-BHQ1
ITR_fr	GGAACCCCTAGTGATGGAGTT
ITR_rv	CGGCCTCAGTGAGCGA
ITR_probe	HEX-CACTCCCTCTCTGCGCGCTCG-BHQ1

2.1.8 Antibodies and other Proteins

Antibodies used for western blot and RBD display are listed in Table 12. Recombinant Human ACE2-Fc (hACE2-Fc) for hACE2 binding assay was purchased from Sino Biological.

Table 12. Antibodies used in this study.

Antibodies	Provider
For western blot	
A1 (anti N-terminal of AAV VP1)	
B1 (anti C-terminal of AAV VP)	
anti -RBD	ACROBiosystems
HRP-conjugated goat anti-mouse IgG	Jackson ImmunoResearch
For RBD display	
RBD_hIgG4_AE1	Friedrich Koch-Nolte
RBD_hinge4_AE1	Friedrich Koch-Nolte
RBD_35GS_AE1	Friedrich Koch-Nolte

2.1.9 Bacterial Strains

MAX Efficiency DH5α Competent Cells (Thermo Fisher Scientific) were used.

2.1.10 Cell lines

Table 13. Cell lines used in this study.

Cell lines	Origin
HEK293T	Human embryomic kidney
U-87 MG	Human glioblastoma
GL261	Mous glioblastoma
Neuro-2A	Mouse neuroblast
Huh-7	Human hepatoma
hACE2+ Huh7	hACE2 expressing Huh7
hACE2+ HEK293T	hACE2 expressing HEK293T

2.1.11 Software

Table 14. Software used in this study.

Name	Provider	Application
ScanR acquisition	Olympus BioSystems GmbH	Microscopy imaging
JEM-1400Plus	JEOL	Electorn microscopy imaging

BD FACSDiva	BD Biosciences	Flow cytometry running
FlowJo	FlowJo LLC	Flow cytometry analysis
Quantity One	Bio-Rad	Agar gel imaging
QuantaSoft™ Software	Bio-Rad	ddPCR droplet reading
Roter Gene 6000 Series	QIAGEN	qRT-PCR running
StepOne Software v2.3	Applied Biosystems	qRT-PCR running
NanoDrop 2000	Thermo Fisher Scientific	Nanodrop
2100 Expert	Agilent Technologies	Bioanalyzer
SnapGene Viewer	SnapGene	DNA viewing
Jalview	Jalview	Aligment
PyMol	The PyMOL Molecular Graphics	Protein structure viewing and editing
ImageJ	Open source	Image analysis
GraphPad Prism	GraphPad Software	Statistical graph making
Adobe illustrator	Adobe	Graph making
Adobe photoshop	Adobe	Graph making
Python 3.6	Python Software Foundation	Data analysis
Microsoft Office 365	Microsoft Corporation	Miscellaneous

2.2 Methods

2.2.1 General Molecular Biology Methods

2.2.1.1 Polymerase Chain Reaction (PCR)

To amplify DNA fragments for subsequent cloning steps, a PCR was performed with Phusion HS II polymerase. In each reaction (50 µl), 5-50 ng template plasmid, 2.5 µl forward primer (10 µM), 2.5 µl reverse primer (10 µM), 1 µl dNTPs (10mM), 0.5 µl Phusion HS II polymerase, 10 µl 5x HF or GC buffer were mixed and filled up to 50 µl with nuclease-free H_2O. PCR was performed in the thermocycler with the program listed in the Table 15. The annealing temperature was calculated for each pair of primers with the online Tm calculator (https://www.thermofisher.com/de/de/home/brands/thermo-scientific/molecular-biology/molecular-biology-learning-center/molecular-biology-resource-library/thermo-scientific-web-tools/tm-calculator.html). After reaction, PCR

products were determined via agarose gel electrophoresis and purified with QIAquick Gel Extraction Kit if needed (see in 2.2.1.3).

Table 15. Cycling program for PCR.

Step	Temperature(°C)	Time	
Initial denaturation	98	5 min	
Denaturation	98	15 s	38 cycles
Annealing	55-68	15 s	
Elongation	72	30-45 s/kb	
Final Elongation	72	5 min	
Hold	4	infinite	

2.2.1.2 Overlap Extension PCR

Overlap extension PCR (OE PCR) was used to join two or more DNA fragments. The reverse primer of the 5'-fragment (R1) and the forward primer of the 3'-fragment (F2) should contain overlapping complementary sequences, which allow the fragments to anneal. Overlap extension PCR were also used for introducing substitutions, insertions or deletions into the plasmids. To this end, R1 and F2 primers carried the desired mutations. The first step is to perform two standard PCRs as described in section 2.2.2.1 to amplify two fragments. The PCR products were purified by gel electrophoresis and QIAquick Gel Extraction Kit (describe in section 2.2.1.3) for the following reactions. Then, equal amounts of each fragment were used in a PCR without primers running for 10 cycles, in which overlapping ends anneal and extend to the full length. Next, forward primer of 5'-fragment (F1) and reverse primer of 3'-fragment (R2) were added, and 30 cycles of standard PCR run to amplify the joint fragment. The final products were determined via agarose gel electrophoresis and purified with QIAquick Gel Extraction Kit if needed.

2.2.1.3 Restriction Digest

To generate sticky ends for ligation, plasmids or PCR amplicons were digested by restriction endonucleases listed in Table 8. In each reaction (50 µl), 1-4 µg plasmid or 5-20 µl purified PCR amplicon, 20 units of each of restriction enzymes, and 5 µl corresponding 10x buffer were mixed and filled up to 50 µl with nuclease-free H_2O, and incubated for 1-4 hours or overnight at 37°C (SfiI at 50 °C). Digested plasmids were applied to gel electrophoresis and sequentially purified with the QIAquick Gel Extraction Kit and DNA clean & concentrator-5 Kit. Digested PCR amplicons were purified with the DNA clean & concentrator-5 Kit directly.

Restriction digest was also performed to confirm the presence and integrity of ITRs. The AAV2-ITR contains an XmaI restriction site and the AAV4-ITR contains a BsaI restriction site. Therefore, XmaI was used for ssAAV plasmids (contain two AAV2-ITRs), and XmaI and BsaI were used for scAAV plasmids (contain AAV2-ITR and AAV4-ITR).

2.2.1.4 Agarose Gel Electrophoresis

After PCR or restriction digest, to determine the size of DNA fragments and separate the DNA fragments with different size, agarose gel electrophoresis was performed. Gels were prepared by dissolving 1% (w/v) agarose in 1x TAE buffer and heating. Ethidium bromide was added to a final concentration of 1 µg/ml. DNA samples were mixed with 6x loading dye and loaded to the solidified gel. 1kb Plus DNA ladder was loaded as a reference. Electrophoresis was performed at 100-120V in TAE buffer. DNA bands were visualized with UV light. If needed, the QIAquick Gel Extraction Kit was used to purify DNA bands after electrophoresis.

2.2.1.5 Annealing and phosphorylation of Oligonucleotides

2.5 µl each of forward and reverse oligonucleotide (100 µM), 5 µl 10x annealing buffer, and 40 µl nuclease-free H_2O were mixed. Annealing was performed in a thermocycler with the following program: heat to 98 °C for 7 min, cool down to 25 °C with 5% ramp, and hold at 4 °C. Annealed oligonucleotides were then phosphorylated by T4 PNK. 4 µl annealed oligonucleotides, 1 µl PNK, 2 µl T4 ligase buffer and 13 µl nuclease-free H_2O were mixed, incubated at 37 °C for 30 min and inactivated at 65 °C for 20 min.

2.2.1.6 Dephosphorylation of digested plasmid

For ligation of annealed and phosphorylated oligonucleotides, the restriction-digested plasmid was dephosphorylated with Quick CIP. Therefore, 2.5 µl Quick CIP were added to 50 µl restriction digest reaction directly, incubated at 37 °C for 10 min and inactivated at 80 °C for 5 min.

2.2.1.7 DNA Ligation

DNA insert and plasmid backbone were used at a 3:1 molar ratio (10:1 molar ratio when the insert was annealed and phosphorylated oligonucleotides). 100 ng of total amount of DNA, 0.5 µl T4 ligase and 1 µl T4 ligase buffer were mixed and adjusted to 10 µl with

nuclease-free H_2O. The reaction was incubated at RT for 30 min to 2 h or at 16 °C overnight. A negative control was performed in the absence of an insert.

2.2.1.8 Transformation

5 µl of the ligation reaction was added to 50 µl of MAX Efficiency™ DH5α™ Competent Cells or One Shot® ccdB Survival™ 2 T1R Competent Cells, mixed, and incubated on ice for 30 min. Then, a heat shock was performed at 42 °C for 45 s. Cells were then cooled down on ice for 2 min, plated on LB-ampicillin agar plates and incubated at 37°C overnight.

2.2.1.9 Bacteria Cultivation and Plasmid Extraction

To prepare plasmids, bacteria were cultivated in LB medium with 50 µg/ml ampicillin at 37°C and 180 rpm shaking for 12-16 h. Depending on the amount of plasmid required, bacteria were grown in three different scales and purified with corresponding kits. (1) Small scale (5-25 µg): bacteria were grown in 2-5 ml LB medium and plasmids were isolated with the QIAprep Spin Miniprep Kit; (2) Medium scale (100-400 µg): bacteria were grown in 80 ml (high-copy) / 150 ml (low-copy) LB medium and plasmids were isolated with the PureYield Plasmid Midiprep Kit; or (3) Large scale (0.5-4 mg): bacteria were grown in 300 ml (high-copy) / 600 ml (low-copy) LB medium and plasmids were isolated with the NucleoBond Xtra Maxi Kit. DNA concentration was measured with the Nanodrop 2000 Spectrophotometer.

2.2.1.10 Sanger Sequencing

Plasmids were submitted to Eurofins Genomics for Sanger sequencing to validate the integrity of the DNA sequences. For each sample, 400-600 ng plasmid was mixed with 2.5 µM corresponding sequencing primer and filled up to 10 µl with nuclease-free H_2O.

2.2.2 Cloning of new constructs

2.2.2.1 Cloning of AAV helper plasmids for hACE2 targeting

All PCR primers used in this section are listed in Table 16. All plasmids used or generated in this section are listed in Table 18.

AAV helper plasmids for VP1-RBD and VP1-RBM were cloned by inserting RBD (T333-P527) and RBM (S438-Q506) amplicons into the pAAV2RA.VP1-nb backbone plasmid[115]. DNA fragment of RBD and RBM with overhangs containing GGGGS linkers and restriction sites for NgoMIV and KasI was ordered from IDT. RBD/RBM_fr, RBD_rv and RBM_rv primers were used to conduct PCRs to generate RBD and RBM amplicons. The pAAV2RA-nb plasmid, RBD amplicon and RBM amplicon were digested by NgoMIV and KasI, and ligated. To generate AAV helper plasmids for $AAV2^{RA}$ (WH-Rep2-Cap2RA), the AAV2 helper plasmid from our lab WH-Rep2-Cap2wt was used as template. OE PCR was used to generate amplicons between BsiWI and SpeI restriction sites with R585A and R588A mutation by using Cap_BsiWI_fr, R585/588A_rv1, R585/588A_fr2 and Cap2_rv as F1, R1, F2, R2, respectively. Then the amplicon was digested by BsiWI and SpeI and ligated with digested WH-Rep2-Cap2wt.

WH-Rep2-Cap2RA plasmid was engineered to generate AAV helper plasmids for V4-/V5-/V8- RBD/RBM- 1L/2L. BspEI and BamHI restriction enzymes were chosen for peptide insertion, which introduce SG and GS flanking amino acids, respectively. At first, WH-Rep2-Cap2RA-VP1 was generated by replacing the sequence between PpuMI and BsiWI restriction sites of WH-Rep2-Cap2wt plasmid with the corresponding sequence from pAAV2RA.VP1-nb plasmid, which introduced SA_M mutation and removed BamHI restriction site in *Rep2* ORF. Next, amplicons of Cap2RA between BsiWI restriction site and V4-/V5-/V8- insertion sites with overhangs containing BsiWI and BamHI restriction sites (1^{st}-fragments), amplicons of RBD-1L/RBD-2L/RBM-1L/RBM-2L with overhangs containing BamHI and BspEI restriction sites (2^{nd}-fragments), and amplicons of Cap2RA between V4-/V5-/V8- insertion sites and SpeI restriction site with overhangs containing BspEI and SpeI restriction sites (3^{rd}-fragments) were generated by PCR and digested with corresponding restriction enzymes. 1^{st}-fragments, 2^{nd}-fragments and 3^{rd}-fragments were cloned to WH-Rep2-Cap2RA-VP1 between BsiWI and SpeI restriction sites.

To generate the plasmid for expressing VP2-RBD, VP2-RBD(1L), VP2-RBM and VP2-RBM(1L), amplicons of RBD, RBD(1L), RBM and RBM(1L) with overhangs containing ATG start codon and restriction sites of HindIII and BamHI and amplicon of VP2 with overhangs containing restriction sites of BamHI and NotI were generated by PCR and digested with corresponding restriction enzymes. Digested RBD or RBM amplicon and VP2 amplicon were cloned into peRF1_e55d_pCDNA5 plasmid between HindIII and NotI,

so that expression was driven by the CMV promoter. The AAV helper plasmid for VP2KO was generated by OE PCR using WH-Rep2-Cap2RA as template.

To generate AAV helper plasmids for VP1-V8-RBMP1 - VP1-V8-RBMP11, sense and anti-sense oligonucleotides (Table 17) for each peptide were ordered, annealed and ligated to WH-Rep2-Cap2RA-VP1-V8-RBD(1L) plasmid between BamHI and BspEI restriction sites.

Table 16. Primers used in cloning of AAV helper plasmids for hACE2 targeting capsids.

Name	Sequence
PCR for RBD/RBM insertion	
RBD/RBM_fr	TAGTCAGCCGGCGTTCGTATC
RBD_rv	ACTAGCGGCGCCTCCTCC
RBM_rv	ACTAGCGGCGCCTTGGTAAC
PCR for new constructs of RBD/RBM insertion	
Cap2_fr	GAGTACCAGCTCCCGTAC
Cap2_rv	AGTTCAACTGAAACGAATCAACC
Cap_453_rv	TCACGAATGCATCCTATCCGGATCCACTTGGAGTGTTTGTTCTG
Cap_454_fr	TCACATATGCATCCAATGGATCCACCACCACGCAGTCAAGG
Cap_496_rv	TCACGAATGCATCCTATCCGGAGTTGTTATCCGCAGATGTCTTTG
Cap_497_fr	TCACATATGCATCCAATGGATCCAACAGTGAATACTCGTGGAC
Cap_586_rv	TCACGAATGCATCCTATCCGGAGCCTGCCTGGAGGTTGG
Cap_587_fr	TCACATATGCATCCAATGGATCCAACGCACAAGCAGCTAC
RBD_1L_fr	TCACGATCCGGAGGAGGAGGATCAAC
RBD_1L_rv	TCACATGGCGCCGGATCCTCCTCCTCCTCCACAAACAGTTG
RBD_2L_fr	TCACGATCCGGAGGAGGAGGATCAGGAGGAGGAGGATCAACAAAC
RBD_2L_rv	TCACATGGCGCCGGATCCACCACCACCTGATCCTCCTCCTCCTCCACAAACAGTTG
RBM_1L_fr	TCACGATCCGGAGGAGGAGGATCATC
RBM_1L_rv	TCACATGGCGCCGGATCCTCCTCCTCCTTGGTAACCAAC
RBM_2L_fr	TCACGATCCGGAGGAGGAGGATCAGGAGGAGGAGGATCATCTAAC
RBM_2L_rv	TCACATGGCGCCGGATCCACCACCACCTGATCCTCCTCCTCCTTGGTAACCAACAC
PCR for VP2-RBD/RBM insertion	
RBD_ATG_fr	TCACGAAAGCTTATGACAAACTTGTGCCCTTTTGG
RBD_rv	TCACATGGATCCTCCACAAACAGTTGCTGG
RBM_ATG_fr	TCACGAAAGCTTATGTCTAACAATCTTGATTCTAAGGTTGG

RBM_rv	TCACATGGATCCTTGGTAACCAACACCATTAGTG
VP2_fr	TCACATGGATCCGCTCCGGGAAAAAAGAGG
VP2_rv	AACACTGCGGCCGCTTACAGATTACGAGTCAGGTATCTG
OE PCR for RA mutation	
Cap2_BsiWI_fr	GAGTACCAGCTCCCGTAC
Cap2_rv	AGTTCAACTGAAACGAATCAACC
R585/588A_rv1	AGCTGCTTGTGCGTTGCCTGCCTGGAGGTTGGTAG
R585/588A_fr2	CCAACCTCCAGGCAGGCAACGCACAAGCAGCTACC
OE PCR for mutation of VP2 start codon	
LSeqFor	GATCTGGTCAATGTGGATTTG
BsiWI_rv	CCGAGGACGTACGGGAG
VP2ko_rv1	CCCGGAGCGGTCTTAACAGG
VP2ko_fr2	CCTGTTAAGACCGCTCCGGGAAAAAAG

Table 17. Oligonucleotides for RBMP peptide inserts

Name	Sequence
RBMP1_fr	CCGGAGGTTTCCAACCCACTAATGGTG
RBMP1_rv	GATCCACCATTAGTGGGTTGGAAACCT
RBMP2_fr	CCGGAGGTTTCCAACCCACTAATGGTGTTGGTTACG
RBMP2_rv	GATCCGTAACCAACACCATTAGTGGGTTGGAAACCT
RBMP3_fr	CCGGAGGACAATCATATGGTTTCCAACCCACTAATGGTGGAG
RBMP3_rv	GATCCTCCACCATTAGTGGGTTGGAAACCATATGATTGTCCT
RBMP4_fr	CCGGAGGACAATCATATGGTTTCCAACCCACTAATGGTGTTGGTTA CGGAG
RBMP4_rv	GATCCTCCGTAACCAACACCATTAGTGGGTTGGAAACCATATGATT GTCCT
RBMP5_fr	CCGGAGGATTTAATTGTTACGGAG
RBMP5_rv	GATCCTCCGTAACAATTAAATCCT
RBMP6_fr	CCGGATGTAATGGTGTTGAAGGTTTTAATTGTTACG
RBMP6_rv	GATCCGTAACAATTAAAACCTTCAACACCATTACAT
RBMP7_fr	CCGGAGGATATCAGGCCGGAG
RBMP7_rv	GATCCTCCGGCCTGATATCCT
RBMP8_fr	CCGGATATCAGGCCGGTAGCACACCTTGTAATGGTG
RBMP8_rv	GATCCACCATTACAAGGTGTGCTACCGGCCTGATAT
RBMP9_fr	CCGGATATCAGGCCGGTAGCACACCTTGTAATGGTGTTGAAGGTT TTAATTGTTACG
RBMP9_rv	GATCCGTAACAATTAAAACCTTCAACACCATTACAAGGTGTGCTAC CGGCCTGATAT

RBMP10_fr	CCGGATCTAAGGTTGGTGGTAATTATG
RBMP10_rv	GATCCATAATTACCACCAACCTTAGAT
RBMP11_fr	CCGGAGGATATAGATTGTTTGGAG
RBMP11_rv	GATCCTCCAAACAATCTATATCCT

Table 18. Plasmids used or generated for producing hACE2-targeting capsids.

Name	Origin
WH-Rep2-Cap2wt	Eike Kienle
pAAV2RA.VP1-nb	Friedrich Koch-Nolte
peRF1_e55d_pCDNA5	Benno Zehnder
WH-Rep2-Cap2RA-VP1stop	Kathleen Börner
WH-Rep2-Cap2RA-VP2/3	Laura Dietz
pAAV2RA.VP1-RBD	This study
pAAV2RA.VP1-RBM	This study
WH-Rep2-Cap2RA	This study
WH-Rep2-Cap2RA-VP1	This study
WH-Rep2-Cap2RA-VP1-V4-RBD(1L)	This study
WH-Rep2-Cap2RA-VP1-V4-RBD(2L)	This study
WH-Rep2-Cap2RA-VP1-V5-RBD(1L)	This study
WH-Rep2-Cap2RA-VP1-V5-RBD(2L)	This study
WH-Rep2-Cap2RA-VP1-V8-RBD(1L)	This study
WH-Rep2-Cap2RA-VP1-V8-RBD(2L)	This study
WH-Rep2-Cap2RA-VP1-V4-RBM(1L)	This study
WH-Rep2-Cap2RA-VP1-V4-RBM(2L)	This study
WH-Rep2-Cap2RA-VP1-V5-RBM(1L)	This study
WH-Rep2-Cap2RA-VP1-V5-RBM(2L)	This study
WH-Rep2-Cap2RA-VP1-V8-RBM(1L)	This study
WH-Rep2-Cap2RA-VP1-V8-RBM(2L)	This study
WH-Rep2-CapRA-VP2KO	This study
pCMV.Cap2RA-VP2-RBD	This study
pCMV.Cap2RA-VP2-RBD(1L)	This study
pCMV.Cap2RA-VP2-RBM	This study
pCMV.Cap2RA-VP2-RBM(1L)	This study
WH-Rep2-Cap2RA-VP1-V8-RBMP1	This study
WH-Rep2-Cap2RA-VP1-V8-RBMP2	This study
WH-Rep2-Cap2RA-VP1-V8-RBMP3	This study
WH-Rep2-Cap2RA-VP1-V8-RBMP4	This study
WH-Rep2-Cap2RA-VP1-V8-RBMP5	This study

WH-Rep2-Cap2RA-VP1-V8-RBMP6	This study
WH-Rep2-Cap2RA-VP1-V8-RBMP7	This study
WH-Rep2-Cap2RA-VP1-V8-RBMP8	This study
WH-Rep2-Cap2RA-VP1-V8-RBMP9	This study
WH-Rep2-Cap2RA-VP1-V8-RBMP10	This study
WH-Rep2-Cap2RA-VP1-V8-RBMP11	This study

2.2.2.2 Cloning of AAV helper plasmids for 1st generation of GBM-targeting

To clone the AAV helper plasmids for double insertion, WH-Rep2-Cap9K449R_PHP.eB was used. Sequences for peptides were introduced directly in the forward primers by PCR. Amplicons and WH-Rep2-Cap9K449R_PHP.eB were digested by XbaI and SpeI and ligated. All PCR primers used in this section are listed in Table 19. All plasmids used or generated in this section are listed in Table 20.

Table 19. Primers used for cloning double-insertion AAV variants.

Name	Sequence
Cap_pA_rv	AACGAATCAACCGGTTTATTG
P1_fr	ATCTCTCTAGAACTATTAACGGTTCTGGACGCGGCGATCTGGGCCTGAGCCAGAATCAACAAAC
P2_fr	ATCTCTCTAGAACTATTAACGGTTCTGGATGCGATTGCCGCGGCGATTGCTTTTGCCAGAATCAACAAAC
P2.2_fr	ATCTCTCTAGAACTATTAACGGTTCTGGACCAGATTGCCGCGGCGATTGCTTTCCACAGAATCAACAAAC
P2.3_fr	ATCTCTCTAGAACTATTAACGGTTCTGGACCATGCGATTGCCGCGGCGATTGCTTTTGCCCACAGAATCAACAAAC
P2.4_fr	ATCTCTCTAGAACTATTAACGGTTCTGGAGCATGCGATTGCCGCGGCGATTGCTTTTGCGGACAGAATCAACAAAC
P2A_fr	ATCTCTCTAGAACTATTAACGGTTCTGGACCAGCAGATGCACGCGGCGATGCATTTGCACCACAGAATCAAC
P2.3A_fr	ATCTCTCTAGAACTATTAACGGTTCTGGACCAGCAGATGCACGCGGCGATGCATTTGCACCACAGAATCAACAAAC
LRGD_fr	ATCTCTCTAGAACTATTAACGGTTCTGGACCAGGACGCGGCGATTCACCACAGAATCAACAAAC

Table 20. Plasmids used or generated for producing AAV capsids for the 1st generation of the GBM-targeting project.

Name	Origin
WH-Rep2-Cap9wt	Eike Kienle
WH-Rep2-Cap9_P1	Eike Kienle
WH-Rep2-Cap9_P2	Eike Kienle
WH-Rep2-Cap9_P2.2	Laura Dietz
WH-Rep2-Cap9K449R_PHP.eB	Jonas Weinmann
WH-Rep2-Cap9K449R_PHP.eB-P1	This study
WH-Rep2-Cap9K449R_PHP.eB-P2	This study
WH-Rep2-Cap9K449R_PHP.eB-P2.2	This study
WH-Rep2-Cap9K449R_PHP.eB-P2.3	This study
WH-Rep2-Cap9K449R_PHP.eB-P2.4	This study
WH-Rep2-Cap9K449R_PHP.eB-P2A	This study
WH-Rep2-Cap9K449R_PHP.eB-P2.3A	This study
WH-Rep2-Cap9K449R_PHP.eB-LRGD	This study

2.2.2.3 Cloning of AAV helper plasmids for 2st generation of GBM-targeting

To clone the plasmids for expressing peptides inserted AAV9 VP, the AAV helper plasmid WH-Rep2-Cap9wt was used. BspEI (T^CCGGA) and BamHI (G^GATCC) restriction enzymes were chosen for peptide insertion, which introduce SG and GS flanking amino acids, respectively. Since the WH-Rep2-Cap9wt plasmid contains two BamHI sites in Rep2 (725-730) and Cap9 (1968-1973) ORF, the first step was to introduce silent mutations to eliminate these two sites by OE PCR. Besides, a silent mutation was also made to introduce an AflII (C^TTAAG) site in Cap9 position 1381-1386 between VR IV and VR VIII peptide insertion sites by OE PCR. Next, OE PCRs were performed to introduce the BamHI and BspEI restriction sites for peptide insertion and to generate two plasmids for peptide insertion, WH-Rep2-Cap9-V4ins and WH-Rep2-Cap9-V8ins. All PCR primers used in this section are listed in Table 21. Then sense and anti-sense oligonucleotides (Table 22) for GBM-targeting and BBB-penetrating peptides were annealed and ligated to the BamHI/BspEI-digested WH-Rep2-Cap9-V4ins and WH-Rep2-Cap9-V8ins. All plasmids used or generated in this section are listed in Table 23.

Table 21. Primers for OE PCR to introduce mutations.

Name	Sequence
Cap9_BsiWI_fr	AGCTCCCGTACGTGCTC
Cap_pA_rv	AACGAATCAACCGGTTTATTG

Cap9_AflIImut_fr2	AATCAACAAACGCTTAAGTTCAGTGTGG
Cap9_AflIImut_rv1	ACACTGAACTTAAGCGTTTGTTGATTCTG
Cap9_BamHImut_fr2	CCTGTACCTGCAGATCCTCCAAC
Cap9_BamHImut_rv1	TGGAGGATCTGCAGGTACAG
Rep2_NcoI_fr	GGTGAAATCCATGGTTTTGG
Rep2_HindIII_rv	CGTAGTTGATCGAAGCTTCC
Rep2_BamHImut_fr2	GCAGTGGATACAGGAGGACC
Rep2_BamHImut_rv1	GGTCCTCCTGTATCCACTGCTTC
Cap9_V4int_fr2	TCCGGAAGATCATGAGTAGTTGGATCCCAGAATCAACAA ACGCTTAAGTTC
Cap9_V4int_rv1	GGATCCAACTACTCATGATCTTCCGGAACCGTTAATAGT CTTTGAG
Cap9_V8int_fr2	TCCGGAAGATCATGAGTAGTTGGATCCGCACAGGCGCA GACC
Cap9_V8int_rv1	GGATCCAACTACTCATGATCTTCCGGATTGGGCACTCTG GTGG
CPP16_fr2	ACCGTGAGCGCGCTGAAAGCACAGGCGCAGACC
CPP16_rv1	TTTCAGCGCGCTCACGGTTTGGGCACTCTGGTGGTTTG
Cap9_W903A_rv1	AGCGAATTTGCTGCTCCTGGAGCTTCTTC
Cap9_W903A_fr2	AGAAGCTCCAGGAGCAGCAAATTCGCTG
Cap9_TT1sub_rv1	GGTGCTCCTGGCGCCCCTCTTGGCACTCTGGTGGTTTG TGG
Cap9_TT1sub_fr2	AAGAGGGGCGCCAGGAGCACCGCGCAGACCGGCTGGG TTC

Table 22. Oligonucleotides for GBM-targeting and BBB-penetrating peptides.

Name	Sequence
Cap9_AflIImut_fr2	AATCAACAAACGCTTAAGTTCAGTGTGG
Ang2_fr	GGAGGAGGTACCTTCTTCTACGGCGGCAGCAGGGGCAAGA GGAACAACTTCAAGACCGAGGAGTACGGAGGA
Ang2_rv	TCCTCCGTACTCCTCGGTCTTGAAGTTGTTCCTCTTGCCCCT GCTGCCGCCGTAGAAGAAGGTACCTCCTCC
Ang2(G)_fr	ACCTTCTTCTACGGCGGCAGCAGGGGCAAGAGGAACAACT TCAAGACCGAGGAGTAC
Ang2(G)_rv	GTACTCCTCGGTCTTGAAGTTGTTCCTCTTGCCCCTGCTGC CGCCGTAGAAGAAGGT
RAP12_fr	GAGGCCAAGATCGAGAAGCACAACCACTACCAGAAG
RAP12_rv	CTTCTGGTAGTGGTTGTGCTTCTCGATCTTGGCCTC
THR_fr	ACCCACAGGCCCCCCATGTGGAGCCCCGTGTGGCCC
THR_rv	GGGCCACACGGGGCTCCACATGGGGGGCCTGTGGGT

THR(G)_fr	GGAGGAGGAGGTACCCACAGGCCCCCCATGTGGAGCCCC GTGTGGCCCGGTGGAGGA
THR(G)_rv	TCCTCCACCGGGCCACACGGGGCTCCACATGGGGGGCCTG TGGGTACCTCCTCCTCC
T7_fr	CACGCCATCTACCCCAGGCAC
T7_rv	GTGCCTGGGGTAGATGGCGTG
CRT_fr	GCCAGGACCATCGGACCCAGCGTGGCC
CRT_rv	GGCCACGCTGGGTCCGATGGTCCTGGC
PB53_fr	CAGTTCGCCGCCCTGCCCGTGAGGGCCCACTACGGC
PB53_rv	GCCGTAGTGGGCCCTCACGGGCAGGGCGGCGAACTG
PB53(G)_fr	GGAGGAGGAGGTCAGTTCGCCGCCCTGCCCGTGAGGGCC CACTACGGTGGAGGA
PB53(G)_rv	TCCTCCACCGTAGTGGGCCCTCACGGGCAGGGCGGCGAAC TGACCTCCTCCTCC
TGN_fr	ACCGGCAACTACAAGGCCCTGCACCCCCACAACGGC
TGN_rv	GCCGTTGTGGGGGTGCAGGGCCTTGTAGTTGCCGGT
GE11_fr	TACCACTGGTACGGCTACACCCCCCAGAACGTGATC
GE11_rv	GATCACGTTCTGGGGGGTGTAGCCGTACCAGTGGTA
GE11(G)_fr	GGAGGAGGAGGTTACCACTGGTACGGCTACACCCCCCAGA ACGTGATCGGTGGAGGA
GE11(G)_rv	TCCTCCACCGATCACGTTCTGGGGGGTGTAGCCGTACCAGT GGTAACCTCCTCCTCC
FAL_fr	TTCGCCCTGGGCGAGGCC
FAL_rv	GGCCTCGCCCAGGGCGAA
LTV_fr	CTGACCGTGAGCCCCTGGTAC
LTV_rv	GTACCAGGGGCTCACGGTCAG
LTV(G)_fr	GGAGGAGGAGGTCTGACCGTGAGCCCCTGGTACGGTGGA GGA
LTV(G)_rv	TCCTCCACCGTACCAGGGGCTCACGGTCAGACCTCCTCCTC C
TT1_fr	GCCAAGAGGGGCGCCAGGAGCACCGCC
TT1_rv	GGCGGTGCTCCTGGCGCCCCTCTTGGC
TT1(G)_fr	GGAGGAGGAGGTGCCAAGAGGGGCGCCAGGAGCACCGCC GGTGGAGGA
TT1(G)_rv	TCCTCCACCGGCGGTGCTCCTGGCGCCCCTCTTGGCACCT CCTCCTCC
TT1(P)_fr	CCAGCCAAGAGGGGCGCCAGGAGCACCGCCCCA
TT1(P)_rv	TGGGGCGGTGCTCCTGGCGCCCCTCTTGGCTGG
Cend1_fr	AGGGGAGAGAGGCCACCCAGG
Cend1_rv	CCTGGGTGGCCTCTCTCCCCT
LRGD1_fr	AGAGGTGACAGCCCA

LRGD1_rv	TGGGCTGTCACCTCT
LRGD2_fr	CCAGGCAGAGGTGACAGCCCA
LRGD2_rv	TGGGCTGTCACCTCTGCCTGG
RTD_fr	CGCACTGATCTGGATAGCCTGCGCACT
RTD_rv	AGTGCGCAGGCTATCCAGATCAGTGCG
P1_fr	CGCGGCGATCTGGGCCTGAGC
P1_rv	GCTCAGGCCCAGATCGCCGCG

Table 23. Plasmids used or generated for producing peptide-modified AAV capsids for the 2st generation of the GBM-targeting project.

Name	Origin
WH-Rep2-Cap9wt	Eike Kienle
WH-Rep2-Cap9(W503A)	This study
WH-Rep2-Cap9_CPP16	This study
WH-Rep2-Cap9(noBamHI)	This study
WH-Rep2-Cap9_V4int	This study
WH-Rep2-Cap9_V8int	This study
WH-Rep2-Cap9_V4-Ang2	This study
WH-Rep2-Cap9_V8-Ang2	This study
WH-Rep2-Cap9_V4-Ang2(G)	This study
WH-Rep2-Cap9_V8-Ang2(G)	This study
WH-Rep2-Cap9_V8-RAP12	This study
WH-Rep2-Cap9_V4-THR	This study
WH-Rep2-Cap9_V8-THR	This study
WH-Rep2-Cap9_V4-THR(G)	This study
WH-Rep2-Cap9_V8-THR(G)	This study
WH-Rep2-Cap9_V8-T7	This study
WH-Rep2-Cap9_V8-CRT	This study
WH-Rep2-Cap9_V4-PB53	This study
WH-Rep2-Cap9_V8-PB53	This study
WH-Rep2-Cap9_V4-PB53(G)	This study
WH-Rep2-Cap9_V8-PB53(G)	This study
WH-Rep2-Cap9_V4-TGN	This study
WH-Rep2-Cap9_V8-TGN	This study
WH-Rep2-Cap9_V4-GE11	This study
WH-Rep2-Cap9_V8-GE11	This study
WH-Rep2-Cap9_V4-GE11(G)	This study
WH-Rep2-Cap9_V8-GE11(G)	This study

WH-Rep2-Cap9_V4-FAL	This study
WH-Rep2-Cap9_V8-FAL	This study
WH-Rep2-Cap9_V4-LTV	This study
WH-Rep2-Cap9_V8-LTV	This study
WH-Rep2-Cap9_V4-LTV(G)	This study
WH-Rep2-Cap9_V8-LTV(G)	This study
WH-Rep2-Cap9_V4-TT1	This study
WH-Rep2-Cap9_V8-TT1	This study
WH-Rep2-Cap9_V4-TT1(G)	This study
WH-Rep2-Cap9_V8-TT1(G)	This study
WH-Rep2-Cap9_V4-TT1(P)	This study
WH-Rep2-Cap9_V8-TT1(P)	This study
WH-Rep2-Cap9_V8-Cend1	This study
WH-Rep2-Cap9_V8-LRGD1	This study
WH-Rep2-Cap9_V8-LRGD2	This study
WH-Rep2-Cap9_V8-RTD	This study
WH-Rep2-Cap9_V8-P1	This study
WH-Rep2-Cap9_V8-TT1sub	This study
WH-Rep2-Cap9_TT1	This study

2.2.2.4 Cloning of AAV helper plasmids for chemically conjugated capsids

A cysteine residue was introduced to WH-Rep2-Cap9wt by OE PCR. All PCR primers used in this section are listed in Table 24. All plasmids used or generated in this section are listed in Table 25.

Table 24. Primers for OE PCR to introduce cysteine into the AAV9 helper plasmid.

Name	Sequence
Cap9_456cys_fr	GGTTCTGGATGTAATCAACAAACGCTTAAG
Cap9_456cys_rv	CGTTTGTTGATTACATCCAGAACCGTTAATAG
Cap9_588+1cys_fr	AGTGCCCAATGTGCACAGGCGCAG
Cap9_588+1cys_rv	GCCTGTGCACATTGGGCACTCTGG
Cap9_660cys_fr	CAGATCCTCCATGTGCCTTCAACAAGGAC
Cap9_660cys_rv	GTTGAAGGCACATGGAGGATCTGCAGG
Cap9_718cys_fr	GAATTTGCTGTTAATACTTGTGGTGTATATAGTGAACC
Cap9_718cys_rv	CACTATATACACCACAAGTATTAACAGCAAATTCAAC
Cap9_588+1TAG_fr	AGTGCCCAATAGGCACAGGCGCAG
AAV9_588+1TAG_rv	GCCTGTGCCTATTGGGCACTCTGG

Table 25. Plasmids used or generated for producing AAV capsids with introduced surface cysteine residue.

Name	Origin
WH-Rep2-Cap9wt	Eike Kienle
WH-Rep2-Cap9_456cys	This study
WH-Rep2-Cap9_588+1cys	This study
WH-Rep2-Cap9_660cys	This study
WH-Rep2-Cap9_718cys	This study
WH-Rep2-Cap9_588+1TAG	This study

2.2.3 Cell Culture

2.2.3.1 Cell maintenance

Cells were cultured in Dulbecco's Modified Eagle's Medium (DMEM) with GlutaMAX™, supplemented with 10% fetal bovine serum (FBS) and 100 U/mL penicillin-streptomycin at 37°C with 5% CO_2. For Huh7 cells, 1% 100X Modified Eagle's Medium Non-essential Amino Acid (MEM NEAA) was supplemented additionally. Cells were split 1:5 to 1:20 every 2-5 days. Cells were detached by adding 2.5% Trypsin-EDTA and incubating at 37°C for 1-10 min, and trypsinization was stopped by adding FBS-containing medium. Incubation time depended on cell types.

2.2.4 AAV Production, Purification and Titration

2.2.4.1 rAAV Production

rAAV vectors were produced by standard triple-transfection of HEK293T cells with (1) AAV vector plasmid, which contains ITR-flanked transgene cassette; (2) AAV helper plasmid, which encodes *rep* and *cap* genes; and (3) adenoviral helper plasmid (AdH), which expresses the adenoviral genes E2A, E4 and VA that are necessary for AAV replication; at a 1:1:1 molar ratio using PEI as transfection reagent. For mosaic rAAV vector production, two AAV helper plasmids encoding different *cap* genes were used at a 1:1 ratio (if not specified otherwise).

For large-scale rAAV vector production, 15 cm dishes were used. HEK293T cells were expanded in T175 flasks to obtain enough cells for seeding. Two days before transfection, 4×10^6 HEK293T cells in 22 ml complete medium per dish were seeded. The number of dishes depended on the yield and required amount of each vector. For transfection, a DNA mix of 44 µg plasmids in 790 µl H_2O and 790 µl 300 mM NaCl per dish, and a PEI mix of 352 µl PEI, 438 µl H_2O and 790 µl 300 mM NaCl per dish, were mixed together, vortexed thoroughly, incubated at RT for 10 min and added to the cells dropwise. Three days after transfection, cells were harvested with cell scrapers, resuspended in medium and centrifuged at 800 g for 15 min. After centrifugation, the supernatant was discarded and cell pellets were resuspended in Benzonase buffer. Cell pellets from 2-10 dishes were suspended in 5 ml Benzonase buffer and loaded onto small iodixanol gradients afterwards. In contrast, cell pellets from 10-40 dishes were suspended in 20 ml Benzonase buffer and purified with large iodixanol gradient afterwards. Cells were lysed via five freeze-thaw cycles in liquid nitrogen and in a 37 °C water-bath. 50 U/ml Benzonase was added to the lysate and incubated at 37 °C for one hour to remove non-encapsidated DNA. To get rid of the cell debris, the lysate was centrifuged at 4000 x g for 15 min, and the supernatant was collected and transferred to a new falcon. Centrifugation and supernatant collection were repeated 1-2 times to obtain a clear lysate for the following purification, i.e., iodixanol gradient centrifugation.

For small-scale AAV productions, 6-well and 12-well plates were used in which 5×10^5 and 2×10^5 HEK293T cells/well were seeded, respectively.

2.2.4.2 AAV Purification via Iodixanol Gradient

rAAV vectors from large-scale productions were purified via Iodixanol gradients. Small gradients were used for up to 10 dishes, and large gradients for 10-40 dishes. For small gradients, a Pasteur pipette was inserted into a 16x76 mm re-seal polyallomer centrifuge tube and the cell lysate from 2.2.4.1 (5 ml) was transferred into the tube through a Pasteur pipette, sequentially followed by 2 ml each of 15%, 25%, 40% and 60% iodixanol solution. Then, the Pasteur pipette was removed and the tube was carefully filled up with benzonase buffer using a syringe. Tubes were sealed with the Tube Sealer and balanced to each other. Balanced tubes were put in 70.1 Ti rotor and centrifuged in an OptimaTM L-90K ultracentrifuge at 50000 rpm and 4 °C for 2 h. After centrifugation, the tube was punctured at the top by a needle to release the pressure. Another needle puncture was made at the bottom to collect fractions. The lowest 1.5 ml fraction was discarded and the

following 1 ml that contained full capsids was collected. For the large gradient, 20 ml of cell lysate, 7 ml of 15%, 5 ml of 25%, 4 ml of 40% and 4ml of 60% iodixanol solutions were filled in 25x89 mm Quick-Seal centrifuge tubes. Balanced tubes were put in 70 Ti rotor and centrifuged at 50000 rpm and 4 °C for 2.5 h. After centrifugation, the lowest 3 ml fraction was discarded and the following 2 ml were collected. All the other steps were the same as for the small gradient. Purified and collected virus was aliquoted (if needed) and stored at -80°C or was subjected to buffer exchange.

2.2.4.3 Buffer Exchange (Dialysis)

For the AAVs that were used for mice injection or chemical modification afterwards, buffer exchange to the proper solution was performed with the Amicon Ultra-15 Centrifugal Filter Unit or Amicon Ultra-4 Centrifugal Filter Unit (MWCO 100,000). For most samples, viruses in 0.8-2 ml iodixanol were mixed with PBS to a total volume of 15 ml, transferred to an Amicon Ultra-15 Centrifugal Filter Unit and then centrifuged at 800-2000 x g until the volume was reduced to 1.5 ml. The sample was again filled to 15 ml and centrifuged to 1.5 ml. For the third time, the sample was filled to 15 ml, centrifuged to 400-600 µL and transferred to a 1.5 ml tube. For P2-displaying variants, PBS with 2 mM DTT was used to prevent formation of disulfide bonds. For variants used for chemical modification, PBS with 2 mM TCEP was used to prevent formation of disulfide bonds, and an Amicon Ultra-4 Centrifugal Filter Unit was used.

2.2.4.4 Titration by qPCR and ddPCR

Purified AAV vectors were quantified by measuring the number of virus genome via qPCR or ddPCR. For qPCR, alkaline lysis was performed first to disassemble viral capsids and release the genome. Therefore, the AAV sample was 1:10 diluted in nuclease-free H_2O. Then, 10 µl diluted sample was mixed with 10 µl TE buffer and 20 µl 2M NaOH, and incubated at 56 °C for 30 min. Afterwards, 38 µl 1M HCl was added to neutralize the reaction and 22 µl nuclease-free H_2O was added up to 100 µl, which caused a further 1:10 dilution. Next, 5 µl was taken and diluted in 45 µl nuclease-free H_2O resulting in a final 1:1000 dilution, which was used for the qPCR reaction. A standard curve was prepared by a serial 1:10 dilution with a reference plasmid. A probe-based qPCR reaction with 10 µl volume was prepared in triplicates as follows (35 µl in total): 17.5 µl 2x Sensimix II Probe mix, 1.4 µl forward primer (10 µM), 1.4 µl reverse primer (10 µM), 0.35 µl probe (10 µM), 9.35 µl nuclease-free H_2O, and 5 µl of sample, standard, or nuclease-free H_2O (negative

control). 10 µl of the mix was transferred to 4-strip tubes or 96-well plates in triplicate. The qPCR was run with the Corbett Rotor-Gene 6000 or StepOnePlus Real-Time PCR machine with the program listed in Table 26.

Table 26. Cycling program for AAV titration by qPCR.

Step	Temperature(°C)	Time	
Initial denaturation	95	10 min	
Denaturation	95	10 s	38 cycles
Annealing	58-60	20 s	

Based on the estimation of the scale of yield, vector samples were diluted 1:10^5 to 1:10^7. The reaction solution was prepared as follows (22 µl in total): 11 µl ddPCR Supermix for probes, 1.1 µl forward primer (18 µM), 1.1 µl reverse primer (18 µM), 1.1 µl probe (5 µM), 2.2 µl nuclease-free H_2O and 5.5 µl diluted sample. 20 µl of the mixture were used for droplet generation with the QX200 Droplet Generator. Droplets were transferred to a 96-well plate and the plate was sealed with pierceable foil with the PX1 PCR Plate Sealer. The ddPCR was run with the C1000 Touch Thermal Cycler with the program listed in Table 27. Capsids were disassembled in the initial denaturation step at 94 °C.

Table 27. Cycling program for AAV titration by ddPCR.

Step	Temperature(°C)	Time	
Initial denaturation	94	10 min	
Denaturation	94	30 s	40 cycles
Annealing	58	1 min	
Final Elongation	58	10 min	
Hold	12	infinite	

2.2.5 SDS-PAGE and Staining

2.2.5.1 Sodium dodecyl-sulfate polyacrylamide gel electrophoresis (SDS-PAGE)

SDS-PAGE was conducted for subsequent Silver staining or Western blotting to analyze the presence of the modified capsid proteins. Samples were purified viruses (from section 2.2.4.2, 2.2.4.3 and 2.2.4.5), unpurified viruses (from section 2.2.4.1), or viruses or capsid proteins from transfected cells. To prepare the samples from transfected cells, cells were resuspended in PBS, transferred to 1.5 ml tubes and centrifuged at 800 x g for 5 min. The

supernatant was discarded, and RIPA buffer was added to the cell pellet and incubated for 20 min on ice to lysate the cells. DNA was degraded by sonication.

7.5% or 4-15% mini-PROTEAN TGX Precast gels, or self-made 8% or 10% gels were used for SDS-PAGE. The Mini-PROTEAN Tetra Handcast System was used to prepare self-made gels. The recipes for the resolving gels and stacking gels are listed in Table 28. The gel was assembled in the Mini-PROTEAN Tetra Cell System filled with 1x Tris/Glycine/SDS (TGS) buffer. Samples were mixed with 4x Laemmli buffer (containing 10% β-ME) and incubated at 95 °C for 5 min. 10-15 µl of each prepared sample and 2-5 µl of PageRuler Plus Prestained Protein Ladder (10 to 250 kDa) was loaded. Electrophoresis was performed at 80 V for 10 min and then at 120 V for ~1.5 h.

Table 28. Components of SDS gels.

Resolving Gel (5 mL)	8%	10%	Staking Gel (2 mL)	
ddH2O	2.65 mL	2.15 mL	ddH2O	1.46 mL
Rotiphorese® Gel 40 (19:1)	1 mL	1.5 mL	Rotiphorese® Gel 40 (19:1)	0.25 mL
1.5 M Tris HCl (pH 8.8)	1.25 mL	1.25 mL	0.5 M Tris HCl (pH 6.8)	0.25 mL
10% SDS	50 µL	50 µL	10% SDS	20 µL
1% APS	50 µL	50 µL	1% APS	20 µL
TEMED	3 µL	3 µL	TEMED	2 µL

2.2.5.2 Silver Staining

After SDS-PAGE, silver staining was performed with the SilverQuest Silver Staining Kit following the manufacturer's instructions.

2.2.5.3 Western Blot

After SDS-PAGE electrophoresis, proteins were transferred to a nitrocellulose membrane using wet transfer with the Mini Trans-Blot Electrophoretic Transfer Cell system. The nitrocellulose membrane was soaked in transfer buffer for 10 min in advance. Sandwich was assembled in the following order: Three layers of Whatman paper, nitrocellulose membrane, gel, and finally again three layers of Whatman paper. Blotting was performed at 4°C, 120 mA/gel for 1.5 h.

After blotting, the membrane was taken out and blocked in blocking buffer (5% milk or BSA in TBS-T) for 1 h at RT. Primary antibodies were diluted in blocking buffer and incubated with the membrane at 4°C overnight. On the next day, the membrane was washed with TBS-T three times, incubated with horseradish peroxidase (HRP) -

conjugated secondary antibody for 1-2 h at RT, and again washed with TBS-T three times. For Biotin-detection, after blocking, the membrane was incubated in diluted HRP-conjugated streptavidin directly for 1 h at RT. The WesternBright Quantum Western blotting detection Kit or SignalFire Elite ECL Reagent Kit were used to visualize proteins. Signals were detected and imaged with the Azure 300 Visible Fluorescent imager.

2.2.6 Pull-down Assay

Binding between engineered AAV capsid and hACE2 was examined by pull-down assay. At first, the recombinant hACE2-Fc proteins were bound to Dynabeads Protein A magnetic beads following the manufacturer's handbook. In brief, 5 μg hACE2-Fc was diluted in 100 μl PBS, added to 150 μl of equilibrated beads in the 1.5 ml tube, mixed and incubated for 1 h at RT on the tube shaker. Then the sample tube was place to the magnetic stand for 10 s and the supernatant was removed. The beads were washed as following for three times: adding 500 μl PBS to the tube and mixing for 5 min, then placing the tube on the magnetic stand for 10 s and removing the PBS.

Then the pull-down assay was done by incubate the 5×10^8 vg AAV virions (diluted in 100 μl PBS) with hACE2-bound beads in 1.5 ml tube for 1 h at RT on the tube shaker. The sample was then washed as following for two times: adding 200 μl PBS to the tube and mixing for 5 min, then placing the tube on the magnetic stand for 10 s and removing the PBS. Then the protein was eluted as following: adding 30 μl elution buffer [50mM glycine-HCl (pH 2.8)] to the beads and mixing for 5 min at RT, placing the tube on the magnetic stand for 10 s, removing and transferring the eluted sample to a new tube containing 6 μl of neutralization buffer [1M Tris buffer (pH 7.5)]. The eluted samples were then applied for western blot to test the present of AAV VPs.

2.2.7 Electron Microscopy

Electron microscopy (EM) allows a direct visualization of the viral particles. Purified dialyzed rAAV vectors (in PBS) were placed on a 200-mesh Formvar/Carbon grid by inversion of the grid on a 20 μl drop of virus. The grid was then washed two times by inversion on a 20 μl drop of ddH_2O followed by inversion of the grid onto a 20 μl drop of 2% uranyl acetate for 30 seconds. The grids were dried by gently touching the edges of

the grids to a Whatman paper. Then the vectors fixed on the grid were visualized using a JEM1400 electron microscope.

2.2.8 *In vitro* Transduction

2.2.8.1 Transduction

One day before transduction, cells were seeded in 96-well plates in 100 µl medium per well. For transduction, 50 µl of medium was removed from each well, then eYFP-expressing AAV vectors were diluted in 50 µl of fresh medium and added to the well. Three days after transduction, fluorescent microscopy and/or flow cytometry were conducted to measure the eYFP signal.

2.2.8.2 Fluorescent Microscopy

An automated imaging procedure was used for imaging of living cells in 96-well plates. Hoechst (10mg/ml) was diluted 1:10 000 in medium and added to cells, incubated for 1 h, and removed. Then, the cells were washed one time in PBS. Measurement was performed using an Olympus microscopy CKX41 and analysis was done by ImageJ.

2.2.8.3 Flow Cytometry

To prepare suspensions of single cells for flow cytometry, medium was removed, and then cells were washed with PBS and treated with 30 µl of 0.25% Trypsin/EDTA per well at 37 °C for 5-15 min until they were fully detached to single cells. 120 µl of 1% BSA/PBS per well was added to inactivate the trypsin. The cell suspension was transferred to a V-Bottom 96-well plate and pipetted up and down several times. Flow cytometry was performed with the FACS Celesta with the 96-well plate HTS loader, and data was analyzed with FlowJo_V10.

2.2.9 Animal Experiments

Animal experiments for the BBB-penetrating and GBM-targeting projects were perfoemed by Khwab Sanghiv and colleagues (German Cancer Research Center, Heidelberg). GBM, GBM peripheral tissue, healthy brain hemisphere, spinal cord, liver, quadriceps, heart,

kidney, spleen, thymus and lung were harvested. Tissue was cut into small pieces and immersed in RNAlater solution at 4 °C for one day, and then stored at -20 °C.

2.2.10 Sample Preparation for NGS

2.2.10.1 DNA and RNA Extraction

The Allprep DNA/RNA mini kit was used to extract DNA and RNA from most of the mouse tissues. A small piece of tissue (about 10-30 mg) was taken from the RNAlater solution, sliced, and transferred to a 2 ml tube containing a stainless-steel bead (two beads for muscle and heart) and 600 µl Buffer RLT Plus with 1% β-ME. Tubes were placed in a TissueLyser LT and homogenization was performed with 45000 rpm for 90 s. 20 µl Proteinase K was added and incubated at 56°C for 30 min. Then, the tubes were centrifuged at 18000 g for 5 min. The supernatants were transferred to Allprep DNA spin columns and extraction of DNA and RNA was performed following the manufacturer's handbook. In the process of RNA purification, instead of washing with 700 µl RW1, 2 wash stept with 350 µl RW1 each were used and an additional step of an on-column DNase digest (see 2.2.8.2) was performed in between.

For the tissues (muscle and heart tissues in the 1st generation of selection) that failed to yield enough DNA or RNA with the Allprep DNA/RNA mini kit, the DNeasy blood & tissue mini kit and RNeasy mini kit were used instead to extract DNA and RNA separately. The sliced tissue was separated into two tubes: one contained two stainless-steel beads and 180 µl Buffer ATL for DNA purification,while the other contained two stainless-steel beads and 600 µl Buffer RLT with 1% β-ME for RNA purification. Homogenization was performed as above and the purification was performed following the manufacturers' handbooks. For the RNA purification, the on-column DNase digest was also performed as above.

Both DNA and RNA were eluted with nuclease-free H_2O, and their concentrations were measured with the Nanodrop 2000. DNA and RNA were stored at -20 °C and -80 °C, respectively.

2.2.10.2 DNase On-column Digest

An RNase-free DNase set was used. One vial of DNase was dissolved in 550 µl RNase-free H_2O as stock solution. For each column, 10 µl DNase and 70 µl RDD buffer was mixed, added and incubated at RT for 15 min.

2.2.10.3 cDNA synthesis

Either the High-Capacity cDNA Reverse Transcription Kit (1st generation of selection) or the SuperScript™ IV VILO™ Master-Mix Kit with ezDNase (2nd generation of selection) was used for cDNA synthesis from RNA. When using the High-Capacity cDNA Revese Transcription Kit, remaining DNA was further removed by the Qiagen RNase-free DNase Set. 450 ng RNA was mixed with 1 µl DNase, 3 µl RDD buffer, and filled up to 30 µl with H_2O, incubated at RT for 40 min and then inactivated at 40 °C for 10 min. Then, 20 µl (equal to 300 ng) DNase-treated RNA was mixed with 4 µl 10x RT buffer, 1.6 µl 25x dNTP mix, 1.6 µl Random Primers, 0.8 µl 100 µM Oligo dT (not provided by the kit, ordered separately from ThermoFisher), 2 µl MultiScribe Reverse Transcriptase and 10 µl H_2O. The cDNA synthesis reaction was performed in a PCR cycler with the program: primer annealing at 25 °C for 10 min, synthesis at 37 °C for 120 min, inactivation at 85 °C for 5 min and hold at 4 °C. When using the SuperScript™ IV VILO™ Master-Mix Kit with the ezDNase kit, remaining DNA was removed by ezDNase from the kit. 320 ng RNA was diluted to 8 µl with H_2O, mixed with 1 µl ezBuffer and 1 µl ezDNase, and incubated at 37 °C for 5 min. 5 µl (equal to 60 ng) ezDNase-treated RNA was mixed with 2 µl RT master mix and 3 µl H_2O. For the no-RT control, 2.5 µl ezDNase-treated RNA was mixed with 1 µl RT master mix and 1.5 µl H_2O. The cDNA synthesis reaction was performed in a PCR cycler with the program: primer annealing at 25 °C for 10 min, synthesis at 50 °C for 10 min, inactivation at 85 °C for 5 min and hold at 4 °C. Synthesized cDNA was stored at -80 °C.

2.2.10.4 Library Preparation for NGS

The Nextera XT Index Kit v2 was used to prepare the samples for Illumina NextSeq 2000 sequencing. Samples were prepared with two PCR steps. In the 1st PCR, the barcode region was amplified with R1 and R2 primers. 150 ng gDNA or 30 ng cDNA was mixed with 12.5 µl 2x Q5 HotStart MasterMix, 1.25 µl 10 mM R1 primer, 1.25 µl 10 mM R2 primer, and filled up to a 25 µl reaction volume with H_2O. The PCR was performed in a

thermocycler with the program listed in Table 28. Proper amplification was confirmed with agarose gel electrophoresis. The PCR products were purified with the ProNex Size-Selective Purification System following the manufacturer's handbook. 22 µl of each sample was mixed with 1.5x volume (33 µl) of ProNex Chemistry and transferred to V-bottom 96-well plates at the beginning, and was eluted in 25 µl elution buffer in the end and transferred into a 96-well PCR plate. Concentration was measured with a Qubit 2.0 Fluorometer and the dsDNA HS Assay kit.

In the 2nd PCR, purified DNA from the 1st PCR was diluted to 2 ng/µl. 4 µl diluted DNA, 4 µl Nextera XT Index Primer 1, 4 µl Nextera XT Index Primer 2, 20 µl 2x KAPA HiFi HotStart Ready Mix and 8 µl nuclease-free H_2O were mixed. The PCR was performed in a thermocycler with the program listed in the Table 29. PCR products were analyzed with a Bioanalyzer and a Qubit. After obtaining all the samples, they were mixed in equal amounts. The final mixture was analyzed with a Bioanalyzer and a Qubit before submission. Sequencing was performed by the EMBL Genomics Core facility (NextSeq).

Table 29. 1st PCR.

Step	Temperature(°C)	Time	
Initial denaturation	98	5 min	
Denaturation	98	15 s	35 cycles
Annealing	64	15 s	
Elongation	72	15 s	
Final Elongation	72	5 min	
Hold	4	infinite	

Table 30. 2nd PCR (Index PCR).

Step	Temperature(°C)	Time	
Initial denaturation	95	5 min	
Denaturation	95	30 s	8 cycles
Annealing	55	30 s	
Elongation	72	30 s	
Final Elongation	72	5 min	
Hold	4	infinite	

2.2.10.5 Quantification of vector genome / diploid genome and eYFP expression by ddPCR

To quantify the numbers of vector genomes per diploid genome (vg/dg) and viral gene expression per host housekeeper gene expression, ddPCR was performed. In the gDNA reaction, HindIII was used to digest the genomic DNA into small fragments.

In the 1st round of selection, vg/dg was measured with eGFP_fr, eGFP_rv and *ddPCR™ Copy Number Assay: Rpp30, Mouse, Mus musculus* from Bio-Rad. 11 µl ddPCR Supermix for Probes (no dUTP), 1.1 µl HindIII / Diluent B mixture (1 HindIII diluted in 3 Diluent B), 1.1 µl 20x RPP30 primers / probe mixture, 0.055 µl 100 µM eGFP probe, 0.2 µl 100 µM eGFP_fr primer, 0.2 µl 100 µM eGFP_rv primer, 2.2 µl 2ng/ µl DNA were mixed and the volume was filled up to µl 22 with H_2O. In the 2nd round of selection, human RPP30 primers and probe were used for GBM tissues from U87-transplanted mice, and mouse RPP30 primers and probe were used for the other tissues.

2.2.11 NGS Data Analysis and Normalization

The NGS results acquired from section 2.2.9.3 were analyzed with two custom Python scripts (as described in the thesis of Jonas Weinmann from our lab and by Rapti *et al.*[220]). In brief, the first script extracts the 15 nt barcode sequences by searching for the defined flanking sequences and then creates a list of the read counts of each barcode that has been assigned to the corresponding variant. The second script performs multistep normalization and calculation of the read counts: (1) Calculate the read counts for each barcode/variant α to the total read counts of each tissue β sample to obtain proportion ($P_{\alpha\beta}$); (2) Normalize $P_{\alpha\beta}$ to the proportion of each variant in the input library (L_α) to obtain normalized proportion $V_{\alpha\beta} = (P_{\alpha\beta}/L_\alpha) / \sum_\alpha (P_{\alpha\beta}/L_\alpha)$, which represents the relative efficiency of each variant in the tissue; (3) Calculate vg/dg of each variant in each sample $A_{\alpha\beta} = P_{\alpha\beta} * G_\beta$ (G_β is vg/dg measured by ddPCR in section 2.2.9.4); (4) Calculate $T_{\alpha\beta} = A_{\alpha\beta} / \sum_\beta A_{\alpha\beta}$, which represents the specificity of each variant across all analyzed tissues; and finally (5) Calculate $B_{\alpha\beta} = P_{\alpha\beta}/L_\alpha * G_\beta$, which are used to generate a heat map comparing the transduction of all variants in all tissues.

2.2.12 Statistical analysis

Statistical analysis and plotting were conducted with the GraphPad Prism 8.0 software. Analysis method was indicated under each figure. Statistical significance is indicated with “ns”, non significant; “ * ”, $p < 0.05$; “ ** ”, $p < 0.01$; “ *** “, $p < 0.001$; and “ **** “, $p < 0.0001$.

3 Results

In this study, I aimed to design AAV vectors to transduce target cells by binding to cell-specific receptors. More specifically, I worked on two major projects: (1) targeting to hACE2-expressing cells (section 3.1); (2) penetration of the BBB and targeting to GBM (section 3.2). To achieve these goals, I displayed the known receptor-binding ligands (peptides and proteins) on AAV capsids. I used three different methods: genetic insertion to the AAV capsid protein (VP), chemical/covalent conjugation to the assembled AAV capsid, and non-covalent binding to the assembled AAV capsid. Furthermore, I adjusted the number of ligands displayed on the AAV capsid by producing mosaic particles composed of wild-type and ligand-displaying VP. Thirdly, I displayed two ligands on the same capsid by producing mosaic capsids of two different ligand-displaying VPs.

3.1 Development of hACE2-targeting AAV Vectors

Immediately at the onset of the Covid-19 pandemic caused by SARS-CoV-2, world-wide research efforts focused on the development of means to treat or prevent SARS-CoV-2 infection. Our group has established an AAV- and RNAi-based method to suppress SARS-CoV-2 gene expression as an effective and direct antiviral strategy[194]. Meanwhile, to specifically transduce the cells that are susceptible to SARS-CoV-2 infection, I aimed to develop AAV vectors possessing the same tropism as SARS-CoV-2. To infect cells, SARS-CoV-2 binds its entry receptor hACE2 on the cell membrane via the RBD on the spike protein (Figure 5, PDB ID: 6M0J). Therefore, I tried to re-target AAV2 to hACE2-expressing cells by displaying RBD or the receptor-binding motif (RBM) of SARS-CoV2 on the AAV capsid.

3.1.1 Genetic fusion

The AAV capsid protein is widely engineered by inserting peptides to VR-VIII and VR-IV, which are the most protrusing parts of the capsid. Even though the inserts are usually short peptides, F. Koch-Nolte's group has previously successfully inserted 110-130 aa residues of nanobodies (nb) to VR-IV of AAV2, AAV8, AAV9 and AAV1P5[115]. Considering that the size of a nb would hamper insertion into all 60 VPs, it was only inserted to VP1.

As a result, 1-5 copies of nb were displayed on each capsid. The nb-displaying AAV vectors specifically transduced the cells expressing the receptor of the nb. This study inspired me to insert the RBD (194 aa in length) or RBM (69 aa in length) of SARS-CoV2 (Figure 5A) into VP1 of AAV2.

At first, I used the same strategy as the nanobody insertion. The VP1-nb expressing plasmid pAAV2RA.VP1-nb was kindly offered by Koch-Nolte's group. In this plasmid, the major splice acceptor SA_M for VP2/VP3 mRNA is mutated so that only VP1 can be expressed. Moreover, residues R585 and R588 are mutated to alanine to impede binding with heparan sulfate proteoglycan (HSPG) (In the following, RA refers to R585A/RB588A mutations). Finally, at VR-IV, seven amino acid residues (453-459) are deleted and the nb-encoding oligonucleotide is inserted between restriction sites NgoMIV (G^CCGGC) and KasI (G^GCGCC). I cloned VP1-RBD and VP1-RBM expressing plasmids pAAV2^{RA}-VP1-RBD and pAAV2^{RA}-VP1-RBM, respectively. Akin to the nb insertion, to increase the feasibility and flexibility of insertion, RBM and RBD were flanked with flexible peptide linkers GGGGS. During virus production, VP2 and VP3 were supplied *in trans* by plasmids WH-Rep2-Cap2RA-VP2/3 or WH-Rep2-Cap2RA-VP1stop (Figure 5B). Both plasmids only express VP2 and VP3, but in plasmid WH-Rep2-Cap2RA-VP2/3, the start codon AUG of VP1 is mutated to AAG. In contrast, in plasmid WH-Rep2-Cap2RA-VP1stop, a stop codon is introduced in VP1u (between the start codons of VP1 and VP2).

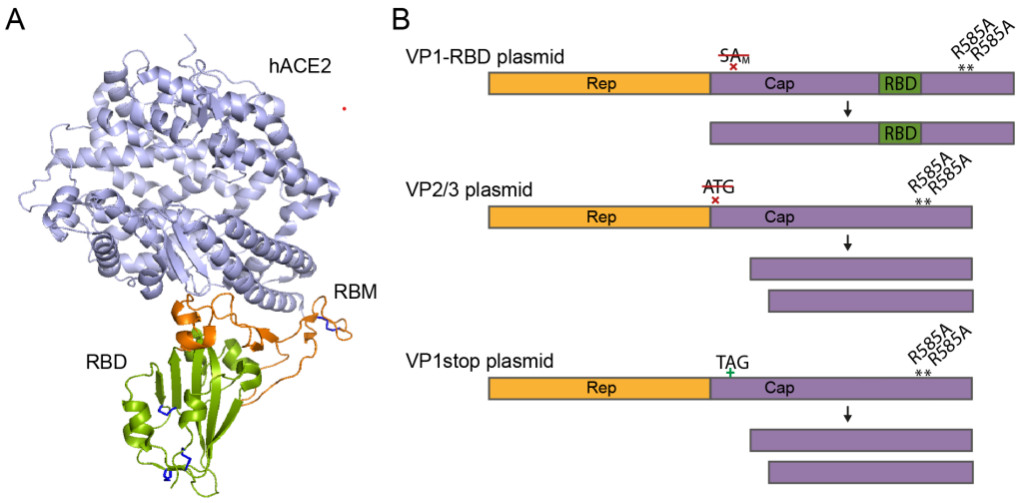

Figure 5. Design and production of RBD- and RBM-displaying AAV capsids.
(**A**) Structure of the interaction between SARS-CoV-2 RBD and hACE2 (PDB ID: 6M0J). hACE2 is shown in light blue, SARS-CoV-2 RBD is shown in green, and RBM is shown in orange. Four pairs

of disulfide bonds in RBD are shown as sticks in blue. (**B**) Expression of VP1-RBD, VP2 and VP3. ×~~SA_M~~ indicates the mutation of SA_M for the VP2/3 transcript. ×~~ATG~~ indicates the mutation of the start codon of VP1, +TAG indicates the introduction of a stop codon.

I investigated the expression of VPs from each plasmid by co-transfection with an adenoviral helper plasmid (pAdH) in HEK293T cells, followed by Western blotting of cell lysates. A mixture of B1 antibody (binding the C terminus of all VPs) and A1 antibody (binding the N terminus of VP1) was used to detect all VPs and boost the signal of VP1. This revealed that the VP1-nb as positive control was expressed, while the expression of VP1-RBM and VP1-RBD was significantly lower than VP1-nb (Figure 6A).

Next, to investigate whether VP1-RBM and VP1-RBD can be assembled into a capsid, I produced RBD-displaying and RBM-displaying rAAV vectors by co-transfection of pAdH, a self-complementary scAAV vector plasmid containing a CMV promoter-driven eYFP reporter, pAAV2^{RA}.VP1-RBD or pAAV2^{RA}.VP1-RBM plasmid, and Rep2-Cap2RA-VP2/3 or WH-Rep2-Cap2RA-VP1stop at a 1:1:1:1 or 1:1:3:1 ratio. I used the 1:1:3:1 ratio to examine whether higher plasmid amounts can compensate for the low expression of VP1-RBM and VP1-RBD. At the same time, I also produced AAV2^{RA} and AAV2^{RA}-VP1-nb as controls. I performed Western blots of cell lysates (Figure 6B, left) and samples after iodixanol gradient purification (Figure 6B, right) again using a mixture of B1 and A1 antibodies. VP1-nb was detected in samples of purified virus, indicating it was incorporated into the assembled capsids, even though the amount was much lower than VP1 in the AAV2^{RA} control. Yields of nb-displaying vectors from the 1:1:3:1 ratio and using Rep2-Cap2RA-VP1stop as AAV helper plasmid were low and below the detection limit of the Western blot. Unlike VP1-nb, VP1-RBD was undetectable in purified virus, and VP1-RBM was found at an extremely low level, indicating they were barely assembled into capsids. Using higher amounts of VP1-RBM- or VP1-RBD-expressing plasmids did not improve their incorporation either. The cell lysate samples indicated the expression of VPs during virus production. VP1-nb was overexpressed compared with VP1 in the standard production of AAV2^{RA}, but expression levels of VP1-RBM and VP1-RBD were low.

To figure out why VP1-RBD and VP1-RBM were not expressed and assembled well, I measured mRNA levels by qPCR. The results showed that VP1-RBD and VP1-RBM mRNAs were transcribed at a scale comparable to AAV2^{RA} and VP1-nb (Figure 6C). Thus, I hypothesized that VP1-RBD and VP1-RBM were misfolded and degraded by the proteasome. To verify this, I transfected HEK293T cells with VP1-RBD and VP1-RBM

plasmids and supplied the proteasome inhibitor Bortezomib (BZM) to the medium. Western blotting of cell lysate samples showed that the expression of VP1-RBD and VP1-RBM was enhanced in the presence of BZM (Figure 6D). However, supplementing BZM during production of AAV2^{RA}-VP1-RBD and AAV2^{RA}-VP1-RBM vectors did not facilitate the incorporation of VP1-RBD or VP1-RBM in the assembled capsids (Figure 6E).

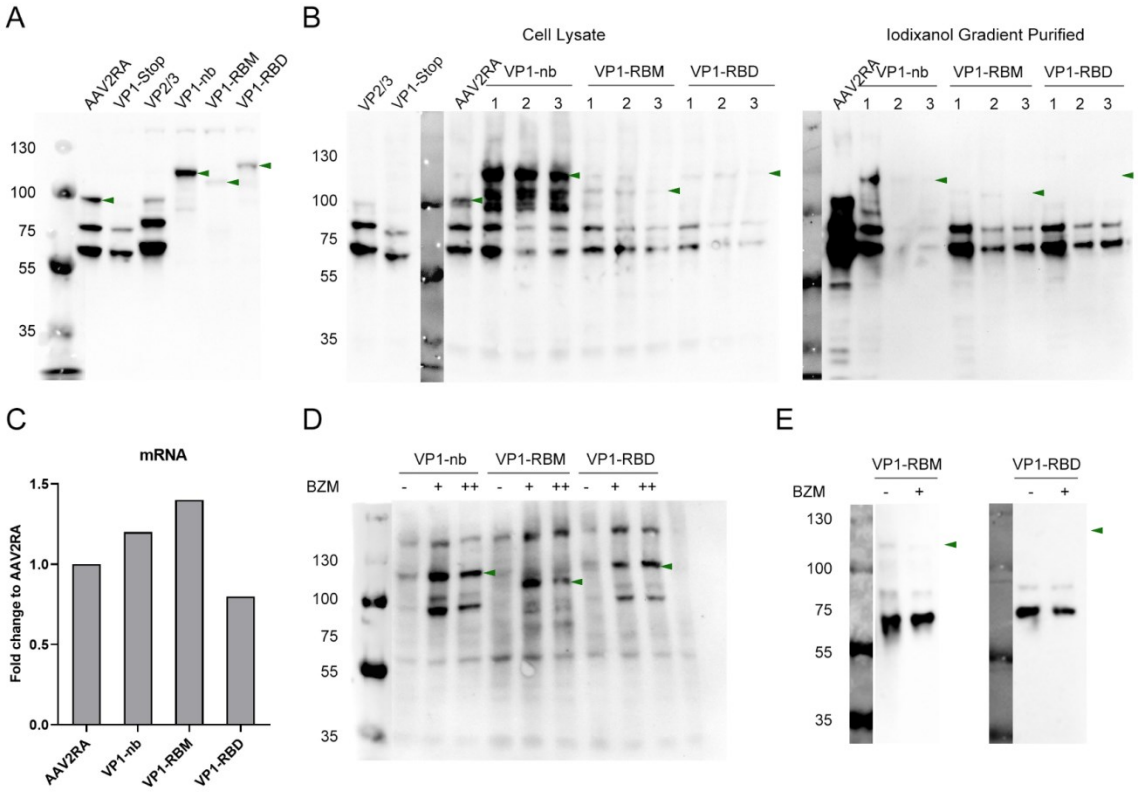

Figure 6. Expression and assembly of VP1-RBD and VP1-RBM.
(**A**) Expression of VPs from each plasmid by co-transfection with a pAdH in HEK293T cells. (**B**) Expression (left, cell lysates) and assembly (right, iodixanol gradient purified samples) of VP1-nb, VP1-RBM and VP1-RBD during vector production. A mixture of B1 and A1 antibodies was used for Western blotting. Three different combinations of plasmids were used for production: (1) Co-transfection of pscAAV-CMV-EYFP-BGHpolyA: AdH: pAAV2RA.VP1-nb, or of pAAV2RA.VP1-RBM or pAAV2RA.VP1-RBD: Rep2-Cap2RA-VP2/3 at a 1:1:1:1 ratio; (2) same plasmids as in (1) at a 1:1:3:1 ratio; (3) Rep2-Cap2RA-VP2/3 was replaced by WH-Rep2-Cap2RA-VP1stop. (**C**) Transcription of *cap* mRNA from each plasmid. mRNA levels were measured by qPCR. (**D**) Expression of VP1-nb, VP1-RBM and VP1-RBD in the presence of the proteasome inhibitor Bortezomib (BZM) at low (+) or high (++) concentrations. The B1 antibody was used for the Western blot. (**E**) Assembly of VP1-RBM and VP1-RBD with BZM supplemented during virus production. A mixture of B1 and A1 antibodies was used for the Western blot. In all the western blotting figures, green arrows indicate the expected positions of VP1 variants.

Next, I attempted to improve the expression and assembly of RBD- or RBM-fused VP by using different insertion sites. Based on previous studies of peptide or protein insertion and structure analysis of VP, I chose VR-IV (V4), VR-V (V5) and VR-VIII (V8) for insertion (Figure 7A), which form the protrusions surrounding the three-fold axis. I cloned VP1 backbone plasmids for each position containing BspEI (T^CCGG^A) and BamHI (G^GATC^C) restriction sites for insertion of RBM- or RBD-encoding DNA sequences. Additionally, GGGGS and longer [GGGGS]×2 linkers were used. I produced and purified vectors as described before. However, the results were still similar as before in that the expression of all RBD- or RBM-modified VP1 variants was low (data not shown). Also, none of the RBD-modified VP1 variants assembled into capsids, and only small amounts of RBM-modified VP1 were found in assembled capsids (Figure 7B).

Another site that I explored subsequently was the N terminus of VP2. Commonly, the principle of fusion of two proteins is to fuse the C terminus of one protein to the N terminus of another protein, because fusing one protein into the center of another protein will likely lead to misfolding. However, the N and C termini of AAV VP are hidden inside the capsid (Figure 2). Therefore, in most prior cases, only short peptides were inserted at VR-IV or VR-IIIV of VP. Interestingly, Münch *et al*. fused a DARPin to the N terminus of VP2, and it was then exposed on the surface of the assembled capsid[114]. Therefore, I used the same strategy to fuse RBD and RBM to the VP2 N-terminus, with or without flanking GGGGS linkers. The fusion protein was cloned into a CMV promoter-driven *cap* expression plasmid. For the expression of VP1 and VP3, I mutated the VP2 start codon in the AAV2^{RA} helper plasmid (Figure 7C). Because the size of VP2-RBM is similar to VP1, expression and assembly of VP2-RBM and VP2-RBM were detected with an anti-RBD antibody. This showed that VP2-RBM and VP2-RBM(1L) (which contained GGGGS linkers) were expressed and assembled into capsids, while VP2-RBD and VP2-RBM were degraded (Figure 7D).

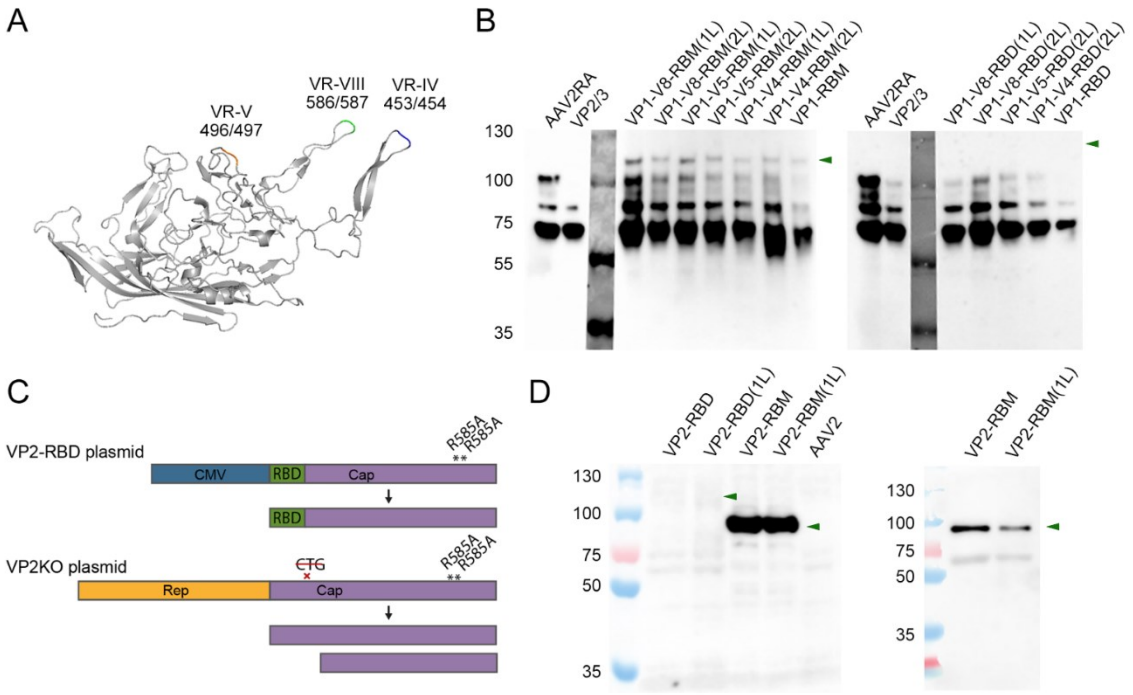

Figure 7. Design and assembly of new constructs with RBD- and RBM-modified VP.
(**A**) Position of three new insertion sites for RBM and RBD display. (**B**) Assembly of new constructs of RBM- or RBD-modified VP1. V4 indicates the VR-IV insertion site, V5 indicates the VR-V insertion site, and V8 indicates the VR-VIII insertion site. 1L indicates the GGGGS linker and 2L indicates the [GGGGS]×2 linker. Green arrows indicate the expected positions of RBM- or RBD-modified VP1 variants. (**C**) Design and production of RBD- and RBM-fused VP2. ×~~CTG~~ indicates the mutation of the VP2 start codon. (**D**) Expression and assembly of VP2-RBM and VP2-RBD. Left: Cell lysates from transfection of VP2-expressing plasmids. Right: Purified VP2-RBM and VP2-RBM(1L) assembled viruses. An anti-RBD antibody was used for Western blotting. Green arrows indicate the expected positions of RBM- and RBD-modified VP2 variants.

Because the insertion of RBD or RBM resulted in degradation, next, I investigated if short peptides derived from RBM can fulfill the binding to hACE2. I selected 11 short peptides RBMP1 – RBMP11 within RBM (Figure 8A) based on the key residues interacting with hACE2 and inserted them into VR-VIII of VP1. I used the same backbone plasmid for VR-VIII insertion as before. Western blotting of purified vectors showed that peptide-modified VP can be expressed and assembled into capsids as expected (Figure 8B).

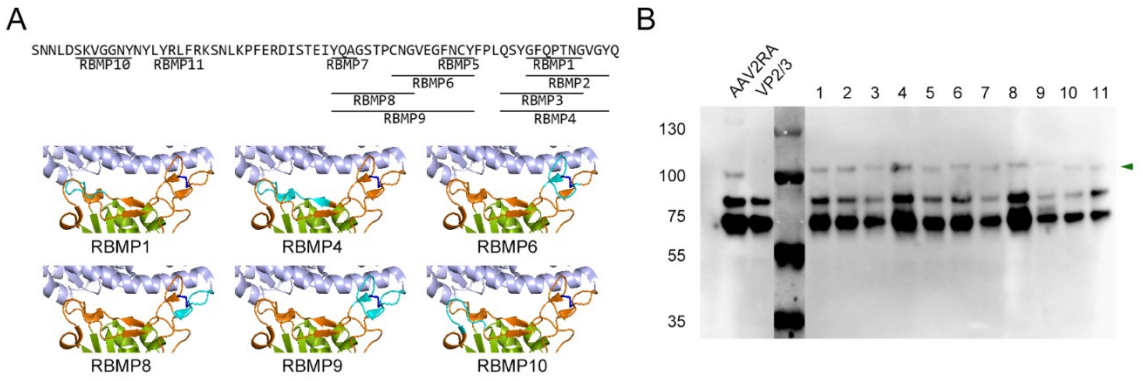

Figure 8. Design and assembly of RBMP-modified VP1.
(A) Top: Sequence and position of RBMP1-RBMP11. Bottom: Structure of the interactions between RBMPs and hACE2 (PDB ID: 6M0J). hACE2 is shown in light blue, SARS-CoV-2 RBD is shown in green, RBM is shown in orange, and RBMP is shown in cyan. (**B**) Expression and assembly of VP1-RBMPs. Western blot of purified and assembled VP1-RBMP viruses. The B1 antibody was used as primary antibody. Green arrows indicate the expected positions of RBMPs-modified VP1 variants.

Next, I investigated whether any of these AAV vectors were able to specifically transduce hACE2-expressing cells. All the vectors packaged a scAAV genome comprising a CMV promoter-driven eYFP. Vectors were used to transduce wild-type or hACE2-expressing Huh7 cells at a MOI of 5×10^4 vg/cell. Three days later, transduction efficiency was evaluated by measurements of YFP signal with a fluorescence microscope. However, none of the vectors was able to transduce hACE2-expressing cells (Figure 9). Next, I investigated whether the failure of transduction was because these vectors were not able to bind to hACE2. To this end, I performed a pull-down assay to examine the binding between hACE2 and AAV capsids. Because only RBM-modified or RBMP-modified VP were assembled into AAV capsids, RBD-modified variants were not investigated with this binding assay. Magnetic Protein A beads were incubated with hACE2-Fc for 1 h at RT and washed with PBS to remove unbound hACE2. Then, the hACE2-loaded beads were incubated with purified AAV vectors or samples from cell lysates for 1 h at RT and subsequently washed with PBS to remove unbound AAV vectors or proteins. hACE2-bound components were eluted, subjected to Western blotting and detected by incubation with B1 antibody. However, none of the RBM or RBMP-modified variants were bound to hACE2, and only truncated VP2-RBMs from cell lysates were bound to hACE2 (Figure 10).

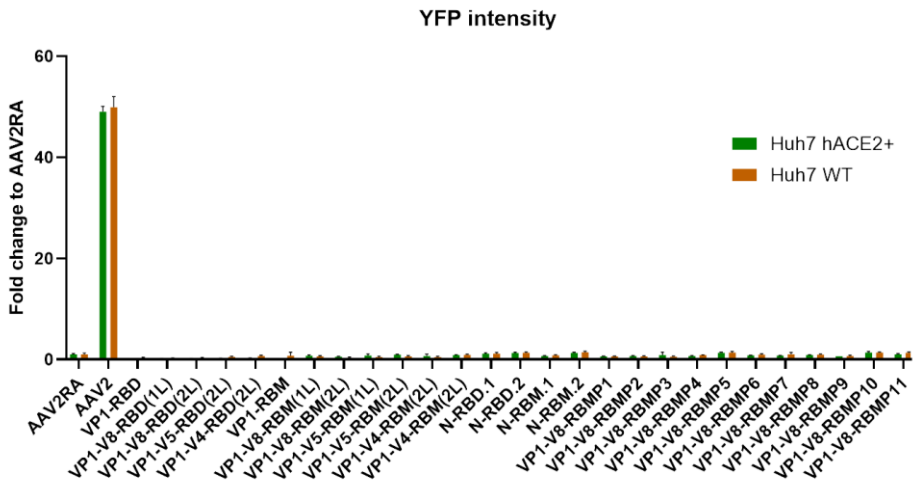

Figure 9. Transduction of RBD-, RBM- or RBMP-displaying AAVs.
eYFP-expressing AAV vectors were used to transduce wild-type or hACE2-expressing Huh7 cells at a MOI of 5×10^4 vg/cell. Three days after transduction, YFP signals were measured with fluorescence microscopy and analyzed with ImageJ. Data represent the mean ± s.d. of *n* = 3 replicates.

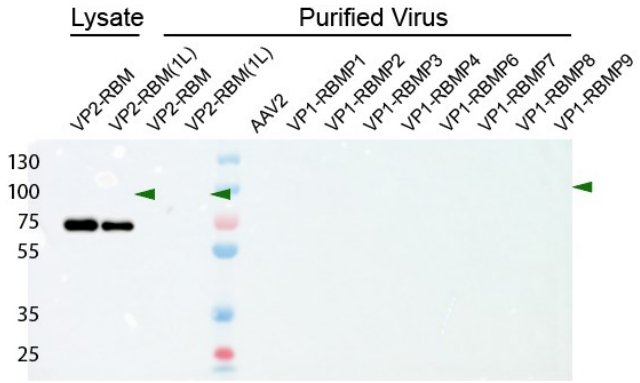

Figure 10. hACE binding of RBM- and RBMP-modified AAVs.
hACE2 pull-down assay were conducted to investigate hACE2 binding affinity of RBM and RBMP-modified AAV vectors. Green arrows indicate the expected positions of RBMPs-modified VP1 variants.

In summary, all of RBD-modified VPs were degraded and were not able to assemble into capsids. In contrast, RBM- and RBMP-modified VPs were able to assemble into capsids. However, the RBM- and RBMP- displaying vectors failed to transduce hACE2-expressing cells and to bind the hACE2 receptor. Later, I realized that the different expression and folding processes between the S-protein of SARS-CoV2 and VP of AAV impeded the

folding of fusion proteins. The S-protein of SARS-CoV2 is synthesized in the endoplasmic reticulum (ER), where chaperones and the oxidative environment facilitate the folding and formation of disulfide bonds. Within the RBD region, four pairs of disulfide bonds form, which are required for binding with hACE2. However, RBD-modified VP1s were synthesized in the cytosol, where disulfide bonds of RBD did not form due to the reducing environment and lack of chaperones. Therefore, an alternative method is required to display RBD on the AAV capsid.

3.1.2 Non-covalent Binding

One such option was inspired by the fact that proteins can be displayed on the AAV capsid by non-covalent binding. For example, bi-specific antibodies that bind with the AAV capsid and target receptors have been used before[161]. Here, I acquired RBD-fused anti-AAV2 (AE1) antibodies and nanobodies, RBD_hIgG4_AE1, RBD_hinge4_AE1 and RBD_35GS_AE1, from our collaboratoring group of Friedrich Koch-Nolte at the University Medical Center Hamburg. Non-covalent binding between AE1 and AAV2 allows for the display of RBD on the AAV capsid surface (Figure 11A). To this end, I incubated eYFP-expressing AAV2^{RA} with RBD_hIgG4_AE1, RBD_hinge4_AE1 and RBD_35GS_AE1 at different concentrations for 30 min on ice before transducing cells. Three days after transduction, YFP signals were measured by microscopy and flow cytometry. Indeed, RBD_IgG4_AE1 facilitated AAV2^{RA} transduction in hACE2-expressing cells in a concentration-dependent manner. Although the transduction was less efficient than AAV2, it was highly specific in hACE2-expressing cells (Figure 11B). In a preliminary study where I used a high ratio of AE1 to AAV (which was impractical for *in vivo* application, thus I excluded this condition in the following studies), RBD_hinge4_AE1 also facilitated specific transduction of hACE2-expressing cells but less efficient compared to RBD_IgG4_AE1, while RBD_35GS_AE1 did not. This might be due to the weaker binding affinity of RBD_hinge4_AE1 and RBD_35GS_AE1 with the AAV capsid.

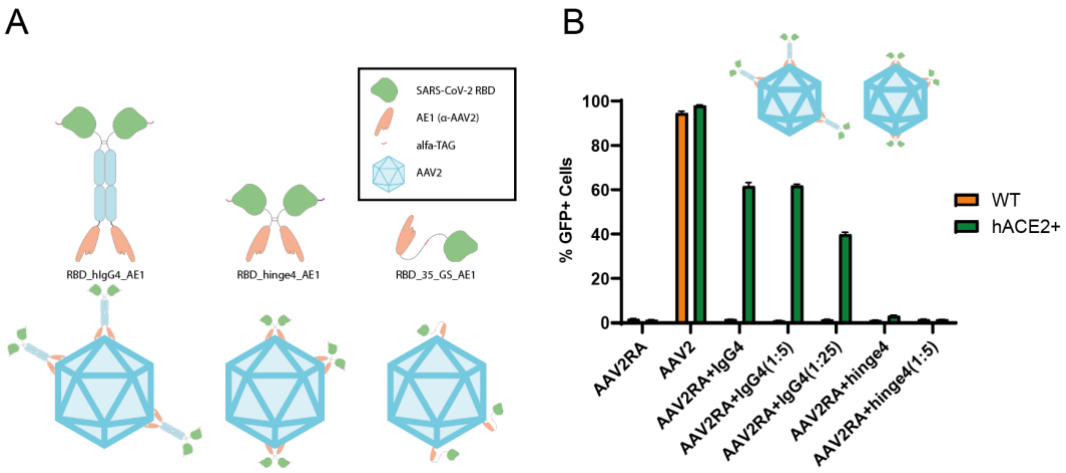

Figure 11. Display of RBD on the AAV capsid via non-covalent binding.
(**A**) Structure of RBD-fused anti-AAV2 antibodies and nanobodies RBD_IgG4_AE, RBD_hinge4_AE1 and RBD_35GS_AE1. (**B**) Transduction of WT and hACE2-expressing HEK293T cells with RBD-displaying $AAV2^{RA}$. 1×10^{11} vg/ml of $AAV2^{RA}$ were incubated with RBD_IgG4_AE (1.8 mg/ml, 1:5 dilution, 1:25 dilution) and RBD_hinge3_AE1 (1.14 mg/ml, 1:5 dilution) for 30 min on ice before transduction. Data represent the mean ± s.d. of *n* = 3 replicates.

3.2 Development of BBB-Penetrating and GBM-Targeting AAV Vectors

GBM is a tumor in the brain and represents the most lethal intracranical tumor, because it is fast-growing, highly invasive and highly resistant to traditional radiotherapy and chemotherapy. As introduced in section 1.4, gene therapy has been developed for several cancers including GBM. Early research on AAV-mediated gene therapy for GBM used wild-type AAVs, but the low efficiency and specificity of transduction in GBM limited the therapeutic effects. One of the major obstacles while transducing GBM is to overcome the blood-brain-barrier (BBB). In this study, I aimed to design AAV vectors with higher transduction efficiency and specificity in GBM by displaying BBB-penetrating and tumor-targeting peptides by genetic insertion and chemical conjugation.

3.2.1 1st generation of design and selection

3.2.1.1 Design and Production of AAV Vectors

Today, one of the most well-known BBB-penetrating engineered AAV variants is PHP.eB, which was identified from an AAV9 peptide display library[216]. It contains a 7mer peptide (TLAVPFK) insertion after AAV9 residue 588 and substitution of A587Q588 to D587G588. It can penetrate the BBB via the Ly6a receptor and transduce brain cells in the C57BL/6 mouse, which motivated me to use this capsid for further engineering in this study.

Upregulated expression of integrins αvβ3 and αvβ5 is one of the hallmarks of tumor cells including GBM[221,222]. RGD is a well-known integrin-binding motif, and several RGD-containing peptides have already been identified and used to target tumor cells[223-225]. The peptide CDCRGDCFC (RGD4C, called P2 in our group and in this study) is one of the widely used integrin-binding peptides, which was initially identified from a phage display peptide library for its binding of αvβ3 and αvβ5 integrins[226]. It has been displayed on small molecule drugs[227-229], therapeutic peptides and proteins[230-233], nanoparticles[234-238], adenoviral vectors[239-242]as well as AAV vectors[110,243 -245] to target tumors. P2-modified AAV variants showed enhanced transduction in several tumors like leukemia or adenocarcinoma cell lines *in vitro*. Another peptide, RGDLGLS (called P1 here), was identified from a peptide-displaying AAV2 library and found to transduce primary breast cancer cells *in vitro*[133]. Our group has previously inserted the P1 and P2 peptides into AAV serotypes 1-13 at VR VIII, and some of the resulting variants showed enhanced transduction in different cell types *in vitro*[246].

The initial idea was to develop AAV variants that transduce GBM with higher efficiency and/or specificity, by combining the BBB-penetrating property of the PHP.eB variant with the tumor-targeting property of RGD-containing peptides. Therefore, I designed AAV vectors displaying both, the PHP.eB peptide and an RGD-containing peptide, on the capsid using three strategies: (1) mosaic vectors, (2) double-insertion vectors, and (3) double-insertion mosaic vectors (Figure 12). (1) To produce the mosaic vectors, I used the PHP.eB helper plasmid and each of the RGD-containing variant helper plasmids at a 1:1 ratio for transfection. Consequently, the two different serotypes of VPs assembled stoichiometrically and formed mosaic capsids. In the mosaic capsid, the PHP.eB and RGD-containing peptides are both inserted at VR-VIII and each VP subunit contains only one peptide. The variants were named in the form of “A/B” (eg. PHP.eB/P2). (2) To produce

double-insertion vectors, I first cloned RGD-containing peptides into the PHP.eB plasmid after position 455 (VR-IV) and then used the corresponding plasmids for production. The variants were named in the form of “A-B” (eg. PHP.eB-P2). In the double-insertion vectors, each VP subunit contains two peptides (3) To produce mosaic double-insertion vectors, I used the PHP.eB helper plasmid and each of the double-insertion helper plasmids at a 1:1 ratio for transfection. The variants were named in the form of “A/A-B” (e.g., PHP.eB/PHP.eB-P2). Into each vector, a scAAV genome containing a CMV promoter-driven eYFP reporter and a unique 15 nt barcode was packaged. The barcode was later used for the NGS analysis in the *in vivo* experiment (section 3.1.1.4).

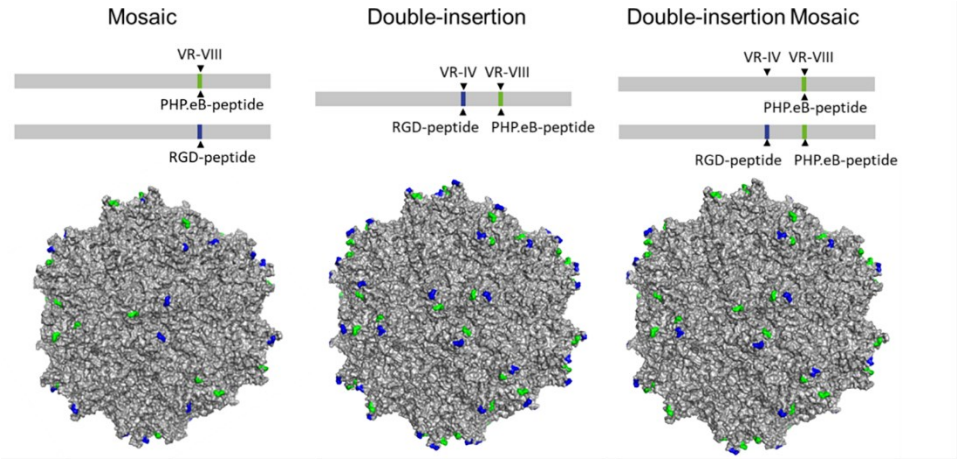

Figure 12. 1st design of BBB-penetrating and GBM-targeting AAV vectors.
Strategies to display BBB-penetrating and GBM-targeting peptides on the same capsid (from left to right): mosaic capsid, double-insertion and double-insertion mosaic. Blue indicates the insertion stie of PHP.eB peptide and green indicates the insertion site of RGD peptides.

3.2.1.2 Designed variants enhanced transduction efficiency of GL261 cells

First, I produced mosaic vectors, double-insertion vectors and double-insertion mosaic vectors that contain the peptides PHP.eB and/or P1, P2 or P2.2 (PDCRGDCFP, derived from P2 with substitution of two terminal C to P). I purified each vector by iodixanol gradient density centrifugation and measured titers by qPCR. To investigate whether the designed variants have a higher transduction efficiency in GBM than the parental AAV9, I *in vitro* transduce GL261 and U87 GBM cells, using the AAV vectors at a MOI of 2.5×10^4 vg/cells. Three days later, transduction efficiency was evaluated by measurement of eYFP signal intensities with a fluorescence microscope and/or by flow cytometry (Figure 13). Display of P2 and P2.2 peptides can enhance the transduction efficiency, especially in the double-

insertion and mosaic double-insertion constructs. Compared with AAV9, double-insertion vectors and mosaic double-insertion vectors PHP.eB-P2 and PHP.eB/PHP.eB-P2 as well as PHP.eB-P2.2 and PHP.eB/PHP.eB-P2.2 showed significantly enhanced transduction efficiencies in both GL261 and U87. AAV9P2 showed a mild enhancement of transduction in U87, while AAV9/9P2 showed a significant enhancement of the transduction efficiency, especially in U87. However, mosaic vector PHP.eB/9P2 showed no enhancement of transduction efficiency. To investigate whether the transduction efficiency of PHP.eB-P2 and PHP.eB/PHP.eB-P2 variants can be further enhanced by changing flanking residues, I also produced double-insertion and mosaic double-insertion vectors containing P2.3 (PCDCRGDCFCP, with additional flanking residues P and P) and P2.4 (ACDCRGDCFCG, with additional flanking residues A and G) for the following study.

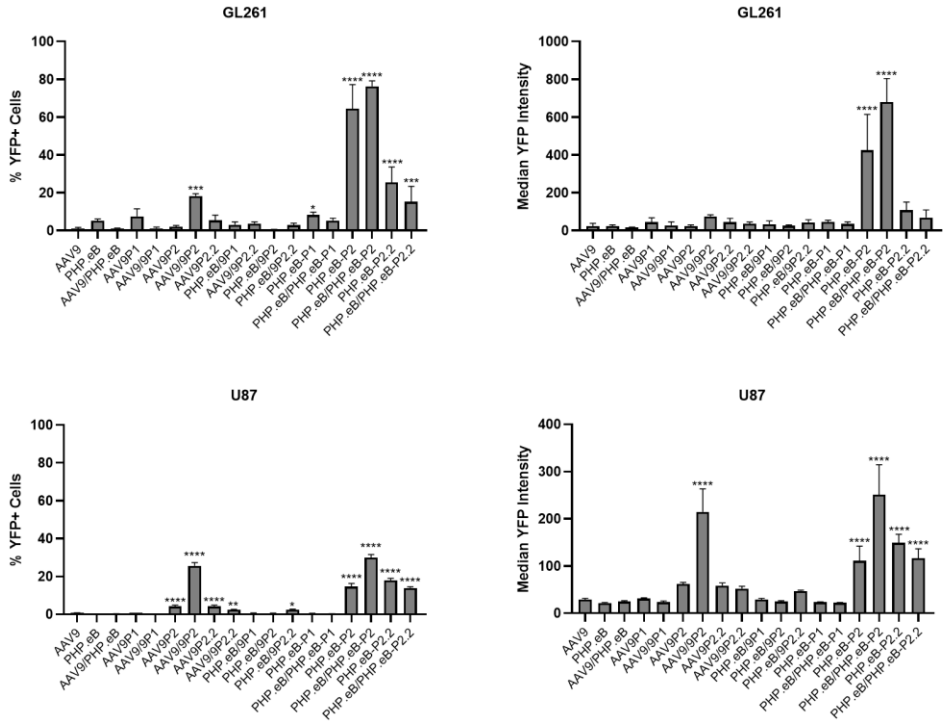

Figure 13. Transduction of PHP.eB and RGD peptide-displaying AAV variants.
eYFP-expressing AAV vectors were used to transduce GL261 mouse GBM cells and U87 human GBM cells at a MOI of 2.5×10^4 vg/cell. Data represent the mean ± s.d. of $n = 3$ replicates. Statistical analysis was conducted by one-way ANOVA comparing with AAV9.

3.2.1.3 Aggregation and Deaggregation of P2-containing AAV vectors

Next, I attempted to produce sufficient amounts of vectors for mouse experiments. Surprisingly, though, I found that P2-containing AAV variants, especially AAV9P2, were difficult to produce to high yields (in the final PBS solution). I then discovered that a large percentage of those AAVs were lost during buffer exchange as a result of precipitation. To figure out whether the precipitation was indeed caused by aggregated AAVs, I first performed a qPCR of the resuspended pellets. The measurement of high titers of vector genomes indicated that the precipitate was indeed AAVs (Figure 14A). For additional confirmation, I performed EM using the JEOL JEM1400 TEM with the help of Vojtech Zila (Department of Infectious Diseases/Virology, University of Heidelberg, Germany). As exemplified in Figure 14B, this showed a bulky aggregation of P2-containing vectors. The aggregate also contained plenty of smaller particles, which were most likely Ferritin, the major contaminant of AAV production discovered by Grieger *et al.* by EM and identified with mass spectrometry[247]. Furthermore, I performed Dynamic Light Scattering (DLS) with the help of Jonah Voigt (Max Planck Institute for Medical Research, Germany), which can measure the diameter of the particles in the sample. The higher particle diameter measured in the PHP.eB-P2 sample compared to PHP.eB provided further evidence for P2-mediated aggregation (Figure 14C).

The P2 peptide contains four cysteine residues, which were designed to form two pairs of disulfide bonds and thus a cyclic structure to enhance the stability of the peptide. However, AAV capsid proteins are synthesized at the cytosolic ribosome where disulfide bonds do not form. Thus, I hypothesized that the aggregation was caused by the formation of inter-particle disulfide bonds when free cysteines were exposed to oxygen during the purification process. To study this hypothesis, AAVs were treated with 50 mM reducing reagent DTT for 30 min at RT to break disulfide bonds. EM and DLS showed that the aggregations dissolved after DTT treatment, which supports the hypothesis (Figure 14B, 14C).

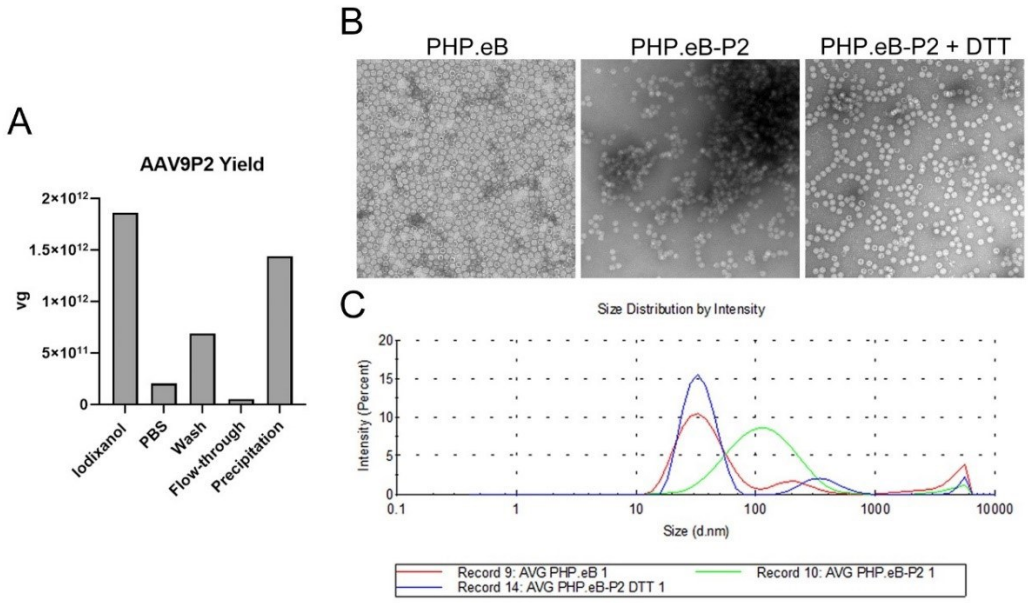

Figure 14. Aggregation and deaggregation of P2-containing AAV vectors.
(**A**) Loss of AAV9P2 vectors during buffer exchange. Iodixanol: viral genomes in iodixanol sample after iodixanol gradient centrifugation and before buffer exchange; PBS: viral genomes in PBS after buffer exchange with Amicon filter unit; Wash: viral genomes in PBS that was used to wash the Amicon filter after collecting the sample; Flow-through: viral genomes in flow-through PBS during the buffer exchange; Precipitation: viral genomes in the precipite. (**B**) EM imaging and (**C**) DLS measurement of purified PHP.eB (red curve), PHP.eB-P2 (green curve), and PHP.eB-P2 treated with 50 mM DTT (blue curve). The X-axis indicates the diameter of the particles in the sample. A higher diameter of the particles in the PHP.eB-P2 sample than PHP.eB sample indicates aggregation of virions. A same diameter of DTT treated PHP.eB-P2 sample as PHP.eB sample indicates dissolvement of aggregation.

Therefore, to avoid the disulfide bond formation in subsequent production runs, DTT was added routinely during production and purification. Specifically, 2 mM DTT was added to cell lysates, 50 mM DTT was added to collected full-capsid-containing fractions after iodixanol gradient centrifugation, and 2 mM DTT was added during buffer exchange and to the final PBS solution. With DTT treatment, P2-containing variants no longer aggregated and loss during the buffer exchange was ameliorated, together restoring the yields to the level of WT AAV9. In addition, because the disulfide-bonds in P2 cannot form as expected, I designed and produced three cysteine-free, RGD-containing double-insertion vectors, PHP.eB-P2A, PHP.eB-2.3A and PHP.eB-LRGD and the corresponding mosaic double-insertion vectors. In PHP.eB-P2A and PHP.eB-P2.3A, the cysteine residues in P2 and P2.3 peptides were substituted to alanine residues. In PHP.eB-LRGD, another peptide PGRGDSP that was also identified as integrin αvβ3 and αvβ5 binding

peptide was inserted. Transduction of GL261 cells showed that DTT treatment did not impact the transduction efficiency (Figure 15). PHP.eB-LRGD and PHP.eB/PHP.eB-LRGD variants showed significantly higher transduction than AAV9. However, substitution of the cysteines in the P2 and P2.3 peptides significantly reduced transduction efficiency (Figure 15).

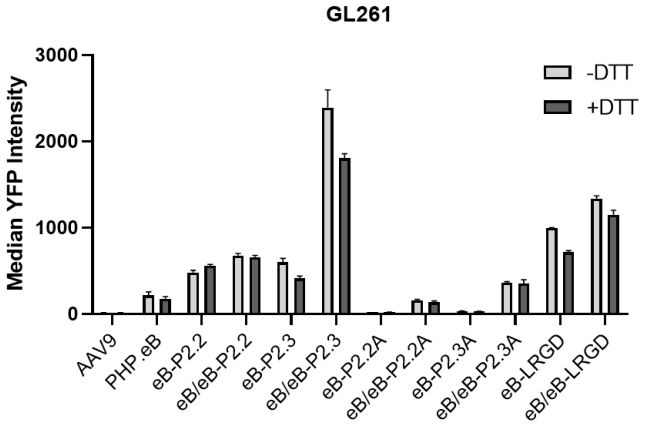

Figure 15. Transduction of AAV variants with and without pre-treatment with DTT.
eYFP-expressing AAV vectors of the shown type were used to transduce GL261 mouse GBM cells at a MOI of 2.5×10^4 vg/cell. Three days after transduction, YFP signals were measured with flow cytometry. +DTT indicates the use of DTT during virus production and storage. Data represent the mean ± s.d. of *n* = 3 replicates.

3.2.1.4 Transduction *in vivo*

The next step was to investigate whether the designed vectors can also transduce GBM with higher efficiency than WT AAV9 *in vivo* after systematic administration (Figure 16A). To this end, I harnessed a barcoded library method that was developed by a former PhD student of our group, Jonas Weinmann, allowing for the evaluation and comparison of hundreds of variants in the same animal. Based on the *in vitro* experiments, I selected 19 variants for the mouse experiment. I produced all barcoded AAV variants and purified them via iodixanol density gradient centrifugation individually. Titers were measured by both ddPCR and qPCR, and equal amounts (calculated based on the ddPCR result) of each vector were mixed and dialyzed to PBS with 2 mM DTT. The titer of the final mixture of AAV vectors was measured by ddPCR. Then, I performed silver staining to validate the purity of the viruses, and EM to rule out aggregation (Figure 16B). Mouse manipulations were conducted by our collaborator, *i.e.*, the group of Michael Platten from DKFZ. GL261

cells were transplanted into C57BL/6 mice, and ten days later, 8×10^{11} vg of barcoded AAVs were administered into each mouse by tail vein injection. Seven days after AAV injection, GBM, healthy brain hemisphere, and five other off-target organs (liver, muscle, heart, kidney, spleen) were harvested. I took over these tissues, performed DNA and RNA extraction, as well as the sample preparation for NGS, ddPCR and qPCR.

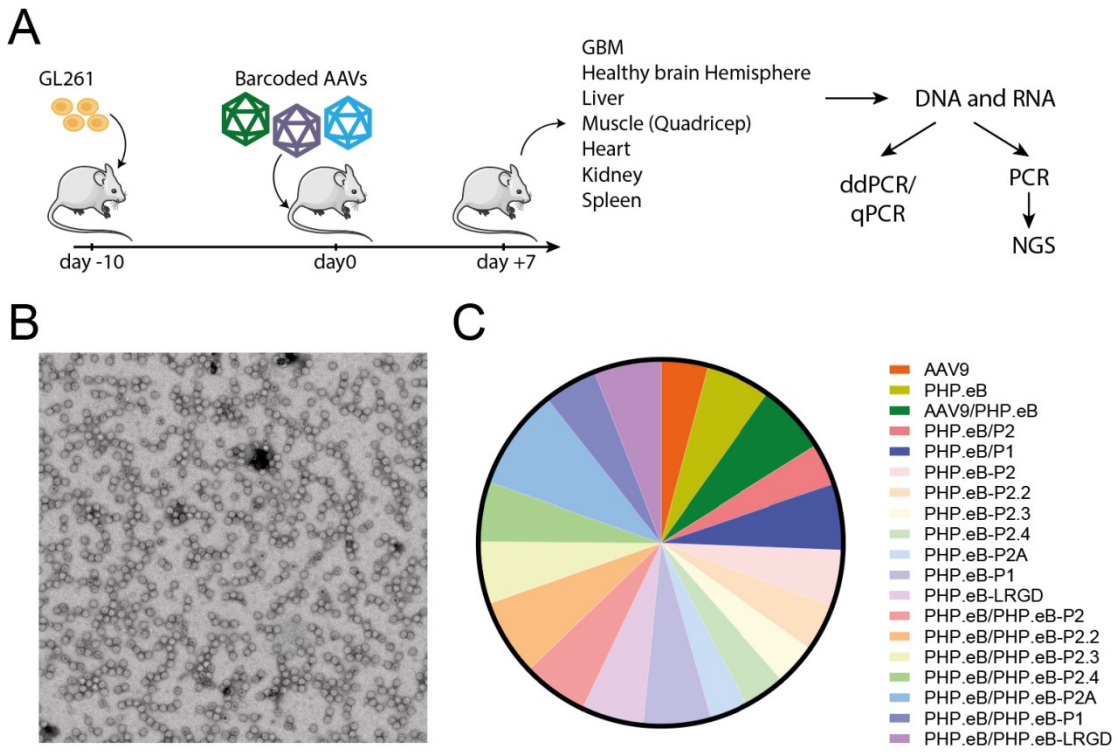

Figure 16. Scheme of first mouse experiment to assess *in vivo* GBM targeting.
(**A**) Workflow of mouse experiment. (**B**) EM image of the mixture of AAV vectors used for injection. (**C**) Composition of the input variants.

The NGS analysis of the input sample showed that the proportions of the 19 variants were fairly even. The most over-represented variant was PHP.eB/PHP.eB-P2A with 8.9% and the most under-represented variant was PHP.eB-P2A with 3.3% (Figure 16C). NGS results were analyzed with custom Python scripts as described in Rapti *et al.* (section 2.2.10)[220].

Normalized proportions $V_{\alpha\beta}$ (corrected to the proportion in the input mixture) were calculated and illustrate the efficiency of each AAV variant within the same tissue (Figure 17, 18). The results showed that, although transduction efficiencies of the designed AAV vectors, especially double-insertion variants containing P2 or P2-derived peptides, in GBM cell lines *in vitro* were significantly higher than AAV9, none of them transduced GBM better

than AAV9 in GL261-transplanted GBM after systematic injection. Instead, wild-type AAV9 was the most efficient variant to transduce GBM on the cDNA level (Figure 17). However, AAV9 mainly transduced the liver (Figure 19). PHP.eB was efficient in normal brain tissue and was depleted in liver (Figure 17-19), which was consistent with published data[216]. Even though PHP.eB was able to penetrate the BBB more efficiently than AAV9, it displayed a tropism to normal brain tissue but not to GBM. In GBM, the genome abundance (gDNA) of PHP.eB was still higher than AAV9, yet gene expression (cDNA) of PHP.eB was lower than AAV9, indicating that AAV9 was more efficient in intracellular trafficking than PHP.eB (Figure 17). The mosaic capsid AAV9/PHP.eB showed a combined transduction profile of AAV9 and PHP.eB, as its transduction efficiencies in GBM, brain and liver were in between AAV9 and PHP.eB. Unexpectedly P2-containing vectors were not enriched in any of the harvested tissues (Figures 17,18). One of the possible reasons is the fast clearance after injection.

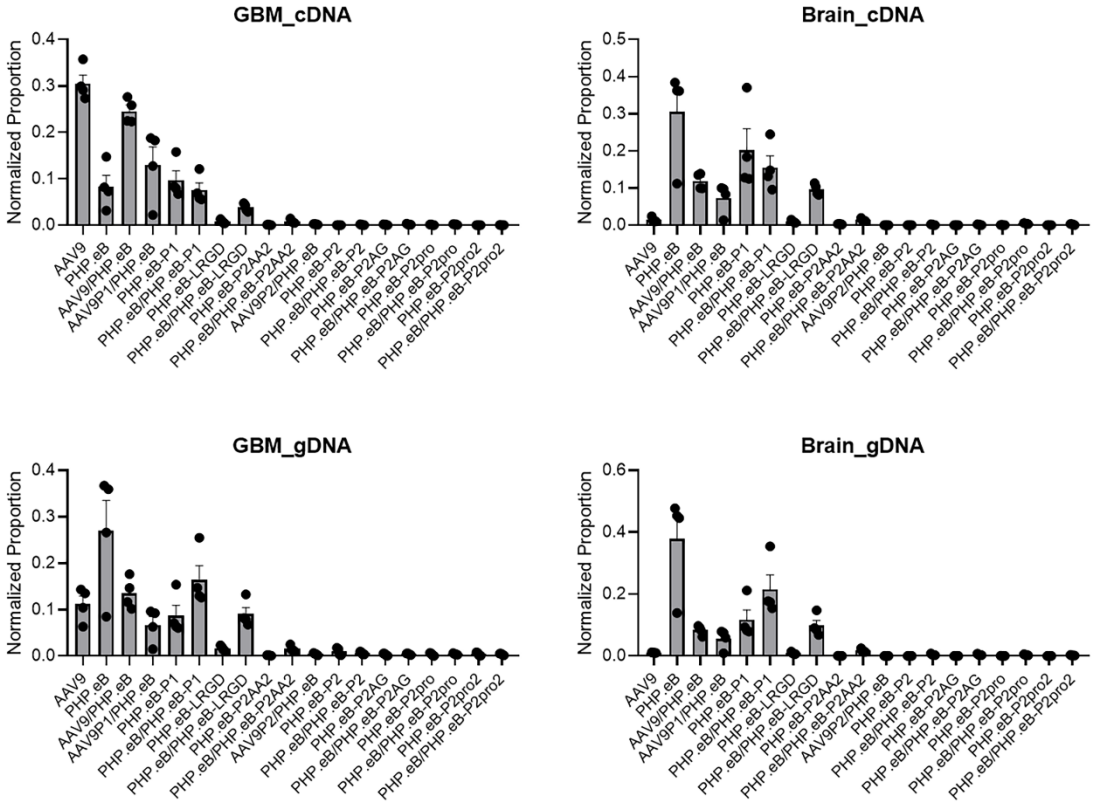

Figure 17. Transduction efficiency in GBM and health brain hemisphere.
Shown are transduction efficiencies (cDNA) and genome abundances (gDNA) as normalized proportions of 19 AAV capsid variants in GBM and normal brain tissue. Data represent the mean ± s.d. of *n* = 4 replicates.

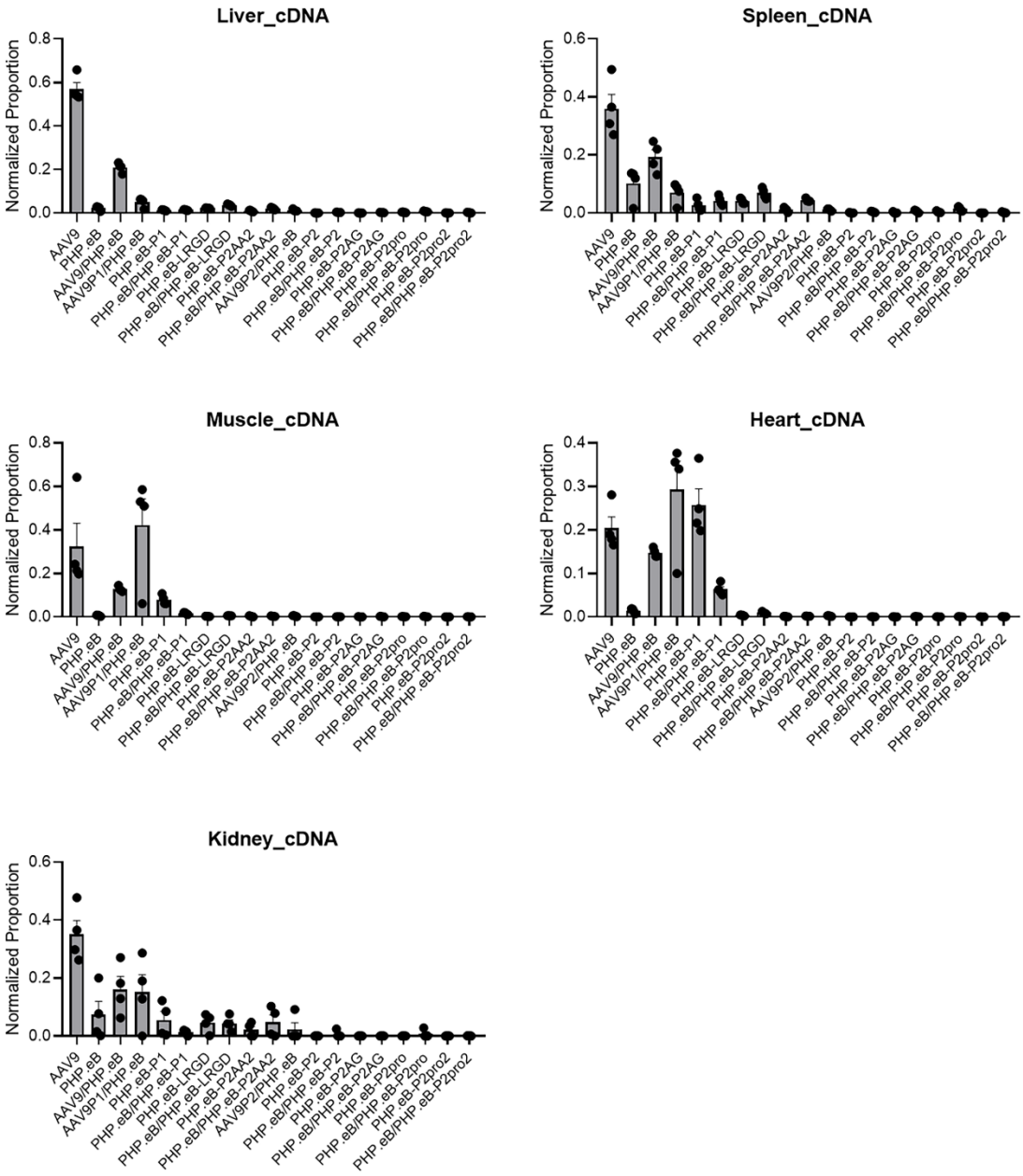

Figure 18. Transduction efficiency in other off-target tissues.
Shown are transduction efficiencies (cDNA) and genome abundances (gDNA) as normalized proportions of 19 AAV capsid variants in the off-target tissues liver, muscle, heart, spleen, and kidney. Data represent the mean ± s.d. of *n* = 4 replicates.

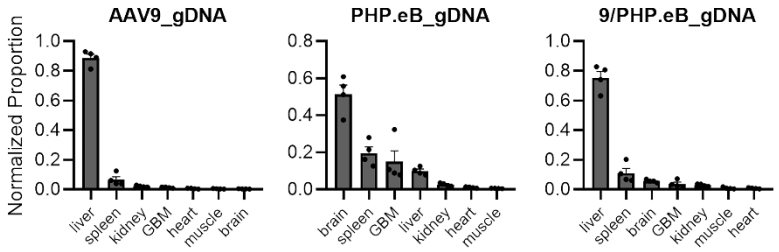

Figure 19. Transduction specificity of AAV9, PHP.eB and 9/PHP.eB.
The figures show the AAV genome abundance as normalized proportion per cell in GBM, brain and other off-target tissues (liver, muscle, heart, spleen and kidney). Data represent the mean ± s.d. of *n* = 4 replicates.

3.2.2 Design and Selection of 2nd Generation Vectors

As shown above, even though the designed 1st generation AAV capsids gave better transduction in GBM cell lines *in vitro*, they transduced GBM less efficiently than wild-type AAV9 in GL261-transplanted C57BL/6 mice after tail vein injection. Therefore, to achieve the original aim of developing GBM-targeting AAV vectors, I designed and selected a 2nd vector generation. My previous data showed that RGD peptide-displaying variants that I used in the 1st vector generation did not improve tumor targeting *in vivo.* Moreover, PHP.eB-displaying variants penetrated the BBB, but displayed a tropism to normal brain tissue instead of GBM. Furthermore, because the receptor of PHP.eB, Ly6A, is only expressed in some mouse strains but not in any other animals, it is not applicable in humans for gene therapy. Therefore, before combining BBB-crossing and GBM-targeting properties in a single vector, I first aimed to identify new BBB-crossing and GBM-targeting variants.

Prior work had identified BBB-penetrating peptides that bind receptors on CNS endothelial cells and facilitate BBB penetration via receptor-mediated transcytosis (RMT), as well as GBM-targeting peptides that bind with receptors that are overexpressed or specifically expressed in GBM. I selected several of these peptides and displayed them on the AAV capsid by genetic insertion and chemical conjugation. The chemical conjugation method allowed for site-specific conjugation and mosaic capsid production. Two animal models, the U87-transplanted nsg mouse and GL261-transplanted C57BL/6 mice, were used for this *in vivo* study.

3.2.2.1 Selection of BBB-crossing and GBM-targeting peptides

All the peptides I used in this study are listed in Table 31. Most of them have previously been identified from phage display peptide libraries, while some were derived from endogenous peptides or by rational design. Overexpression of epidermal growth factor receptor (EGFR) is a hallmark of most forms of GBM[248-252]. Some GBM types also express the EGFRvIII mutant, which is a tumor-specific receptor[253-255]. Hence, I selected GE11, one of the most widely used EGFR-binding peptides[256-262], and FAL, an EGFR and EGFRvIII dual binding peptide[263-267]. Another member in the human EGFR family, human epidermal growth factor receptor 2 (HER2), is also overexpressed in many forms of GBM[268,269]. Hence, the HER2-binding peptide LTV was also included[270-272]. Other than the EGFR family, a few tumor-specific receptors are also expressed in GBM, including p32 (binding peptide TT1)[273-276] and Neurophilin-1 (binding peptide Cend1)[277,278]. Besides, integrin is one of the earliest and most-studied targets for tumor. Even though the effects of targeting are controversial, many researchers continue to work on it[279]. Therefore, I included integrin αvβ5 and αvβ3 binding peptides LRGD1 and LRGD2[280,281], as well as the integrin αvβ6 and αvβ8 binding peptide RTD[282] in this study, too.

Several receptors that are expressed on CNS endothelial cells were identified for aiding BBB-crossing via RMT. Several BBB-penetrating peptides that bind with these receptors were also identified, including Low density lipoprotein receptor-related protein 1 (LRP1) binding peptides Ang2[283-289] and RAP12[290-292], and transferrin receptor (TfR) binding peptides THR[293,294], T7[293,295,296] and CRT[297-302]. Besides, PB53[304] and TGN[303] that were selected as BBB-penetrating peptides in mice were also included. Notably, PB53 was selected from a phage display library that can non-covalently bind to the AAV9 capsid and penetrate the BBB. Incubation with PB53 enhanced BBB penetration and CNS transduction of the AAV9 capsid[304].

Table 31. BBB-penetrating peptides and GBM-targeting peptides used in 2nd round of design and selection.

Name	Sequence	Receptor	Origin
BBB-penetrating peptides			
Ang2	TFFYGGSRGKRNNFKTEEY	LRP1	Derived from human aprotinin
RAP12	EAKIEKHNHYQK	LRP1	Derived from human RAP
THR	THRPPMWSPVWP	TfR1	Phage display peptide library (human receptor)
T7	HAIYPRH	TfR1	Phage display peptide library (human receptor)
CRT	ARTIGPSVA	TfR1	Phage display peptide library (human receptor)
PB5-3	QFAALPVRAHYG	unknown	Phage display peptide library (mice)
TGN	TGNYKALHPHNG	unknown	Phage display peptide library (mice)
Tumor-targeting peptides			
GE11	YHWYGYTPQNVI	EGFR	Phage display peptide library(human receptor)
FAL	FALGEA	EGFR&EGFRvIII	Designed (human receptor)
LTV	LTVSPWY	HER2	Phage display peptide library (human receptor)
TT1	AKRGARSTA	p32	Phage display peptide library(human receptor)
Cend1	RGERPPR	Neuropilin-1	Phage display peptide library (human receptor)
LRGD1	RGDSP	Integrin αvβ5, αvβ3	Designed
LRGD2	PRGDSP	Integrin αvβ5, αvβ3	Designed
RTD	RTDLDSLRT	Integrin αvβ6	Phage display peptide library (human receptor)
P1	RGDLGLS	Integrin	AAV peptide display library (mice)

3.2.2.2 Production of Peptide-modified AAV Vectors

Peptides were inserted into VR-IV (V4) and VR-VIII (V8) of AAV9 VP. Similar to the production of the 1st generation vectors, scAAV genomes with a CMV promoter-driven eYFP reporter and a 15 nt unique barcode were packaged into each capsid variant. Besides, I produced AAV9, PHP.eB[216], and another BBB-penetrating variant CPP16[112] as benchmarks. However, even though most of the peptides are short and should thus be compatible with AAV display, variants containing the Ang2, THR, TT1, GE11 and LTV peptides gave low yields (Figure 20, top). Even when I introduced longer and more flexible GGG or GGGG linkers, in most cases, this did not enhance the yields.

As a possible explanation, I assumed that the insertion of these peptides impeded capsid assembly and stability, in turn resulting in the observed low yields. Therefore, I produced mosaic vectors that consisted of VPs of AAV9 and the peptide-modified variants by using the corresponding plasmids at a 1:1 ratio during virus production. Indeed, this facilitated capsid assembly and enhanced stability by reducing the number of peptides displayed on the capsid, as evidenced by the finding that the yields of AAV9 mosaic vectors were rescued to those of wild-type AAV9 (Figure 20, bottom).

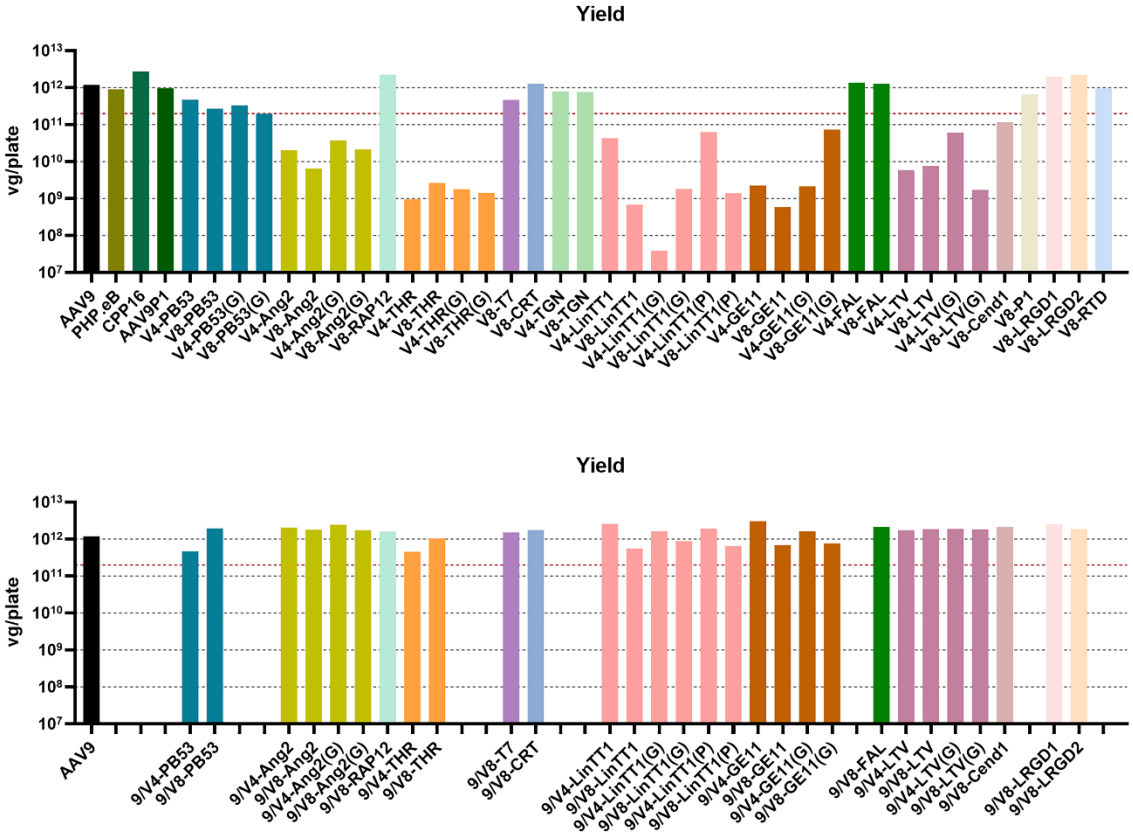

Figure 20. Yields of BBB-penetrating and tumor-targeting peptide-modified rAAV vectors. Shown are yields of AAV vectors of each peptide-displaying variant (top) and of the mosaic vectors composed of AAV9 and peptide-modified VPs (bottom). Variants containing the same peptide are shown in the same color. V4 represents the VR-IV insertion site, and V8 indicates the VR-VIII insertion site. (G) indicates additional GGGG or GGG flanking residues, while (P) indicates additional single P flanking residues.

To investigate whether AAV9 mosaic vectors consisted of VPs of both, wild-type AAV9 and peptide-displaying variants, I performed SDS-PAGE and silver staining of purified AAVs. The finding that the bands of VP1, VP2 and VP3 were shifted up indicated the presence of peptide-modified variants (Figure 21). Notably, the bands in V4-peptide-displaying variants ran at a higher molecular weight than expected. A possible reason is that the peptide insertion resulted in post-translational modifications, likely the glycosylation on S454, which is rare in wild-type AAV serotypes[305,306]. Due to the small size of the peptides, not all VPs of V8-peptide-displaying serotypes were distinguishable from the corresponding VPs of AAV9. Notably, the mosaic vectors showed a different *in vitro*

transduction, indicating that the peptide-modified VPs were assembled into capsids, or else they should perform identical to AAV9 (Figure 22).

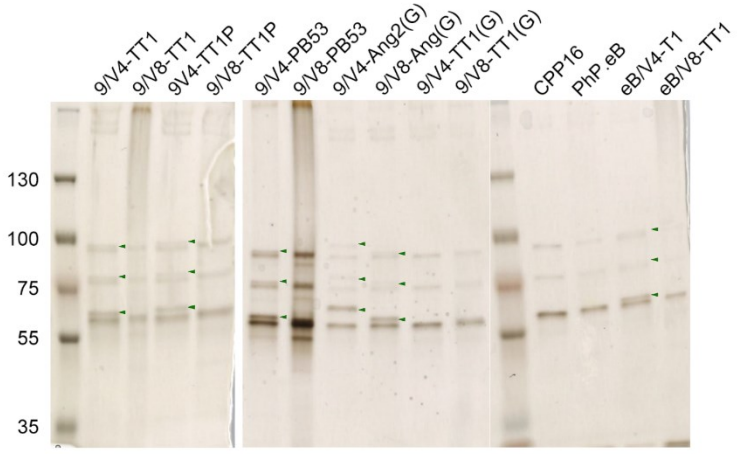

Figure 21. Silver staining of purified AAVs.
Bands marked with arrows indicate peptide-modified VPs.

As I already knew that results of *in vitro* transduction hardly translate to an *in vivo* setting, I decided to mainly focus on *in vivo* experiments. Still, I performed selected *in vitro* transduction experiments to investigate whether the peptide insertion had changed the transduction profile from AAV9. Accordingly, a subset of all vectors was used to transduce U87 human GBM cells, GL261 murine GBM cells, and Neuro-2A (N2A) murine neuroblastoma cells. Three days after transduction, I conducted flow cytometry to quantify transduction efficiencies via measurement of eYFP signals. In preliminary experiments, TT1-displaying AAV9 mosaic variants, especially AAV9/V8-TT1, showed significantly higher transduction efficiency than AAV9 in U87 cells. Therefore, I chose this peptide to produce mosaic capsids with PHP.eB. The results showed that display of the BBB-penetrating and tumor-targeting peptides on the AAV capsid changed its transduction *in vitro* (Figure 22). In particular, display of TT1 at VR-VIII significantly enhanced transduction in U87 cells.

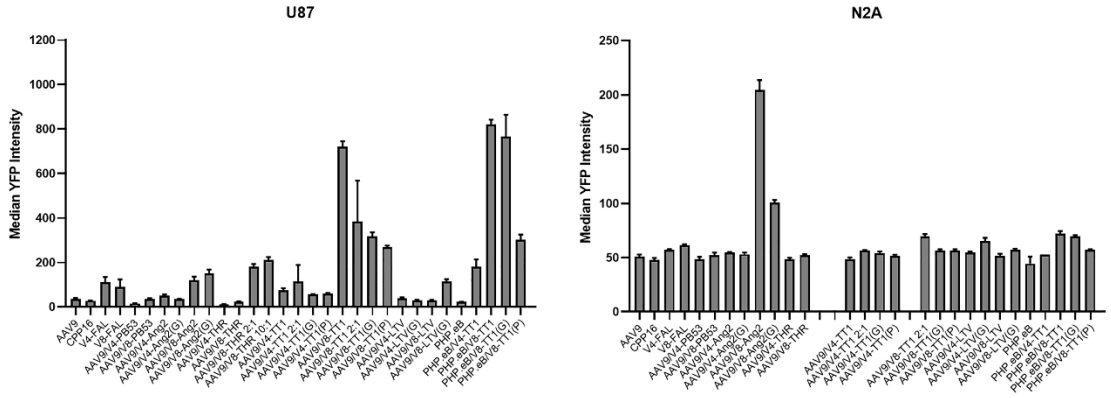

Figure 22. Transduction of GBM-targeting and BBB-penetrating AAVs.
eYFP-expressing AAV vectors were used to transduce U87 human GBM and N2A murine neuroblastoma cells at a MOI of 2.5×10^4 vg/cell. Three days after transduction, YFP signals were measured with flow cytometry. Data represent the mean ± s.d. of *n* = 3 replicates.

To investigate the reason for the low yields of some of the variants, I predicted the structures of peptide-modified VP monomers with AlphaFold3. Next, I created the structure of the 3-fold axis trimer by aligning the predicted structure to the X-ray diffraction capsid structure of AAV9 (PDB ID: 3UX1). The THR peptide (THRPPMWSPVWP), for instance, contains two tryptophan residues and four prolines that constrain its structural flexibility. The predicted AAV9-V8-THR structure showed a conformational conflict of the side chain of W597 within the THR peptide with W611 (W595 on wild-type AAV9 VP) from another monomer, which may impede its assembly (Figure 23A). VR VIII (VR) in the predicted AAV9-V8-THR VP bends to the gap between VR VIII and VR IV, which is likely to impede the positioning of VR V of the other monomer to the gap during assembly (Figure 23B). Nonetheless, for most of the variants, it is challenging to identify the reasons for their low yields from this simplified modeling.

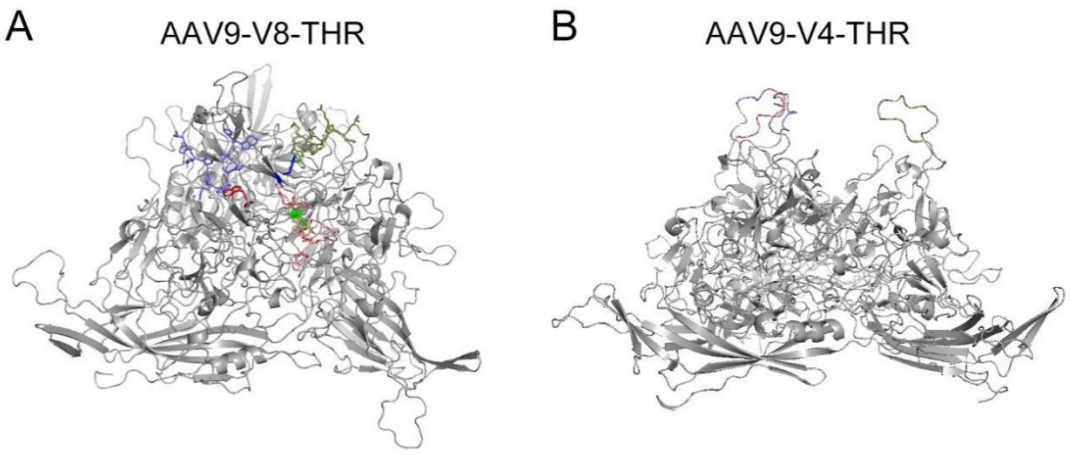

Figure 23. Predicted structures of AAV9-V8-THR and AAV9-V4-THR.
Show are ribbon diagrams of the 3-fold axis VP trimer of AAV9-V8-THR (**A**) and AAV9-V4-THR (**B**). Light red, light green and light blue represent the THR insertion in the different monomers. Red, green and blue indicate W611 (W595 on wild-type AAV9 VP). Side chains of these residues are shown in (**A**).

3.2.2.3 Production of Peptide-conjugated AAV Vectors

Peptide insertion influences the folding and assembly of AAV VPs, which can result in low yields or even failure of production. Furthermore, it is likely that the binding ability of the peptide is changed or lost due to the interaction with surrounding residues and conformational changes. Post-production chemical conjugation is an alternative display method that has potential to solve these issues. Besides, chemical conjugation allows for the display of ligands other than peptides, *e.g.*, small molecules, antibodies, nanobodies, DNA and RNA aptamers, or peptides containing modified amino acids. The traditional conjugation method is to conjugate to the primary amine group (-NH2) on lysine residues. However, each AAV9 VP contains several surface-exposed lysine residues, which makes the modification not site-specific. In contrast, AAV VP does not contain any surface-exposed cysteines (Figure 24A). Here, I developed a site-specific conjugation method by introducing a cysteine residue at the site of interest. Subsequent site-specific conjugation can then be achieved between the thiol group (-SH) on the cysteine and any substrate that bears a maleimide group (Figure 24B).

I first cloned AAV9 helper plasmids with substitution of Q456, G660, or E718 to cysteines, or insertion of a cysteine after Q588 (588+1), respectively (Figure 24C). 456cys or

588+1cys are located at the peak of VR-IV and VR-VIII, respectively, which were used for peptide conjugation in this study. 660cys and 718cys face away from receptor binding motifs. Therefore, they were chosen for fluorescent labeling, which minimizes the impact on infection and enables capsid tracing in the future. The yields of these variants were the same as AAV9. Then, I used maleimide-PEG3-Biotin to validate and optimize the conjugation method. Therefore, 5×10^{12} vg purified AAV9-456cys and AAV9 (as negative control) vectors were dialyzed to approximately 500 µl of PBS buffer with 5 mM TCEP, and incubated for 20 min to reduce disulfide bonds in case they formed. Next, viruses were incubated with maleimide-PEG3-Biotin at different concentrations for 2 h at RT. The reaction was quenched by excess BME in the loading dye. Samples were loaded on SDS-PAGE and transferred to a nitrocellulose membrane, and conjugated Biotin was detected by Streptavidin-HRP. Biotin-conjugated VPs were only detected for AAV9-456cys but not for AAV9, which proved the specific conjugation on the cysteine residues.

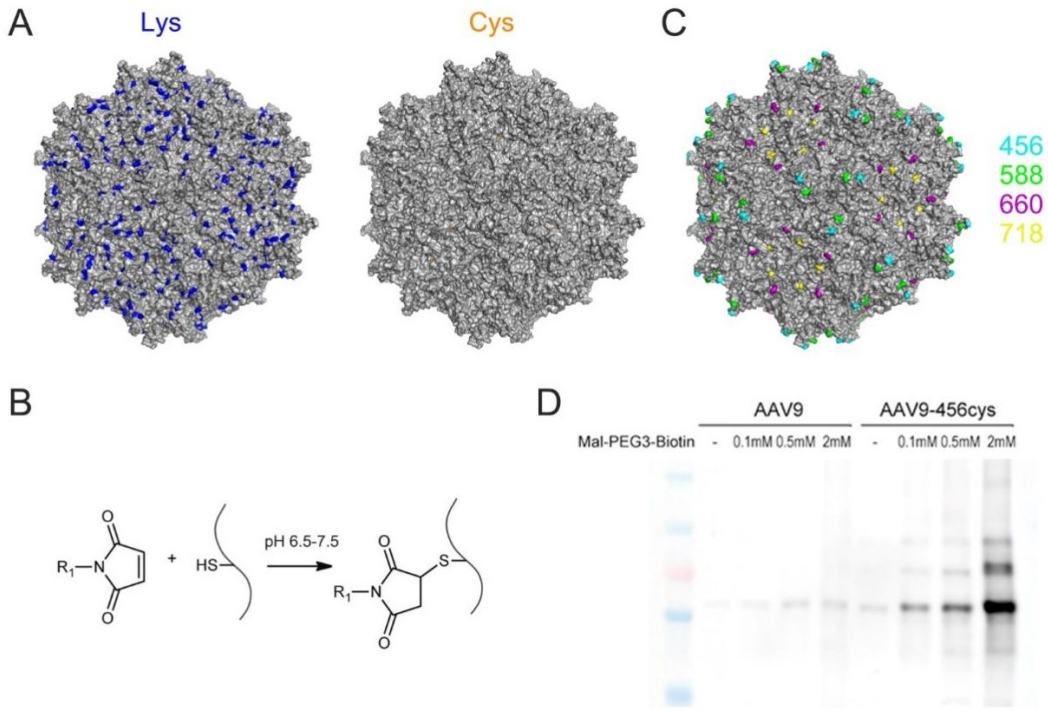

Figure 24. Chemical conjugation of the AAV capsid.
(**A**) Lysine (blue) and cysteine (orange) residues on the surface of the AAV9 capsid. (**B**) Four sites of introduced cysteine residues for chemical conjugation. (**C**) Reaction between maleimide and cysteine residue. (**D**) Validation of chemical conjugation on the AAV capsid with Mal-PEG3-Biotin.

Five peptides with N-terminal maleimide modification were ordered and used for conjugation (Table 32). Besides, as noted before, chemical conjugation can display non-peptide molecules. In 2023, Puzzo *et al*. conjugated a tumor-targeting DNA aptamer onto the AAV capsid and found that it increased transduction efficiency in a HeLa cell-derived tumor in mice. Inspired by their work, I also ordered and used two tumor-targeting aptamers with 5' maleimide modification (Table 33). Conjugation of the peptide and aptamer were validated by AAV silver staining (Figure 25A). The upshifting of the VP bands indicated successful conjugation of peptide and aptamer on the AAV capsid. Furthermore, the number of molecules conjugated on the capsid can easily be adjusted by changing the number of cysteines on the capsid. To study this, I produced mosaic capsids of AAV9/AAV9-456cys and AAV9/AAV9-588+1cys. After conjugation with the peptide, both, peptide-conjugated VPs and wild-type AAV9 VPs, were observed in silver staining (Figure 25B).

Then, I used GBM-targeting peptide-conjugated vectors AAV9-588+1cys[TT1] and AAV9-588+1cys[GE11] for transduction of U87 cells *in vitro*. Remarkably, AAV9-588+1cys[TT1] showed significantly enhanced transduction, which was even pronouncedly higher than the TT1-genetically-modified variant AAV9/V8-TT1 (Figure 25C).

Table 32. Synthesized peptides with N-terminal maleimide modification for conjugation.

BBB crossing peptides	
PB5-3	Mal-QFAALPVRAHYG-NH2
Ang2	Mal-TFFYGGSRGKRNNFKTEEY-NH2
THR	Mal-THRPPMWSPVWP-NH2
Glioblastoma targeting peptide	
LinTT1	Mal-AKRGARSTA
GE11	Mal-YHWYGYTPQNVI-NH2

Table 33. Synthesized ssDNA aptamers with 5' maleimide and 5' tetrazine modification for conjugation.

	Sequence	**receptor**	**resource**
As1411	GGTGGTGGTGGTTGTGGTGGTGGTGG	Nucleoli	screened for Nucleoli
GMT8	TGACGAGCCCAAGTTACCTCGATCTTGTGTGTTTAATTGT TTATTGCTGTACCGTGAGAATCTCCGCTGCCTACA		screened for U87MG

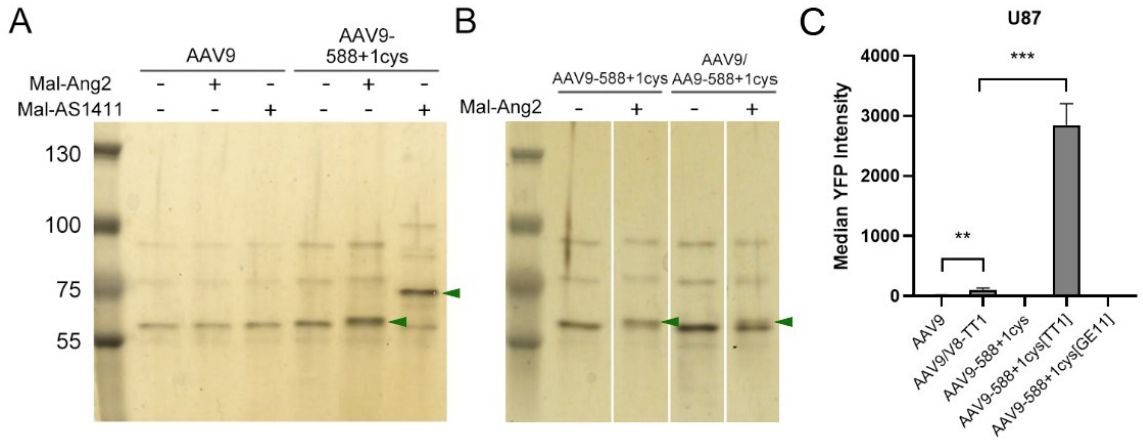

Figure 25. Conjugation of peptide and aptamer on the AAV capsid.
(**A**) Validation of sccessful chemical conjugation of peptide Mal-Ang2 and aptamer Mal-AS1411 on the AAV9-588+1cys capsid. 5×10^{12} vg/dg AAV9-588+1cys, AAV9/AAV9-588+1cys and AAV9 (as negative control) were incubated with 0.5 mM Mal-Ang2 or Mal-AS141 for 2 h at RT. After the reaction, unconjugated peptides and aptamers were washed off by dialysis in Amicon Ultra-4 Centrifugal Filters. Samples were loaded on an SDS-PAGE and silver stained. The shift of the VP bands (marked with green arrows) indicates the presence of Mal-Ang2 or Mal-AS1411 conjugated VPs. (**B**) Validation of chemical conjugation of peptide Mal-Ang2 on the mosaic AAV9/AAV9-588+1cys capsid. Green arrows indicated the Mal-Ang2 conjugated VPs. (**C**) Transduction with GBM-targeting peptide-conjugated AAVs. eYFP-expressing AAV vectors were used to transduce U87 human GBM at a MOI of 2.5×10^{4} vg/cell. Three days after transduction, YFP signals were measured with flow cytometry. Data represent the mean ± s.d. of n = 3 replicates. A T-test was conducted between AAV9 and AAV9/V8-TT1, and AAV9/V8-TT1 and AAV9-588+1cys[TT1].

3.2.2.4 Transduction *In vivo*

AAV variants that reached a yield of 2×10^{11} vg/plate (1×10^{12} in total) were used for a mouse experiment. To prepare a pool of barcoded vectors, I purified barcoded vectors by iodixanol density gradient centrifugation separately and measured their titers by qPCR. For AAV9 and peptide-modified AAV variants, I pooled equal amounts of each vector together, dialyzed and concentrated the pooled vectors to PBS buffer by using Amicon Ultra-15 Centrifugal Filters, and measured the titer of the mixture by qPCR and ddPCR. For peptide-conjugated vectors, I dialyzed and concentrated each vector to PBS with 10 mM TCEP separately by using Amicon Ultra-4 Centrifugal Filters. Vectors were then incubated with peptides for 2 h at RT, and unconjugated peptides were washed off by dialysis with Amicon Ultra-4 Centrifugal Filters. I measured the titer of each virus by qPCR and ddPCR. Right before injecting into the mice, I mixed the pools of peptide-modified

viruses and individual peptide-conjugated viruses. The final pool was composed of equal amounts of each vector (the calculation was based on the ddPCR results). Two GBM mouse models were used this time, namely, the GL261-transplanted C57BL/6 mouse model and the U87-transplanted nsg mouse model. Mouse manipulations were again performed by our collaborator, the group of Michael Platten at the DKFZ. For GL261-transplanted C57BL/6 mice, 4×10^{11} vg AAV vectors were administered by tail vein injection ten days after cell transplantation, and tissues were harvested eight days after AAV administration. For the U87-transplanted nsg mouse, 4×10^{11} vg AAV were administered by tail vein injection 28 days after cell transplantation, and tissues were harvested nine days after AAV injection. I isolated DNA and RNA for the subsequent ddPCR and NGS analysis, using the same methods as in the 1st round of selection.

The variants used in the two mouse models were slightly different. Pooled AAVs injected to the nsg mice included 68 variants: AAV9, PHP.eB, CPP16 as benchmarks, 16 peptide-modified variants, 33 AAV9/peptide-modified mosaic variants, 4 BBB-penetrating peptide-modified / tumor-targeting peptide inserted mosaic variants, 7 peptide-conjugated variants, 3 AAV9/peptide-conjugated variants, 1 dual-peptides-conjugated variant, and 1 aptamer-conjugated variant. Pooled AAVs injected to the C57BJ/6 mice included ten more variants: 1 peptide-modified variant, 1 AAV9/peptide-modified mosaic variants, 2 BBB-penetrating peptide inserted / tumor-targeting peptide inserted mosaic variants, 2 peptide-conjugated variants, and 4 AAV9/peptide-conjugated variants. Proportions of variants varied as some of them were lost during dialysis. Still, most of the variants were in the range of 5-fold to the theoretical mean proportion (Figure 26).

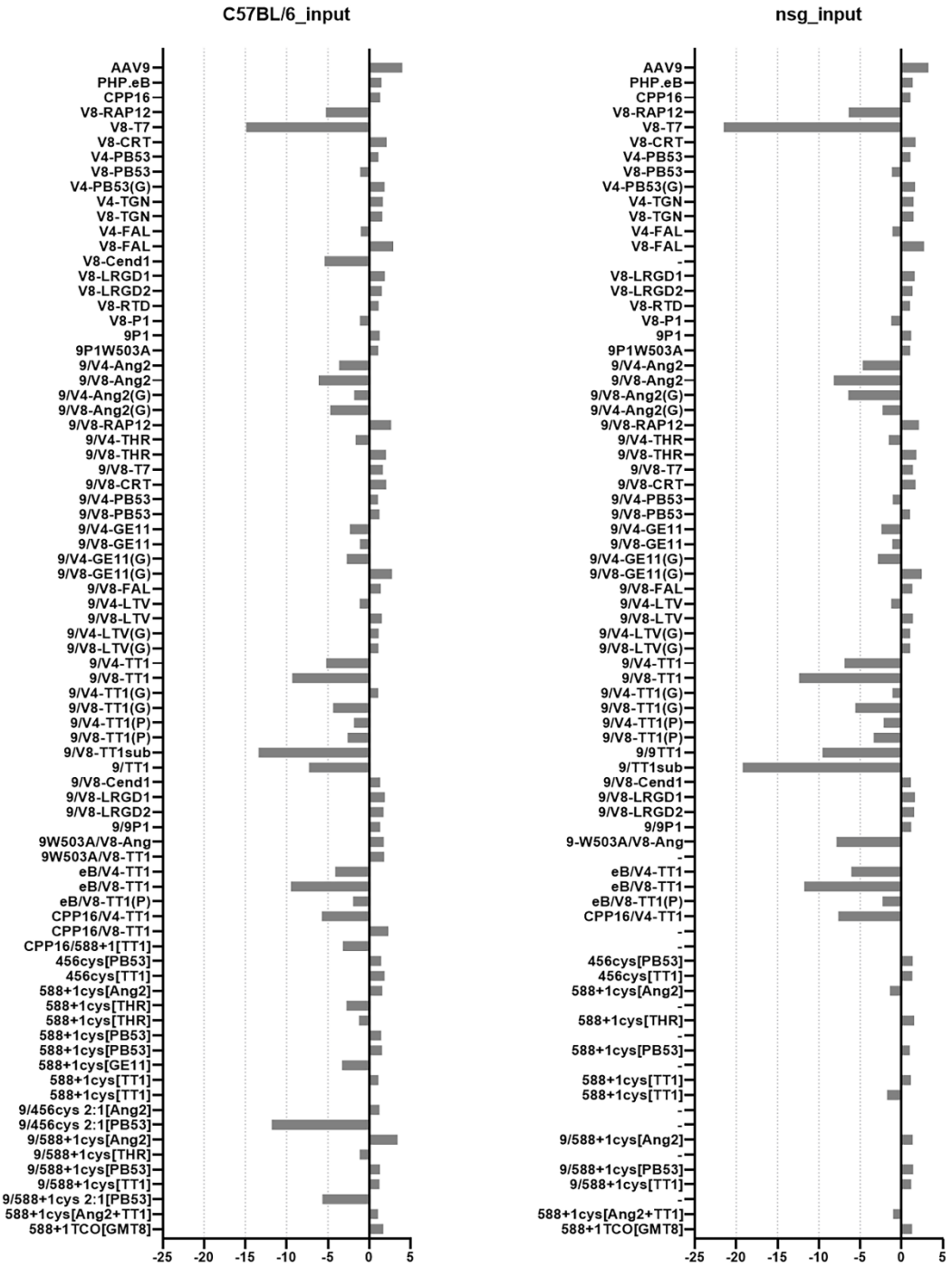

Figure 26. Composition of input libraries for nsg and C56BL/6 mouse injections.
Shown are the fold changes to the theoretical average proportion of each barcoded variant. Negative values indicate under-representation of the variant, while positive values indicate over-representation.

Normalized proportions $V_{\alpha\beta}$ were calculated and illustrate the efficiency of each AAV variant within the same tissue as the analysis in the 1st round. The profiles of transduction in U87 and GL261 GBM were again completely different from the *in vitro* experiments. Display of the TT1 peptide by either insertion or conjugation had enhanced transduction of U87 and GL261 GBM cells *in vitro* significantly (Figure 22 and Figure 25C). *In vivo*, though, none of the TT1-displaying variants showed higher transduction of GBM than AAV9 in U87- and GL261-transplanted mice.

In the U87-transplanted nsg mice, AAV9-V4-FAL became the most efficient variant in GBM, which was 2.2- and 3.5-fold higher than AAV9 at the gene expression (cDNA) and genome abundance (gDNA) levels, respectively (Figure 27). The other two FAL-displaying vectors AAV9-V8-FAL and AAV9/V8-FAL were also among the most efficient variants. Another variant, V4-TGN, was also highly efficient, and was 2.2- and 2.2-fold higher than AAV9 at the gDNA and cDNA levels, respectively. AAV9-V8-TGN, on the other hand, was not enriched in GBM. Importantly, AAV9-V4-FAL, AAV9-V8-FAL and AAV9-V4-TGN were significantly depleted from the liver, where they were 33.1-, 9.7- and 9.1-fold lower than AAV9 at the cDNA level, respectively, and 12.7-, 4.9- and 8.3-fold lower at the gDNA level, respectively. Mosaic AAV9/V8-FAL showed a milder 2-fold depletion at the cDNA and a 1.7-fold depletion at the gDNA level, probably because the capsid contained AAV9 VP. Furthermore, transduction with these four variants was specific to GBM when compared to normal brain tissue. Even though the specificity to GBM was not high, it was significantly enhanced compared to AAV9 (Figure 28). Considering the difficulty of transducing GBM and the fast proliferation of GBM, which dilutes virus genomes and thus decreases vg/dg, this result is promising. In contrast, in the GL261-transplanted mice, none of the variants transduced GBM with significantly higher efficiency than AAV9 (Figure 29).

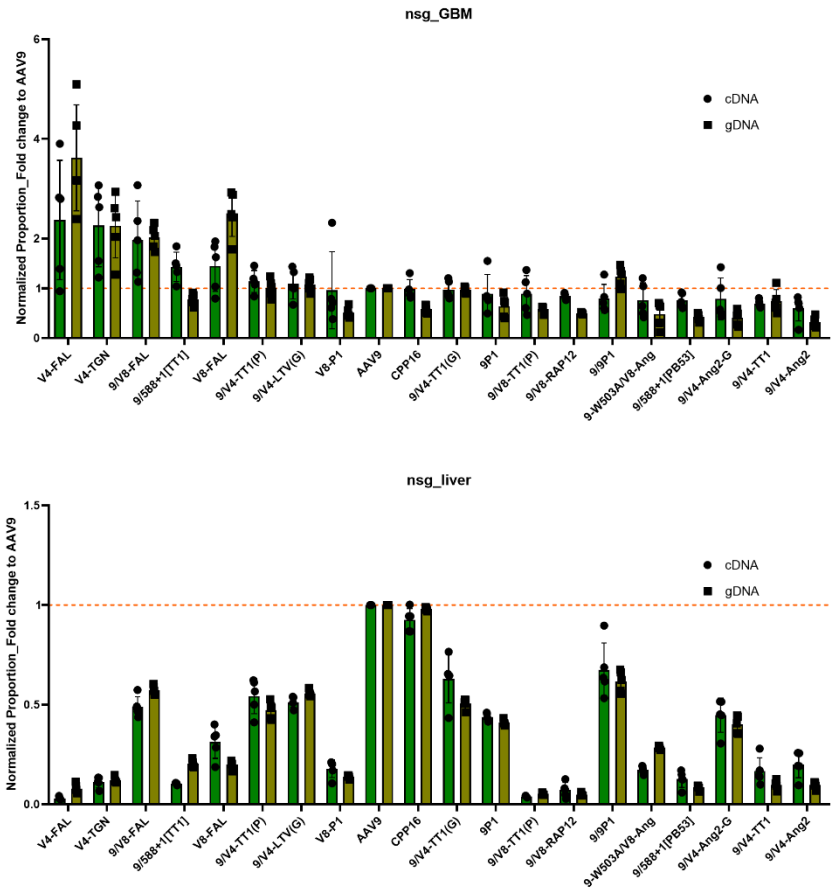

Figure 27. Transduction efficiency in GBM and liver in nsg mice.

Shown is the transduction efficiency (cDNA) and genome abundance (gDNA) in GBM and liver in nsg mice as fold change to AAV9 of the normalized proportion ($V_{\alpha\beta}$) of the top 20 AAV variants (cDNA level) in GBM. Data represent the mean ± s.d. of *n* = 5 replicates.

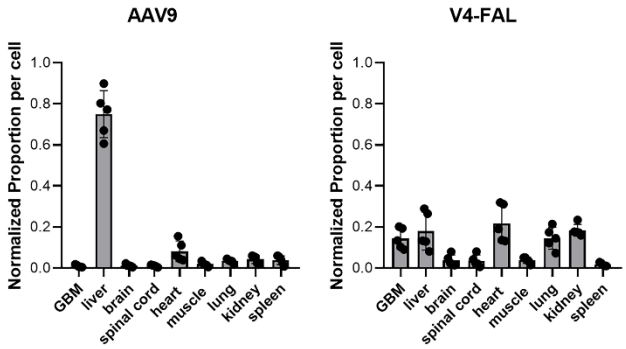

Figure 28. Transduction specificity of AAV9 and AAV9-V4-FAL in nsg mice.
Figures show the transduction specificity (cDNA) as normalized proportion per cell ($T_{\alpha\beta}$) of AAV9 and AAV9-V4-FAL in nsg mice. Data represent the mean ± s.d. of *n* = 5 replicates.

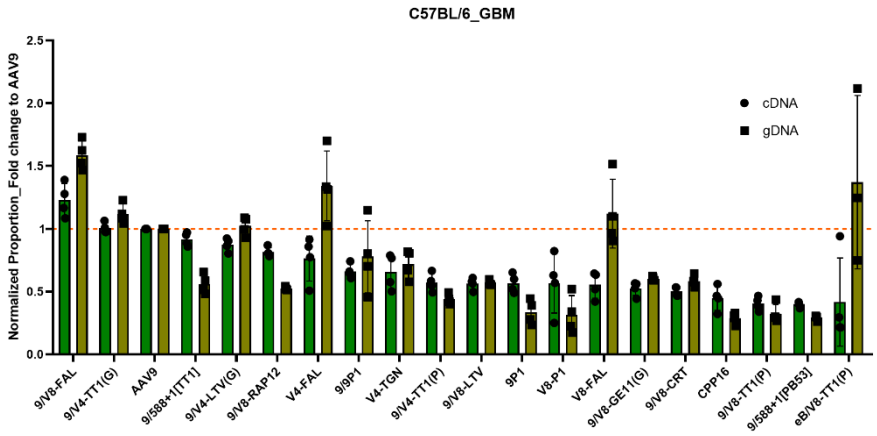

Figure 29. Transduction efficiency in GBM in C57BL/6 mice.
Figures show the transduction efficiency (cDNA) and genome abundance (gDNA) in C57BL/6 mice as fold change to AAV9 of the normalized proportion ($V_{\alpha\beta}$) of the top 20 AAV variants (cDNA level) in GBM. Data represent the mean ± s.d. of *n* = 4 replicates.

In normal brain tissue, none of the designed variants showed an enhanced transduction efficiency (Figure 30). PHP.eB and PHP.eB mosaic variants were the most efficient in C57BL/6 mice, but not in nsg mice that lack the Ly6a receptor PHP.eB. This result was consistent with published studies[216]. CPP16, however, conflicting with Yao's study[112], did not exhibit increased transduction efficiency in brain.

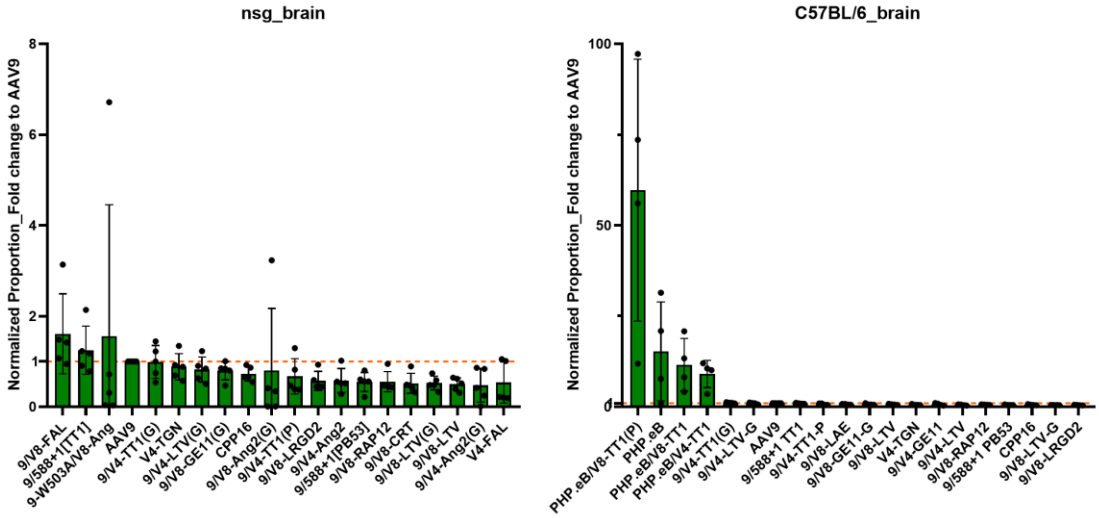

Figure 30. Transduction efficiency in brain in nsg and C57BL/6 mice.
Figures show the transduction efficiency (cDNA) in C57BL/6 mice as fold change to AAV9 of the normalized proportion ($V_{\alpha\beta}$) of the top 20 AAV variants (cDNA level) in GBM. Data represent the mean ± s.d. of *n* = 5 replicates of nsg mice and *n* = 4 of C57BL/6 mice.

AAV9-V8-RTD, AAV9-V8-P1 and AAV9P1 were the three most efficient vectors in heart and muscle (*quadriceps*) in both C57BL/6 mice (Figure 31) and nsg mice (data not shown, similar to the data in C57BL/6 mice). AAV9P1 was reported to exhibit a pronounced muscle tropism by a former member in our group, Jonas Weinmann[169]. In the present study, AAV9P1 showed a 6.6- and 2.4-fold higher transduction efficiency (cDNA) than AAV9 in muscle and heart, respectively. AAV9-V8-P1 contains the same peptide (RGDLGLS), but it was inserted into the backbone that I used for peptide insertion in this study and that contains different flanking amino acids compared to AAV9P1. AAV9-V8-P1 showed a 9.1- and 6.3-fold higher transduction efficiency (cDNA) than AAV9 in muscle and heart, respectively. AAV9-V8-RTD showed a 12.9- and 10.6-fold higher transduction efficiency (cDNA) than AAV9 in muscle and heart, respectively. AAV9-V8-RTD contains an integrin αvβ6/αvβ8-binding peptide RTD. Interestingly, integrin αvβ6 was also identified to be responsible for the muscle transduction observed in the studies of Tabebordbar *et al*.[136] and Hong *et al*.[307] Notably, genome abundances (gDNA) of AAV9-V8-RTD, AAV9-V8-P1 and AAV9P1 were also increased in heart, while in muscle they were the same as AAV9, indicating that the enhanced transduction efficiencies in muscle were likely mediated by more efficient intracellular trafficking and gene expression. While AAV9-V8-RTD and AAV9-V8-P1 exhibited better transduction in muscle and heart, the reductions of transduction in liver were not as significant as for AAV9P1. Still, AAV9-V8-RTD and AAV9-V8-P1 showed good specificity in heart and muscle, especially in the heart (Figure 32).

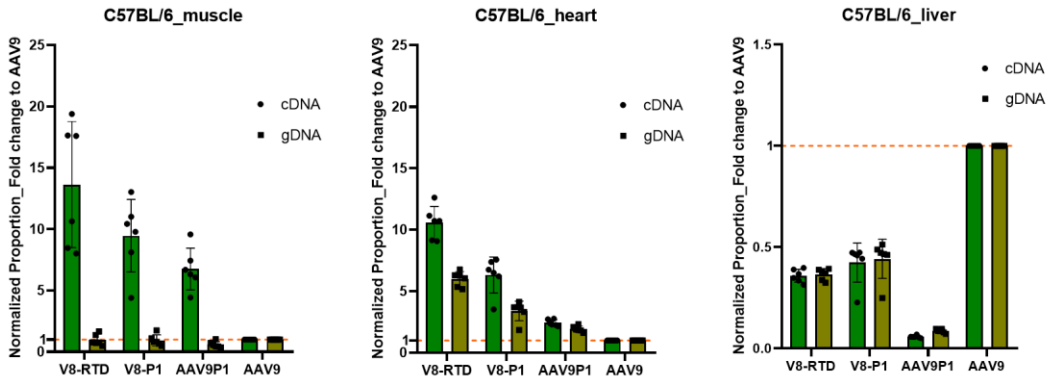

Figure 31. Transduction efficiency of AAV9-V8-RTD, AAV9-V8-P1, AAV9P1, and AAV9 in muscle, heart and liver in C57BL/6 mice.
Show are the transduction efficiencies (cDNA) and genome abundances (gDNA) as fold changes to AAV9 of the normalized proportion of V8-RTD, V8-P1, AAV9P1 and AAV9 in muscle, heart and liver in C57BL/6 mice.

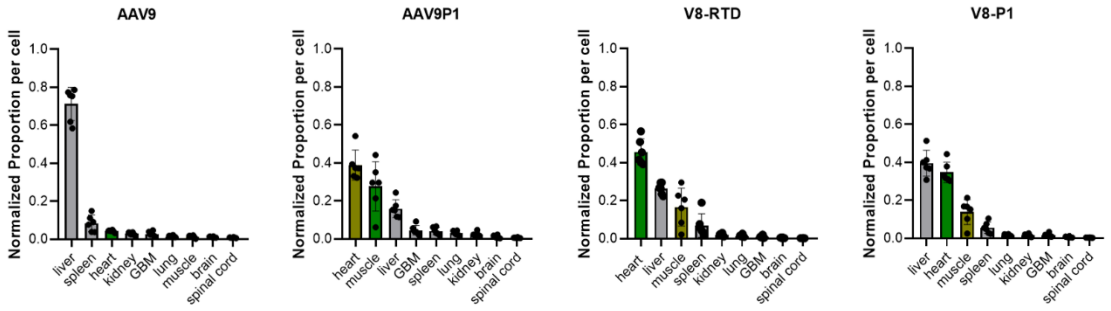

Figure 32. Transduction specificity of V8-RTD, V8-P1, AAV9P1, and AAV9 in C57BL/6 mice.
Figures show the transduction specificity (cDNA) as normalized proportion per cell ($T_{\alpha\beta}$) of V8-RTD, V8-P1, AAV9P1 and AAV9 in liver in C57BL/6 mice. Data represent the mean ± s.d. of *n* = 6 replicates.

In lung, insertion of another type of integrin-binding peptides, LRGD1 and LRGD2, which bind to integrin αvβ5 and αvβ3, enhanced the transduction efficiency (cDNA) by 1.7- and 2.9-fold, respectively (Figure 33A). However, liver remained the major target tissue for these variants (Figure 33B).

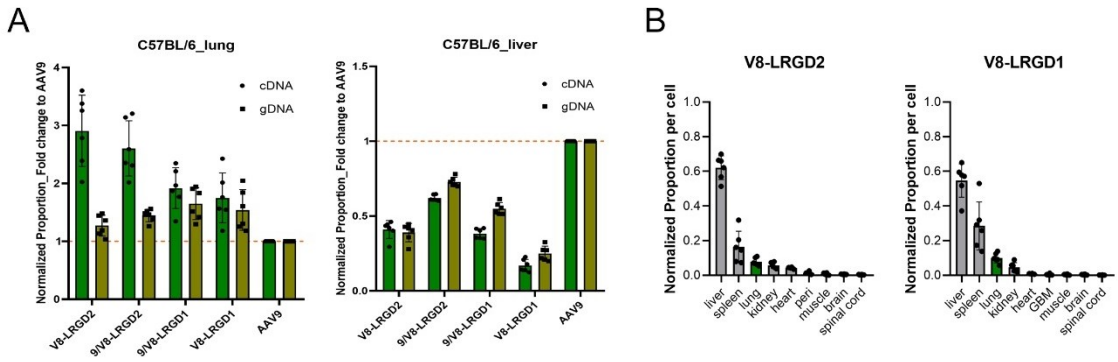

Figure 33. Transduction efficiency in lung in C57BL/6 mice.
(A) Transduction efficiency (cDNA) and genome abundance (gDNA) as fold change to AAV9 of the normalized proportion of the top 5 variants in lungs in C57BL/6 mice. (B) Transduction specificity (cDNA) as normalized proportion per cell ($T_{\alpha\beta}$) of V8-LRGD2 and V8-LRGD1 in C57BL/6 mice. Data represent the mean ± s.d. of *n* = 6 replicates.

4 Discussion

AAV capsid engineering is the principal strategy to develop AAV vectors for gene therapy with high transduction efficiency and specificity to a desired target tissue. Nowadays, directed evolution has become the most widely used method for AAV capsid engineering because it does not require preliminary knowledge of the interaction between AAVs and target cells. Typically, several rounds of selection are conducted in animal models to identify variants enriched in target tissues or cells. However, in recent years, more and more studies in different animal models have revealed that frequently, variants selected in animals fail to translate across species. One of the main reasons is the difference of receptors across species. As mentioned before, a well-known case is the PHP.B and PHP.eB variants, which exhibit a striking BBB-penetrating ability and CNS tropism in C57BL/6 mice, but not in other animals, because the receptor of these two variants, Ly6a, is specifically expressed in only some mouse strains. Therefore, to develop AAV capsids that can be used in humans for gene therapy, it is important to know the viral attachment and entry receptors.

In the study, I aimed to rationally design AAV vectors to transduce target cells by binding to cell-specific receptors. I worked on two major projects: (1) targeting to hACE2-expressing cells; and (2) penetration of the BBB followed by targeting to GBM. To achieve these goals, I decided to display already known receptor-binding ligands (peptides and proteins) on the AAV capsid. I used three different methods, namely, genetic insertion into the AAV capsid protein, chemical/covalent conjugation to the assembled AAV capsid, and non-covalent binding to the assembled AAV capsid. To achieve the site-specific chemical conjugation, I developed a novel method which allowed the conjugation on the desired site by introducing a cysteine residue. Furthermore, I adjusted the number of ligands displayed on the AAV capsid by producing mosaic capsids composed of wild-type VPs and ligand-displaying VPs. Thirdly, I displayed two ligands on the same capsid by producing mosaic capsids composed of two ligand-displaying subunits.

In the hACE2-targeting project, I tried to display RBD or RBM of SARS-CoV2, which bind to hACE2, on the AAV capsid. While the genetic insertion strategy failed, most likely due to viral protein misfolding and degradation, display of RBD on the AAV capsid via non-covalent binding was successful and achieved the desired specific transduction of hACE2-expressing cells. In the BBB-penetration and GBM-targeting project, I displayed BBB-

penetrating and tumor-targeting peptides on the AAV capsid by genetic insertion and chemical conjugation. I identified two variants, AAV9-V4-FAL and AAV9-V8-FAL, displaying the EGFR and EGFRvIII binding peptide FALGEA, which transduced GBM efficiently in U87-transplanted nsg mice after tail vein injection and which were depleted from the major off-target tissue liver. Meanwhile, from the analysis of off-target tissues, I identified another variant, AAV9-V8-RTD, displaying the integrin αvβ6/αvβ8 binding peptide RTDLDSLRT, which transduced heart and muscle with high efficiency.

During this work, I encountered numerous challenges, as can be expected from a project focused on technology development and application. This includes interesting findings that inserting a peptide/protein on the AAV capsid can lead to unexpected impacts on the expression and assembly of the capsid protein as well as modulate the binding affinity of the inserted peptide/protein. Importantly, the observations I made and the lessons I learned enabled me to come up with promising solutions and improved strategies for the future.

4.1 Challenges of Peptide and Protein Insertion

Peptide or protein insertion is a widely used method of AAV capsid modification. Many studies have previously used this method to identify AAV vectors that gained specific transduction profiles. Therefore, I used this method because, unlike directed evolution, it does not require the generation of an AAV library and several rounds of selections, granted the inserted moiety exhibits desired targeting properties. However, my studies showed that many factors can affect these properties, which can have an unpredicted impact on capsid folding, assembly and binding affinity.

4.1.1 Disulfide Bonds pose a Risk of inter-particle Aggregation

Many previously reported peptides isolated from phage display libraries and rationally designed peptides contain cysteines that form disulfide bonds, in order to create a cyclic structure that enhance peptide stability and improves target interaction. One example studied here is the P2 peptide, CDCRGDCFC, which was selected from a CX_7C (X = any amino acid) phage display library for binding with αvβ5 integrin and which is predicted to

form two pairs of disulfide bonds (C1-C9 and C3-C7)[226]. In the past, it was widely used in combination with small molecule drugs[227-229], therapeutic peptides and proteins[230-233], nanoparticles[234-238], adenoviral vectors[239-242]as well as AAV vectors[110,243 -245] to target tumors or tumor sections. Strikingly, when I produced P2-displaying AAV vectors, I observed precipitation caused by particle aggregation during vector purification and especially dialysis. This had not been reported before in publications using AAV vectors displaying this peptide. Notably, though, previous work in our own group had already noticed the production deficiency of P2-displaying AAV particles. In the present study, I discovered the reason for the low yields, namely, a loss of aggregated viral particles. This is reminiscent of a 2021 study by Stepanenko *et al.* who reported aggregation of adenovirus particles displaying this peptide due to intermolecular disulfide bonds[308]. Here, I figured that the aggregation of P2-displaying AAV capsids was also caused by the formation of intermolecular disulfide bonds. VP of wild-type AAV serotypes contains five conserved cysteine residues, which are buried inside the capsid. Based on molecular dynamics simulations, intra-subunit disulfide bonds between cys289 and cys361 and inter-subunit disulfide bonds between cys230 and cys394 are plausible, while disulfide bonds have not been observed in structural studies. Pulicherla and colleagues also proved that mutations of these cysteine residues of AAV2 VP did not impede the titer or transduction efficiency[309]. Notably, proteins can form disulfide bonds when they are translated in the endoplasmic reticulum and the mitochondrial intermembrane space, where the sulfhydryl oxidase enzymes catalyze the pairing and oxidation of the cysteine residues[310-313]. In contrast, AAV VP is expressed in the cytosol (section 1.1.3, Figure 3), where disulfide bonds cannot form due to the lack of sulfhydryl oxidases and the reducing environment maintained by NADPH-dependent reductases in healthy cells[310-313]. As a result, free cysteines can form intermolecular disulfide bonds next to the expected intramolecular disulfide bonds as soon as they are exposed to oxygen during harvest, purification and dialysis, which can readily explain my observations. Interestingly, in several studies using random peptide display AAV libraries, it was found that cysteine was depleted from the products of AAV libraries[314-317], which is possibly also due to the intermolecular disulfide bond and aggregation.

In my study, adding reducing reagent like DTT during virus harvest, purification and dialysis prevent the formation of disulfide bond and the aggregation, meanwhile the assembly and transduction efficiency of AAVs are maintained. In the future, when producing AAV vectors that contains surface-exposed cysteine residues, taking production

of cysteine-containing proteins as reference, strict redox control is required in every step of production (e.g., by using reducing agents or working in anaerobic conditions) and the final formulation (e.g., use of antioxidants) [318] (also see section 4.3). Vice versa, due to the lack of disulfide bond formation, peptides and proteins that need to form disulfide bond(s) should be excluded from the design of AAV capsid in the future.

The mechanism outlined above can possibly also explain the degradation of VP-RBD fusion proteins that I consistently observed, regardless of the insertion sites or linkers I used. Unlike AAV VP, the S-protein of SARS-CoV2 is expressed on the ER. Four pairs of disulfide bonds form in RBD, which are necessary for its correct folding, stability and binding with the hACE2 receptor[319]. Therefore, I hypothesize that the VP-RBD fusion proteins were not able to express and fold properly in the cytosol. Early study fused scFv to the N-terminus of VP2, but the titers were extremely low[320]. The following study (unpublished data, mentioned in the review[321]) figured out that this was due to the failure of disulfide bond formation in scFv in the cytosol and nucleus, which interfered with the correct folding. Notably, all proteins that have been successfully fused to the N-terminus of VP2 or inserted to the VR of VP, including DARPin[114,322-329], affibody[329], GFP[330], mCherry[117] and luciferase[331], are all non-cysteine-containing proteins. Nanobody[115,332], as an exception, has two cysteine residues, which form one pair of conserved disulfide bond. Yet, unlike conventional antibodies or antibody fragments, removal of disulfide bonds in the nanobody did not compromise its folding, mechanical stability and binding affinity[333,334].

4.1.2 Properties of the Peptide, Insertion site and Flanking Amino Acids influence the Properties of Peptide-modified AAV Variants

The length and sequence of the peptides, as well as the interaction between the peptide and surrounding amino acid residues in the AAV backbone, play important roles for the properties of the engineered capsid. As the N and C termini of VP are hidden inside the assembled capsid, the peptide can only be inserted into the central portion of VP, which is more likely to interfere with the folding of VP and therefore more challenging than its fusion to one of the termini. This is why usually only short peptides are inserted. Capsid assembly is a precise and complicated process. Therefore, even with short peptides, strong secondary structure, interaction with residues in VP, charge or other properties may impede capsid assembly. For instance, in Yao. *et al*'s study published in 2022, they

selected and inserted 14 CPPs into the AAV9 capsid between amino acids 588 and 589 in their initial round of screening, and only 5 out of 14 variants were produced efficiently[112]. In their study, it appears that amphipathic or hydrophobic CPPs are better structurally tolerated than cationic CPPs. Furthermore, in the random short peptide display AAV library, only some of all the variants are produced efficiently. Analysis of the composition of amino acid residues revealed that the bulky aromatic residues tyrosine, phenylalanine and especially tryptophan, as well as the positively charged arginine are unfavorable for production[335]. In the GBM-targeting project, insertion of several short peptides including THR, GE11, LTV and TT1 resulted in low yields. The THR peptide, for instance, contains two tryptophan and four proline residues that constrain its structural flexibility. Moreover, the predicted structure of the AAV9-V8-THR variant indicated a conformational conflict of VP trimers at the 3-fold axis. Similarly, GE11 and LTV are also rich in aromatic tryptophan and phenylalanine residues. Even though the predicted structures did not show a conformational conflict, it is likely that hydrophobic aromatic residues form strong hydrophobic cores on the surface, which compromise the stability of the capsid[336,337]. The TT1 peptide, which contains two arginine and one lysine residues, is a positively charged peptide, and therefore can repel the other subunits during assembly. To solve the difficulty of assembly, I produced mosaic capsids which are composed of the peptide-displaying VPs and the wild-type AAV9 VPs (see section 4.2).

In addition, the insertion site and the flanking amino acid residues can significantly influence the properties of the capsid. VR-IV and VR-VIII of VP form the protrusions surrounding the 3-fold axis. While VR-VIII is the first and the most commonly used insertion site, a few studies have also begun to use VR-IV as the insertion site[338,339]. Especially for proteins like DARPins and nanobodies, VR-IV was used as insertion site. In the GBM-targeting project, I therefore inserted GBM-targeting and BBB-penetrating peptides to VR-IV and VR-VIII of AAV9 VP. Interestingly, inserting into VR-IV and VR-VIII triggered differences in yield and transduction profile. For most peptides, insertion into VR-IV resulted in higher yields than insertion into VR-VIII. A recent study by Jackson and colleagues also observed that, when inserting a 36 amino acid insulin-mimetic peptide S519 to AAV9 VP, insertion in VR-IV led to a higher yield than insertion in VR-VIII[338]. Based on the structure of the AAV capsid, one possible explanation is that because VR-IV is more protruded than VR-VIII and because VR-IV is at the outer side of the protrusion, the inserted peptide at VR-IV faces less interference from neighboring residues on the same monomer during folding and from the other monomers during assembly, which leads to a

better tolerance for peptide insertion. Concurrently, it is more common that insertion into VR-IV results in lower transduction efficiency *in vitro* and significant depletion from the liver (the major target tissue for AAV9). One possible explanation is that display of peptides on VR-IV exerts a higher probability to interfere with the binding with galactose, AAVR or other unknown receptors of AAV9. Both galactose- and AAVR- binding regions of AAV9 are located at the 3-fold protrusion and 2/5-fold wall on the capsid, which are closer to VR-IV than VR-VIII[340].

Remarkably, even a minor change in the insertion site or the flanking residues can already result in significant differences. Our previous work compared the insertion of peptides in VR-VIII at two different positions with a +1 or +2 residue shift and frequently found the transduction efficiencies to be different[246]. Hong *et al*. performed computational molecular dynamics analysis of different flanking residues (two residues on each side) during their attempts to insert the 8mer peptide GRGDLGRL in VR-IV. The predicted energies for different constructs with unique flanking residues were dramatically different[307]. As another example, the difference between PHP.eB and PHP.B is a substitution of only two residues upstream of the inserted peptide, but PHP.eB exhibits a higher BBB penetration ability[216]. In my study, I mainly used GS and SG as flanking amino acids because they are small and offer flexibility. AAV9P1 (AAVmyo) was originally identified as a muscle-tropic capsid[169]. Here, I found that the AAV9-V8-P1 variant, which has the same P1 insertion in VR-VIII as AAV9P1 but different flanking residues, showed even higher transduction in muscle and heart (but less depletion from the liver) than the AAV9P1 variant. This makes this new capsid highly interesting for further investigation and development, and ultimately for application in muscle gene therapy.

In summary, the properties of the inserted peptide itself, the insertion site as well as the flanking amino acids can influence the expression, assembly and binding affinity of the peptide-displaying AAV variant. Consequently, the results of this work show that when inserting new peptides into the AAV capsid, optimizations need to be considered and performed for each peptide and each capsid backbone. A common optimization method is to generate and screen subtle changes in the insert and flanking amino acids. For example, the PHP.eB variant was selected from an AAV capsid library in which the PHP.B was modified by randomizing three consecutive amino acids in an overlapping fashion across the heptamer insert and flanking amino acids. Santon *et al.* discovered a PAL motif for transduction in macaque CNS from an AAV peptide display library. Similarly, they

conducted a second round of selection of a library in which the second and sixth residues of the heptamer insert and the three upstream flanking residues were varied.

4.2 Mosaic Capsids and Double-Modified Capsids

Producing mosaic capsids can be used to: (1) adjust the number of inserted peptides or conjugated molecules on the capsid, and (2) combine the properties of two different capsid variants.

When the displayed peptide or protein is large, to enable capsid assembly, the number of peptides or proteins on each capsid may need to be reduced. This can be achieved by producing a mosaic capsid, which is composed of the peptide- or protein-displaying VPs and the corresponding wild-type VPs. For instance, nanobodies and DARPins are only displayed on VP1 or VP2, which results in 1-5 copies on each capsid[114,115,322-329,332]. When I attempted to produce SARS-CoV-2 RBD- and RBM-displaying vectors, I used the same strategies. Mosaic capsid can also be produced by mixing AAV helper plasmids encoding VP1-VP3 of two different serotypes, and the ratio can be changed by changing the ratio of the plasmids. In my study, because several peptide-displaying AAV variants were not able to assemble and be produced efficiently, I produced mosaic capsids consisting of the peptide-displaying VPs and wild-type AAV9 VPs. Indeed, this enabled the assembly of capsids and rescued the yields to amounts comparable to wild-type AAV9.

The change of number of peptides on the capsid can also change the transduction profile, with the optimal number varying for different peptides. In the study where the insulin-mimetic peptide S519 was displayed on AAV9, Jackson *et al.* found that using 1:10 ratio of AAV9-S519 and AAV9 resulted in the highest transduction in HEK293T cells[338]. In my study, I mainly used a 1:1 ratio of peptide-displaying variant and AAV9. AAV9P2 exhibited improved transduction efficiency in GL261 and U87 cells *in vitro*, while AAV9/AAV9P2 further enhanced the efficiency significantly. At the same time, AAV9/PHP.eB showed a significantly higher transduction in the brain of C57BL/6 mice than AAV9, but lower than PHP.eB. Meanwhile, AAV9/AAV9-V8-FAL showed a similar GBM transduction efficiency as AAV9-V8-FAL in U87-transplanted mice. Notably, in the *in vivo* study, AAV9 mosaic capsids retained the liver tropism of AAV9. In some previous studies, the W503A mutation was used to deplete the binding with galactose[128]. Here, I produced two variants, AAV9^{W503A}/AAV9-V8-Ang2 and AAV9^{W503A}/AAV9-V8-TT1, which were substantially

detargeted from the liver compared with AAV9/AAV9-V8-Ang2 and AAV9/AAV9-V8-TT1. Therefore, in the future, using AAV9 with mutations of galactose-binding residues (e.g., D271A, N272A, Y446A, N470A and W503A) may aid in liver detargeting of the AAV9 mosaic capsid.

Mosaic capsids can also be produced to combine the properties of two different serotypes. Therefore, mosaic capsids of wild-type AAVs have been generated before. In 2003, Hauck *et al.* generated AAV1/2 mosaic vectors (AAV1 and AAV2 at a 1:1 ratio), which exhibited transduction similar to AAV1 in muscle after local injection and similar to AAV2 in liver after intravenous administration[164]. A recent study in 2023 generated an AAV2.1 mosaic vector (AAV1 and AAV2 at a 1:9 ratio), which exhibited the same high efficiency as AAV1 and the identical high specificity as AAV2 for neurons after cortical injection[341]. In my study, I attempted to combine the properties of two peptide-displaying serotypes. Indeed, PHP.eB/AAV9-V8-TT1 showed enhanced transduction in GBM cells *in vitro* as AAV9-V8-TT1, and enhanced BBB penetration and transduction in brain in C57BL/6 mice as PHP.eB. PHP.eB/AAV9P1 showed brain tropism as PHP.eB and muscle tropism as AAV9P1 in C57BL/6 mice. Even though the aim was not fully achieved *in vivo* because displaying P2, P1 and TT1 peptides failed to target GBM *in vivo*, the mosaic capsid strategy is still promising once a peptide-displaying variant that can target GBM efficiently *in vivo* has been identified.

Yet another way to potentially combine the properties of two peptides on the capsid is to display one peptide on VR-VIII and another peptide on VR-IV. Goertsen *et al.* generated this kind of double-modified AAV library in which 7 amino acids (453-459) in VR-IV of PHP.eB were substituted with random heptamer peptides[342]. They identified CAP-B10 and CAP-B22 variants that crossed BBB of C57BL/6 mice as PHP.eB, and obtained a novel property of crossing the BBB in marmosets. In my study, the double-modified PHP.eB-P2 showed enhanced transduction in GBM cells *in vitro*, but failed in mice for the same reason as mosaic capsids.

4.3 Site-Specific Chemical Modification Method

As noted above, due to the interaction between the inserted peptide and neighboring amino acid residues in AAV VP, genetic insertion can lead to several problems including failure of expression and assembly of VP, changes in the binding affinity of the peptide,

etc. Chemical conjugation after AAV production is an alternative method, which has the benefit that it does not influence VP expression and assembly, while largely preserving the binding affinity of the peptide. Furthermore, chemical conjugation allows to link a wide variety of components, which can bring novel properties to the AAV capsid.

Chemical modification of the AAV capsid requires a bioconjugation method, which allows for the conjugation under physiological conditions to avoid disrupting AAV capsid functionality. The traditional method relies on the primary amine group (-NH2) of lysine residues. A concern with this method is the lack of control over the exact site, as each VP contains several lysine residues. In turn, this can lead to undesired modifications of functional lysine residues and a heterogenous mixture of particles with different conjugation patterns. In particular, this modification method is not applicable to a capsid that contains genetic insertion of a peptide with lysine residues. A solution may be provided by GCE technology that enables site-specific modification of proteins.

In this study, I established and validated a workflow for a novel site-specific modification method relying on the thiol (-SH) of a cysteine residue. Because no cysteine exists on the surface of the AAV capsid, site-specific conjugation was achieved by first introducing a cysteine on the desired surface-exposed site and subsequential reaction with maleimide-bearing molecules. When using the GCE technology, because the efficiency of orthogonal aaRS/tRNA in eukaryotic cells is not high, the yield of ncAA-containing AAVs is decreased compared with corresponding wild-type AAVs. Furthermore, ncAAs are large, which leads to limited flexibility of incorporation sites. Notably, cysteine is small and encoded by endogenous aaRS/tRNA. Therefore, the expression of cysteine-modified VP is efficient and cysteine introduction is tolerated in many surface-exposed sites. The yields of all cysteine-containing AAVs that I tested in my study (incorporation site 456, 588+1, 660, 718) were the same as, or even higher than, wild-type AAV9. AAV9-456cys and AAV9-588+1cys were used for peptide conjugation, which solved the aforementioned issue that genetic insertion of some peptides had resulted in very low yields. As a proof-of-concept experiment, conjugation of the TT1 peptide on 588+1 site significantly enhanced the transduction efficiency in U87 cells *in vitro,* which also strongly surpassed the performance of variants with genetic insertion of TT1 peptide.

Furthermore, as a second benefit over GCE, it is easier to produce mosaic capsids containing cysteine-incorporated VPs. The number of peptides conjugated on the capsid influences the transduction. Even though this can be adjusted by restricting the degree of

conjugation, obtaining an accurate control is difficult, therefore this approach leads to a highly heterogeneous mixture of products. In 2023, Erickson and colleagues developed ncAA-incorporated mosaic capsids by incorporating ncAAs in VP1 or VP1+VP2, which led to 1-10 conjugation sites on each capsid[343]. For cysteine-modified VP, because it does not require the orthogonal aaRS/tRNA, the expression of cysteine-carrying VP is the same as wild-type VP. Therefore, mosaic capsids can also be produced simply by mixing the helper plasmids, and the number of cysteine-incorporated VP can be flexibly adapted by changing the ratio of AAV helper plasmids. Here, I produced AAV9/AAV9-456cys and AAV9/AAV9-588+1cys. Besides, mosaic capsids that consist of cysteine-modified VP and peptide-modified VP were also produced without difficulty (eg. CPP16/AAV9-588+1cys).

A noteworthy advantage of chemical conjugation is that it allows for the display of non-peptide molecules. GalNac, mannose, eosin, folic acid, DNA aptamer have all been conjugated before to change the transduction of AAV capsids. Interestingly, ncAA itself also changed particle transduction properties in many cell lines and tissues. In this study, I obtained a preliminary validation of this concept by tethering small molecules such as biotin or DNA aptamers onto the capsid. Furthermore, other than chemically synthesized components, this method allows for the conjugation of proteins. Hence, I tried to conjugate SARS-CoV-2 RBD onto the AAV2^{RA}-454cys and AAV2^{RA}-587cys capsids. The idea is to first conjugate AAV capsids with Maleimide-PEG4-Tetrazine linker, which can then react with TCO-modified RBD. While the AAV2^{RA}-454cys and AAV2^{RA}-587cys could be successfully produced, work on producing TCO-modified RBD with the GCE technology is ongoing. During the time of the writing of this thesis, a nanobody-conjugated AAV capsid was reported[159]. In this study, a Azk-modified AAV capsid was produced and conjugated with a DBCO-Tetrazine linker. A Azk-modified nanobody was produced and conjugated with the DBCO-PEG4-TCO linker, and the final conjugation was between Tetrazine and TCO.

To date, chemical conjugation has not been used as widely as genetic engineering of the AAV capsid, but pilot studies have already clearly demonstrated the capacity of this method to modify the AAV capsid's tissue tropism and to evade its detection by the immune system. In my study, a new method of site-specific chemical modification of AAV capsids has been established and its impact on transduction efficiency was shown *in vitro*. However, the conjugation sites, the number of ligands on each capsid, the length of the

linker as well as the process of production and storage need to be further optimized to enhance the performance of ligand-conjugated capsids especially *in vivo.*

Another application of site-specific conjugation is to conjugate tracer molecules like fluorescent dyes or positron emitters. Live-cell imaging is a powerful method to study the infection pathway of viruses. Early studies conjugated fluorescent dyes on lysine residues to enable real-time imaging in live cells[59,66,344]. Positron emitters were also conjugated for positron emission tomography, which can trace the biodistribution of the AAVs *in vivo*. Site-specific conjugation can minimize the impact on the infection pathway and biodistribution, especially when choosing a conjugation site located away from receptor binding regions. For this purpose, I introduced cysteines at 660 and 718 residues, respectively, which are apart from the receptor binding region of AAV9 and peptide-modified AAV9 variants.

4.4 Challenges of BBB-penetrating and GBM-targeting attempts

Besides the inherent difficulties of displaying receptor-binding peptides on the AAV capsid, another major obstacle to rationally develop AAV variants that transduce target cells via binding to a given receptor is choosing the target receptor itself. For most tissues, specific receptors that can be targeted remain unknown. GBM is particularly hard to transduce because it is located in the CNS, hence the AAVs need to penetrate the BBB to reach it. Moreover, it is typically heterogenous so that no overexpressed or specifically expressed receptors exist on all cells within these tumors.

4.4.1 Design of AAV Vectors to Penetrate BBB via Binding to Receptors that Mediate RMT

In recent years, many AAV variants with enhanced BBB-penetrating and CNS-transducing efficiency have been discovered by directed evolution. Early studies mainly performed screenings in mice. However, AAV variants selected in mice often failed to translate to NHPs, which raised concerns about directed evolution and in particular the selection models. In 2023, Stanton *et al.* compared the results of screenings in mice and macaques, which revealed that the variants selected in CNS of mice and macaques have largely different sequences[345]. Moreover, the variants selected in mice were unable to improve BBB penetration in macaques, and, vice versa, the variants selected in macaques were

unable to improve BBB-penetration in mice. Even more surprisingly, the two variants CAP-10 and CAP-B22, which were selected in mice and showed enhanced CNS transduction in marmosets, failed to enhance CNS transduction in macaque. In 2023, a comprehensive study of variant CAP-Mac, which was selected in marmosets, showed that even though it has enhanced CNS transduction in mice, marmosets, and macaques, cell-type tropisms are different in different animal models[346]. The complexity of the CNS poses additional challenges in cross-species transduction. Therefore, to achieve successful translation from animal models to clinical applications in human, transduction via a known and translatable mechanism is required.

For large molecules like AAV vectors, one of the most promising methods to penetrate the BBB is RMT. LRP1 and TfR are well-known receptors for RMT. Several LRP1-binding and TfR-binding peptides have been discovered from phage display peptide libraries or derived from the endogenous binding proteins. Therefore, I attempted to display LRP1-binding peptides (Ang2 and RAP12) and TfR-binding peptides (THR, T7 and CRT) on AAV9 capsids by means of genetic insertion and chemical conjugation. Several studies have used BBB-penetrating peptides or CPPs to facilitate AAV to penetrate the BBB and transduce the CNS. For instance, Yao *et al*. designed AAV9 variants with CPPs inserted between residues 588 and 589 of VP. They identified two variants that displayed Ku70-derived Bip1 (VPALR) and Bip2 (VSALK) peptides with enhanced brain transduction in mouse after intravenous injection. They further modified Ku70-derived peptides and identified AAV.CPP16 and AAV.CPP21, displaying TVSALK and TVSALFK peptides, respectively, with further improved transduction efficiencies in the CNS after systemic administration in four mouse strains and macaques[112]. In another example. Zhang *et al*. showed that incubation with the TfR-binding peptide THR, enhanced AAV8 transduction in the brain after retro-orbital injection in C57BL/6 mice. In that study, instead of insertion into the AAV VP, BBB-penetrating peptides were simply incubated with AAV8[162]. A similar study reported by Meng *et al*. exemplfied how incubation with the CPP peptide LAH4 enhanced AAV9 transduction in the brain after tail vein injection in C57BL/6 mice[163]. However, notably, the enhancement of transduction in these two studies was not brain-specific. A more recent study by Zhang *et al*. identified a novel BBB-penetrating peptide, PB5-3, which enhanced AAV9 transduction specifically in the CNS[304] in mice, thus I used PB5-3 in my own study as well.

When conjugated to drugs, proteins or nanoparticles, Ang2, RAP12, THR, T7 and CRT have been validated for binding with human receptors, facilitating uptake by receptor-expressing cells *in vitro* and aiding penetration of the BBB in mouse[283-302]. Surprisingly, in my study, none of the peptide-displaying variants exhibited enhanced transduction in normal brain tissue or GBM. These results may again illustrate how a change in the method of displaying peptides can change the binding affinity to the receptors and the transduction of the associated AAV vectors. Taking the PB5-3 peptide as an example, while its incubation significantly enhanced BBB penetration with AAV9 in the study by Zhang and colleagues, neither genetic insertion nor chemical conjugation of this peptide to AAV9 had an effect in my own study. Therefore, further improvements of peptide grafting (see sections 4.1 and 4.3) or alternative methods (see section 4.5) are required to develop AAV variants that can bind with RMT receptors and penetrate the BBB. Nonetheless, targeting the RMT receptor remains a promising area of further research and development. In 2024, Huang *et al.* identified TfR-binding AAVs that can penetrate the BBB and transduce CNS cells efficiently in human TfR-transgene mice, by screening a random peptide display AAV library for binding to human TfR and transducing human TfR-overexpressing cells[347]. This is the first successful development of AAV variants to cross the BBB based on a known receptor and mechanism of action. Interestingly, four identified variants only bound to human TfR but not macaque, marmoset or mouse TfR, which emphasizes the importance of selecting AAVs for binding with known and desired receptors.

In my study, consisting with the published data, the benchmark PHP.eB showed a robust enhancement of transduction in healthy brain tissue in C57BL/6 mice. I also found that the PHP.eB mosaic capsid maintained efficient transduction in brain. However, it is worth nothing that enhancement of BBB penetration does not automatically yield enhancement of GBM transduction. In fact, PHP.eB and PHP.eB-derived variants showed a tropism towards healthy brain cells and transduced GBM even less efficiently than AAV9. Therefore, it remains an important and challenging goal for future work to develop a vector that can concurrently penetrate the BBB and exhibit GBM tropism from systemic delivery.

4.4.2 Design of AAV Vectors to target GBM via Binding to Receptors that Are Overexpressed or Specifically Expressed in GBM

In this study, I displayed the EGFR-binding peptide GE11, the EGFRvIII and EGFR dual binding peptide FAL, the HER2-binding peptide LTV, the p32-binding peptide TT1, the neuropilin-1-binding peptide Cend1, and the integrin-binding peptides LRGD1, LRGD2, RTD, P1, P2 as well as P2-derived peptides on the AAV capsid. Prior studies had reported the conjugation of these peptides on drugs, micelles and other nanoparticles to deliver therapeutic materials to GBM.

Here, I found that the FAL-displaying variant AAV9-V4-FAL gave a 2.2-fold higher transduction in GBM and a 33.1-fold lower transduction in the liver (the major off-target tissue) compared to wild-type AAV after tail vein injection of U87-transplanted nsg mice. Furthermore, it showed tropism to the GBM compared with to the normal brain tissue. Another FAL-displaying variant, AAV9-V8-FAL, also yielded a 1.4-fold higher transduction in GBM and a 9.7-fold lower transduction in liver. The FAL peptide was first reported to bind with EGFRvIII[263] and later found to also exhibit a lower binding affinity with EGFR[264]. Both EGFR and EGFRvIII are prominent target receptors for GBM. EGFR has been identified as a prime oncogene in several tumors including GBM. It is amplified in approximately 40% and overexpressed in approximately 60% of GBM, while its expression is very low in normal brain tissues. EGFRvIII is an EGFR mutant with a deletion of amino acid residues 6-273 in the extracellular domain, which leads to a constitutive activity. EGFRvIII is found in 20-30% of GBM and is a tumor-specific surface marker, which is only present in tumors, in particular ovarian, breast cancer and GBM. Further experiments are required to validate whether AAV9-V4-FAL and AAV9-V8-FAL indeed bind with EGFRvIII and EGFR, and whether the observed enhanced transduction in U87 xenografts were indeed mediated by EGFR or EGFRvIII. In GL261-transplanted C57BL/6 mice, AAV9-V4-FAL and AAV9-V8-FAL did not give higher transduction in GBM compared to AAV9. One possible reason that could be studied in the future is that the expression level of EGFR is lower in GL261 cells. In fact, the expression levels of EGFR, and especially EGFRvIII, are not high in either U87 or GL261 cell lines. To further investigate the biology of AAV9-V4-FAL and AAV9-V8-FAL, GBM cells that express high levels of EGFR or EGFRvIII (e.g., U87-EGFR or U87-EGFRvIII) should be used. To target a specific receptor, using cell lines that overexpress the receptor will give a better result, making this approach also more reasonable for future investigations. However, one should be aware that, compared to the

realistic clinical application, using overexpressing cell lines may lead to an over-estimation of transduction results.

All other peptides tested in this work failed to enhance transduction in GBM. Possible explanations include that (1) the binding affinities of the peptides were lost after insertion in the AAV capsid, (2) expression levels of the targeted receptors were too low in the two cell types, (3) binding with receptors was not enough for efficient and specific transduction in GBM, or (4) the vectors cannot cross the BBB. Further experiments are needed to elucidate and overcome the exact mechanism(s).

In recent years, several AAV vectors that target tumor receptors have been developed. In 2020, Feiner *et al*. designed an AAV variant with an EGFR-binding peptide insertion between residues 587 and 588 of AAV2^{RA} VP, which showed specific transduction to EGFR-overexpressing cell and tumor xenografts in chicken egg chorioallantoic membrane assays[348]. In this study, the authors computationally designed two novel β-hairpin peptides that bind to the EGFR dimerization domain and inserted these peptides into the AAV2 capsid. A HER2-binding DARPin was inserted into AAV capsids and mediated the specific transduction in subcutaneously SK-OV-3-derived tumors and RENCA-Her2/neu-derived tumors after intravenous injection[322,323]. In 2021, Strecker *et al.* used this HER2-DARPin-displaying AAV (HER2-AAV) to transduce HER2-expressing GL261 and LN-319 GBM transplants in mice[349]. They investigated transduction of GBM cells by HER2-AAV via intravenous or intratumoral injections in subcutaneous or orthotopic intracranial tumors. HER2-AAV transduced subcutaneous tumor cells via both of intravenous and intratumoral injections, while transducing intracranial tumors only via intratumoral injection, which indicated that HER2-AAV can transduce HER2-expressing tumors but cannot penetrate the BBB. This study again emphasizes the importance of developing AAV vectors that can target GBM and penetrate the BBB as well. It is noteworthy that in these studies, receptor-overexpressing cells were used.

Thus far, direct targeting of these receptors with conventional drugs has yielded mixed results. The major reasons include: (1) The inhibition of these receptors by drugs provided no therapeutic benefits; (2) the receptors are not expressed in all of the GBM cells, leaving cells not expressing the receptors are resistant to the drugs; (3) the receptors are not specific for the tumor cells, resulting in adverse side effects in normal cells. Theoretically, using AAV-mediated gene therapy promises to overcome these constrains. Firstly, it does not exert its therapeutic effect through direct targeting of these receptors. Instead,

targeting mainly serves for AAV binding and transduction, while the actual therapeutic effect is executed by the transgene. Secondly, therapeutic transgenes can exert bystander effects on the neighboring cells. For instance, the toxic metabolites expressed from a suicide gene can be transferred from transduced tumor cells to neighboring tumor cells[350-352]. Thirdly, specificity can be further improved by using tumor-specific promoters (e.g., alpha-fetoprotein promoter (AFP), thyroid transcription factor 1 (TTF-1), glypican-3 protein (GPC3), etc.) for detargeting from healthy cells[353,354,].

4.5 Integrin as Target Receptor

Integrins, especially αvβ3/αvβ5, have been extensively pursued for tumor targeting, because they are overexpressed in many tumor cells and in cells in the tumor microenvironment, such as endothelial cells. RGD is recognized as a well-known integrin binding motif, which can bind with αvβ3, αvβ5 as well as six other integrins (αvβ1, αvβ6, αvβ8, α5β1, α8β1, and αIIbβ3)[355]. Different RGD-containing peptides have been identified and incorporated on the surface of vectors to deliver therapeutic drugs and genes to the tumor. RGD-containing peptides have also been genetically inserted[110,243,245,246] or chemically conjugated[156,157] to AAV capsids to transduce tumor cells, while only a few studies conducted systematic administration of AAV vectors *in vivo*[245] and the other studies only conducted *in vitro* transduction[156,243, 246] or local injection of AAV *in vivo*[110,157]. In my study, displaying of αvβ3/αvβ5 binding peptides P2 and LRGD on the AAV capsid dramatically enhanced the transduction efficiency in GBM cell lines *in vitro.* However, they failed to enhance the transduction in GBM in mice after systematic intravenous injection. In Michelfelder *et al.*'s study, when conducting directed evolution of an AAV peptide display library for transducing breast cancer cells *in vitro*, they found that the top variants often contain an RGD motif. However, these variants were not efficient for transduction *in vivo* after intravenous administration[133].

Beyond cancer, integrins may also be explotied as target receptors for other tissues. A striking finding from our group is that the AAVmyo (AAV9P1) variant, which contains RGDLGLS peptides, showed efficient and specific transduction in skeletal muscle in mice after intravenous injection[169]. Interestingly, when conducting directed evolution of an AAV peptide display library in mice, Tabebordbar *et al*. observed that the top candidates selected in skeletal muscle and heart also contain the RGD motif[136]. They further identified

that integrin αvβ6 mediates the transduction of these variants. Later on, Hong *et al.* designed a variant displaying peptide GRGDLGRL that is derived from the endogenous αvβ6 binding protein human TGF-β3, which also transduced skeletal muscle efficiently[307]. In my study, I found that a novel variant AAV-V8-RTD, which displays peptide RTDLDSLRT, showed 2.1- and 4.4-fold higher transduction efficiency than AAVmyo in muscle and heart, respectively. RTDLDSLRT, as a non-RGD αvβ6/αvβ8 binding peptide, has high binding specificity to αvβ6/αvβ8 integrins[281,282]. Besides, RTDLDSLRT was initially selected for binding with human αvβ6 integrin and showed efficient transduction in muscle and heart in mice in my study, which indicates a high chance of successful translation across species. Further optimization of the RTDLDSLRT-modified capsid can potentially create novel variants with even higher transduction efficiency and specificity.

4.6 Conclusions and Prospectives

Directed evolution in animals has become the preferred method for capsid engineering because it does not require prior understanding of the AAV infection pathway. However, it also comprises concerns about the translation of evolved capsids across species due to the differences of receptors in different species. Therefore, I aimed to engineer AAVs that bind to specific and already known receptors using SARS-CoV2 and GBM as model systems. Specifically, I used the most direct way by grafting known receptor-binding peptides onto the AAV capsid. However, this yielded several unexpected findings including perturbances of folding and assembly, or changes in the binding affinity. Therefore, in the future, an optimization of peptide display or the exploration of alternative ways to generate receptor-binding AAVs are required. I also developed a site-specific chemical modification method, which can conjugate peptides on the AAV capsid without influencing capsid assembly and genome encapsidation, albeit the *in vivo* performance of chemically modified vectors still needs to be improved. In the future, performing selection for receptor binding of an AAV peptide display library is a direct, effective and high-throughput way, which can overcome the difficulties of grafting peptides selected from other contexts.

Even when a capsid specifically binds to a given receptor, this does not guarantee that it can functionally transduce the receptor-expressing cells, especially *in vivo*. Furthermore, one of the predominant challenges of AAV capsid engineering is that in the most cases, transduction results in cells *in vitro* are not necessarily translatable to animals *in vivo*,

especially when the particles are administered systematically. This was also observed in my study during the GBM-targeting project. Possible explanations include that the composition of the extracellular matrix changes when the cells are cultured *in vitro*. For example, it was found that the HSPG-binding motif of AAV2 was evolved during passaging of cells in culture, which can explain why AAV2 is one of the most efficient natural AAV serotypes *in vitro* but not efficient for *in vivo* transduction[356]. AAV9, on the other hand, is not efficient *in vitro* but is one of the most potent natural AAV serotypes *in vivo*. Moreover, AAVs are taken up by other tissues during their circulation in the organism after systemic administration, which emphasizes the importance of performing *in vivo* studies.

In the future, a promising approach is the combination of *in vitro* receptor-binding screening to generate a sub-library of AAVs that can bind with the specific receptor, and a subsequent *in vivo* study to identify the AAV variants that can transduce target tissue also in a living organism. With this strategy, it will ideally be possible to identify variants that can be translated from *in vitro* to *in vivo*, and that function across species. It is noteworthy that in Huang *et al.* 's study, the AAV variants selected for binding human TfR cannot bind mouse or macaque TfR[357]. Moreover, Shay *et al.* found that the variants 9P31 and 9P36 that were selected for BBB-penetrating in mice bind Carbonic anhydrase IV (CA-IV) for RMT, yet they can only bind mouse CA-IV but not human or macaque CA-IV[358]. This suggests that one should select variants that can bind with the receptors of animal models and also humans, or that the field should use human receptor-transgenic animals for *in vivo* selection.

As mentioned before, the specific receptors of most target tissues that can be used as target receptors remain unknown. Fortunately, though, with the help of *in vivo* AAV library screenings, additional receptors have been identified in recent years, including the well-known example of Ly6A for PHP.eB. Notably, this receptor is lacking in humans, which once again exemplifies the relevance of a proper selection model. In 2023, a study by Shay *et al.* identified CA-IV as a novel receptor for crossing the BBB, by screening potential receptors that are highly and specifically expressed in the endothelial cells of the brain of various engineered BBB-penetrating AAV variants[358]. In 2024, the same group identified another receptor, LRP6, for several BBB-penetrating AAV variants by using microarray screening of over 6400 cell membrane proteins[359]. These two receptors may thus be useful as target receptors for selection of further BBB-penetrating AAV variants in the future. Additionally, as noted before, in Tabebordbar *et al*.'s study, they identified

integrin αvβ6 as the target receptor for skeletal muscle and heart[136]. Accordingly, there is every reason to hope and believe that continued bioinformatic analysis and experimental studies will unravel many more receptors for transduction of target tissues and cells, which will pave the way for a new generation of rationally designed AAVs with maximum efficiency, specificity and safety in humans or across species.

Reference

1. Atchison, Robert W., Bruce C. Casto, and William McD Hammon. "Adenovirus-associated defective virus particles." Science 149.3685 (1965): 754-756.
2. Hoggan, M. David, Neil R. Blacklow, and WP224346 Rowe. "Studies of small DNA viruses found in various adenovirus preparations: physical, biological, and immunological characteristics." *Proceedings of the National Academy of Sciences* 55.6 (1966): 1467-1474.
3. Buller, Robert ML, *et al*. "Herpes simplex virus types 1 and 2 completely help adenovirus-associated virus replication." *Journal of virology* 40.1 (1981): 241-247.
4. Weindler, Friedrich W., and R. E. G. I. N. E. Heilbronn. "A subset of herpes simplex virus replication genes provides helper functions for productive adeno-associated virus replication." *Journal of virology* 65.5 (1991): 2476-2483.
5. You, Hong, *et al*. "Multiple human papillomavirus genes affect the adeno-associated virus life cycle." *Virology* 344.2 (2006): 532-540.
6. Rose, James A., *et al*. "Evidence for a single-stranded adenovirus-associated virus genome: formation of a DNA density hybrid on release of viral DNA." *Proceedings of the National Academy of Sciences* 64.3 (1969): 863-869.
7. Green, MICHAEL R., and ROBERT G. Roeder. "Transcripts of the adeno-associated virus genome: mapping of the major RNAs." Journal of Virology 36.1 (1980): 79-92.
8. Berns, K. I., and S. Adler. "Separation of two types of adeno-associated virus particles containing complementary polynucleotide chains." *Journal of Virology* 9.2 (1972): 394-396.
9. Srivastava, Arun, E. W. Lusby, and KENNETH I. Berns. "Nucleotide sequence and organization of the adeno-associated virus 2 genome." *Journal of virology* 45.2 (1983): 555-564.
10. Balakrishnan, Balaji, and Giridhara R Jayandharan. "Basic biology of adeno-associated virus (AAV) vectors used in gene therapy." Current gene therapy 14.2 (2014): 86-100.
11. Koczot, Frank J., *et al*. "Self-complementarity of terminal sequences within plus or minus strands of adenovirus-associated virus DNA." *Proceedings of the National Academy of Sciences* 70.1 (1973): 215-219.
12. Becerra, S. P., *et al*. "Synthesis of adeno-associated virus structural proteins requires both alternative mRNA splicing and alternative initiations from a single transcript." Journal of virology 62.8 (1988): 2745-2754.
13. Trempe, JAMES P., and BARRIE J. Carter. "Alternate mRNA splicing is required for synthesis of adeno-associated virus VP1 capsid protein." *Journal of virology* 62.9 (1988): 3356-3363.
14. Bennett, Antonette, Mario Mietzsch, and Mavis Agbandje-McKenna. "Understanding capsid assembly and genome packaging for adeno-associated viruses." Future virology 12.6 (2017): 283-297.
15. Wörner, Tobias P., *et al*. "Adeno-associated virus capsid assembly is divergent and stochastic." Nature communications 12.1 (2021): 1642.
16. Chiorini, J. A., *et al*. "The roles of AAV Rep proteins in gene expression and targeted integration." Adeno-Associated Virus (AAV) Vectors in Gene Therapy (1996): 25-33.
17. McCARTY, DOUGLAS M., *et al*. "Identification of linear DNA sequences that specifically bind the adeno-associated virus Rep protein." Journal of virology 68.8 (1994): 4988-4997.
18. Im, D. S., and N. I. C. H. O. L. A. S. Muzyczka. "Partial purification of adeno-associated virus Rep78, Rep52, and Rep40 and their biochemical characterization." Journal of virology 66.2 (1992): 1119-1128.
19. Recchia, Alessandra, and Fulvio Mavilio. "Site-specific integration by the adeno-associated virus rep protein." *Current gene therapy* 11.5 (2011): 399-405.
20. Sonntag, Florian, Kristin Schmidt, and Jürgen A. Kleinschmidt. "A viral assembly factor promotes AAV2 capsid formation in the nucleolus." Proceedings of the National Academy of Sciences 107.22 (2010): 10220-10225.

21. Sonntag, F., *et al*. "The assembly-activating protein promotes capsid assembly of different adeno-associated virus serotypes." *Journal of virology* 85.23 (2011): 12686-12697.
22. Naumer, Matthias, *et al*. "Properties of the adeno-associated virus assembly-activating protein." Journal of virology 86.23 (2012): 13038-13048.
23. Ogden, Pierce J., *et al*. "Comprehensive AAV capsid fitness landscape reveals a viral gene and enables machine-guided design." Science 366.6469 (2019): 1139-1143.
24. Galibert, Lionel, *et al*. "Functional roles of the membrane-associated AAV protein MAAP." Scientific reports 11.1 (2021): 21698.
25. Aksu Kuz, Cagla, *et al*. "Role of the membrane-associated accessory protein (MAAP) in adeno-associated virus (AAV) infection." Journal of Virology 98.6 (2024): e00633-24.
26. Kronenberg, Stephanie, Jürgen A. Kleinschmidt, and Bettina Böttcher. "Electron cryo-microscopy and image reconstruction of adeno-associated virus type 2 empty capsids." EMBO reports 2.11 (2001): 997-1002.
27. Xie, Qing, *et al*. "The atomic structure of adeno-associated virus (AAV-2), a vector for human gene therapy." Proceedings of the National Academy of Sciences 99.16 (2002): 10405-10410.
28. Govindasamy, Lakshmanan, *et al*. "Structurally mapping the diverse phenotype of adeno-associated virus serotype 4." *Journal of virology* 80.23 (2006): 11556-11570.
29. Agbandje-McKenna, M. A. V. I. S., and MICHAEL S. Chapman. *Correlating structure with function in the viral capsid*. Edward Arnold, New York, New York, 2006.
30. Van Vliet, Kim M., *et al*. "The role of the adeno-associated virus capsid in gene transfer." *Drug Delivery Systems* (2008): 51-91.
31. Kronenberg, Stephanie, *et al*. "A conformational change in the adeno-associated virus type 2 capsid leads to the exposure of hidden VP1 N termini." Journal of virology 79.9 (2005): 5296-5303.
32. Venkatakrishnan, Balasubramanian, *et al*. "Structure and dynamics of adeno-associated virus serotype 1 VP1-unique N-terminal domain and its role in capsid trafficking." *Journal of virology* 87.9 (2013): 4974-4984.
33. Rayaprolu, Vamseedhar, *et al*. "Comparative analysis of adeno-associated virus capsid stability and dynamics." *Journal of virology* 87.24 (2013): 13150-13160.
34. DiMattia, Michael A., *et al*. "Structural insight into the unique properties of adeno-associated virus serotype 9." *Journal of virology* 86.12 (2012): 6947-6958.
35. Wu, Pei, *et al*. "Mutational analysis of the adeno-associated virus type 2 (AAV2) capsid gene and construction of AAV2 vectors with altered tropism." *Journal of virology* 74.18 (2000): 8635-8647.
36. Bleker, Svenja, Florian Sonntag, and Jürgen A. Kleinschmidt. "Mutational analysis of narrow pores at the fivefold symmetry axes of adeno-associated virus type 2 capsids reveals a dual role in genome packaging and activation of phospholipase A2 activity." *Journal of virology* 79.4 (2005): 2528-2540.
37. Srivastava, Arun. "In vivo tissue-tropism of adeno-associated viral vectors." *Current opinion in virology* 21 (2016): 75-80.
38. Maurer, Anna C., and Matthew D. Weitzman. "Adeno-associated virus genome interactions important for vector production and transduction." *Human Gene Therapy* 31.9-10 (2020): 499-511.
39. Summerford, Candace, and Richard Jude Samulski. "Membrane-associated heparan sulfate proteoglycan is a receptor for adeno-associated virus type 2 virions." *Journal of virology* 72.2 (1998): 1438-1445.
40. Qing, Keyun, *et al*. "Human fibroblast growth factor receptor 1 is a co-receptor for infection by adeno-associated virus 2." *Nature medicine* 5.1 (1999): 71-77.
41. Kashiwakura, Yuji, *et al*. "Hepatocyte growth factor receptor is a coreceptor for adeno-associated virus type 2 infection." *Journal of virology* 79.1 (2005): 609-614.
42. Akache, Bassel, *et al*. "The 37/67-kilodalton laminin receptor is a receptor for adeno-associated virus serotypes 8, 2, 3, and 9." *Journal of virology* 80.19 (2006): 9831-9836.

43. Summerford, Candace, Jeffrey S. Bartlett, and Richard Jude Samulski. "αVβ5 integrin: a co-receptor for adeno-associated virus type 2 infection." *Nature medicine* 5.1 (1999): 78-82.
44. Asokan, Aravind, *et al*. "Adeno-associated virus type 2 contains an integrin α5β1 binding domain essential for viral cell entry." *Journal of virology* 80.18 (2006): 8961-8969.
45. Pillay, S., *et al*. "An essential receptor for adeno-associated virus infection." *Nature* 530.7588 (2016): 108-112.
46. Dudek, Amanda M., *et al*. "GPR108 is a highly conserved AAV entry factor." *Molecular Therapy* 28.2 (2020): 367-381.
47. Meisen, W. Hans, *et al*. "Pooled screens identify GPR108 and TM9SF2 as host cell factors critical for AAV transduction." *Molecular Therapy-Methods & Clinical Development* 17 (2020): 601-611.
48. Wu, Zhijian, *et al*. "α2, 3 and α2, 6 N-linked sialic acids facilitate efficient binding and transduction by adeno-associated virus types 1 and 6." *Journal of virology* 80.18 (2006): 9093-9103.
49. Handa, Atsushi, *et al*. "Adeno-associated virus (AAV)-3-based vectors transduce haematopoietic cells not susceptible to transduction with AAV-2-based vectors." *Journal of General Virology* 81.8 (2000): 2077-2084.
50. Ling, Chen, *et al*. "Human hepatocyte growth factor receptor is a cellular coreceptor for adeno-associated virus serotype 3." *Human gene therapy* 21.12 (2010): 1741-1747.
51. Akache, Bassel, *et al*. "The 37/67-kilodalton laminin receptor is a receptor for adeno-associated virus serotypes 8, 2, 3, and 9." *Journal of virology* 80.19 (2006): 9831-9836.
52. Kaludov, Nikola, *et al*. "Adeno-associated virus serotype 4 (AAV4) and AAV5 both require sialic acid binding for hemagglutination and efficient transduction but differ in sialic acid linkage specificity." *Journal of virology* 75.15 (2001): 6884-6893.
53. Pasquale, Giovanni Di, *et al*. "Identification of PDGFR as a receptor for AAV-5 transduction." *Nature medicine* 9.10 (2003): 1306-1312.
54. Ng, Robert, *et al*. "Structural characterization of the dual glycan binding adeno-associated virus serotype 6." *Journal of virology* 84.24 (2010): 12945-12957.
55. Weller, Melodie L., *et al*. "Epidermal growth factor receptor is a co-receptor for adeno-associated virus serotype 6." *Nature medicine* 16.6 (2010): 662-664.
56. Shen, Shen, *et al*. "Terminal N-linked galactose is the primary receptor for adeno-associated virus 9." *Journal of Biological Chemistry* 286.15 (2011): 13532-13540.
57. Duan, Dongsheng, *et al*. "Dynamin is required for recombinant adeno-associated virus type 2 infection." *Journal of virology* 73.12 (1999): 10371-10376.
58. Nonnenmacher, Mathieu, and Thomas Weber. "Adeno-associated virus 2 infection requires endocytosis through the CLIC/GEEC pathway." *Cell host & microbe* 10.6 (2011): 563-576.
59. Sanlioglu, Salih, *et al*. "Endocytosis and nuclear trafficking of adeno-associated virus type 2 are controlled by rac1 and phosphatidylinositol-3 kinase activation." *Journal of virology* 74.19 (2000): 9184-9196.
60. Bantel-Schaal, Ursula, Birgit Hub, and Juergen Kartenbeck. "Endocytosis of adeno-associated virus type 5 leads to accumulation of virus particles in the Golgi compartment." *Journal of virology* 76.5 (2002): 2340-2349.
61. Nonnenmacher, Mathieu E., *et al*. "Syntaxin 5-dependent retrograde transport to the trans-Golgi network is required for adeno-associated virus transduction." *Journal of virology* 89.3 (2015): 1673-1687.
62. Sonntag, Florian, *et al*. "Adeno-associated virus type 2 capsids with externalized VP1/VP2 trafficking domains are generated prior to passage through the cytoplasm and are maintained until uncoating occurs in the nucleus." *Journal of virology* 80.22 (2006): 11040-11054.
63. Stahnke, Stefanie, *et al*. "Intrinsic phospholipase A2 activity of adeno-associated virus is involved in endosomal escape of incoming particles." *Virology* 409.1 (2011): 77-83.
64. Lins-Austin, Bridget, *et al*. "Adeno-associated virus (AAV) capsid stability and liposome remodeling during endo/lysosomal pH trafficking." Viruses 12.6 (2020): 668.

65. Douar, Anne-Marie, *et al*. "Intracellular trafficking of adeno-associated virus vectors: routing to the late endosomal compartment and proteasome degradation." *Journal of virology* 75.4 (2001): 1824-1833.
66. Seisenberger, Georg, *et al*. "Real-time single-molecule imaging of the infection pathway of an adeno-associated virus." *Science* 294.5548 (2001): 1929-1932.
67. Johnson, Jarrod S., and R. Jude Samulski. "Enhancement of adeno-associated virus infection by mobilizing capsids into and out of the nucleolus." *Journal of virology* 83.6 (2009): 2632-2644.
68. Kelich, Joseph M., *et al*. "Super-resolution imaging of nuclear import of adeno-associated virus in live cells." *Molecular Therapy Methods & Clinical Development* 2 (2015).
69. Bevington, Joyce M., *et al*. "Adeno-associated virus interactions with B23/Nucleophosmin: identification of sub-nucleolar virion regions." *Virology* 357.1 (2007): 102-113.
70. Sutter, Sereina O., *et al*. "Adeno-associated virus type 2 (AAV2) uncoating is a stepwise process and is linked to structural reorganization of the nucleolus." *PLoS Pathogens* 18.7 (2022): e1010187.
71. Ni, Tie-Hua, *et al*. "In vitro replication of adeno-associated virus DNA." *Journal of virology* 68.2 (1994): 1128-1138.
72. Nakai, Hiroyuki, Theresa A. Storm, and Mark A. Kay. "Recruitment of single-stranded recombinant adeno-associated virus vector genomes and intermolecular recombination are responsible for stable transduction of liver in vivo." *Journal of virology* 74.20 (2000): 9451-9463.
73. McCarty, Douglas M., Samuel M. Young Jr, and R. Jude Samulski. "Integration of adeno-associated virus (AAV) and recombinant AAV vectors." *Annu. Rev. Genet.* 38.1 (2004): 819-845.
74. Samulski, R. J., *et al*. "Targeted integration of adeno-associated virus (AAV) into human chromosome 19." *The EMBO journal* 10.12 (1991): 3941-3950.
75. Linden, R. Michael, *et al*. "Site-specific integration by adeno-associated virus." *Proceedings of the National Academy of Sciences* 93.21 (1996): 11288-11294.
76. Pereira, Daniel J., Douglas M. McCarty, and Nicholas Muzyczka. "The adeno-associated virus (AAV) Rep protein acts as both a repressor and an activator to regulate AAV transcription during a productive infection." *Journal of virology* 71.2 (1997): 1079-1088.
77. Brister, J. Rodney, and Nicholas Muzyczka. "Mechanism of Rep-mediated adeno-associated virus origin nicking." *Journal of virology* 74.17 (2000): 7762-7771.
78. Dubielzig, Ralf, *et al*. "Adeno-associated virus type 2 protein interactions: formation of pre-encapsidation complexes." *Journal of virology* 73.11 (1999): 8989-8998.
79. King, Jason A., *et al*. "DNA helicase-mediated packaging of adeno-associated virus type 2 genomes into preformed capsids." *The EMBO journal* (2001).
80. Samulski, Richard Jude, Long-Sheng Chang, and T. Shenk. "Helper-free stocks of recombinant adeno-associated viruses: normal integration does not require viral gene expression." *Journal of virology* 63.9 (1989): 3822-3828.
81. Matsushita, T., *et al*. "Adeno-associated virus vectors can be efficiently produced without helper virus." *Gene therapy* 5.7 (1998): 938-945.
82. Ylä-Herttuala, Seppo. "Endgame: glybera finally recommended for approval as the first gene therapy drug in the European union." *Molecular Therapy* 20.10 (2012): 1831-1832.
83. Smalley, Eric. "First AAV gene therapy poised for landmark approval." Nature biotechnology 35.11 (2017): 998-1000.
84. Hoy, Sheridan M. "Onasemnogene abeparvovec: first global approval." *Drugs* 79.11 (2019): 1255-1262.
85. Keam, Susan J. "Eladocagene exuparvovec: first approval." *Drugs* 82.13 (2022): 1427-1432.
86. Blair, Hannah A. "Valoctocogene roxaparvovec: first approval." *Drugs* 82.14 (2022): 1505-1510.
87. Navale, Mr Sachin, *et al*. "Hemgenix as first gene therapy for treatment of haemophilia B." *Haemophilia* 2.1 (2022).
88. Mullard, Asher. "FDA approves first gene therapy for Duchenne muscular dystrophy, despite internal objections." *Nat Rev Drug Discov* 22.8 (2023): 610.

89. Dhillon, Sohita. "Fidanacogene elaparvovec: first approval." *Drugs* 84.4 (2024): 479-486.
90. Shen, Weiran, Shengjiang Liu, and Li Ou. "rAAV immunogenicity, toxicity, and durability in 255 clinical trials: A meta-analysis." *Frontiers in immunology* 13 (2022): 1001263.
91. Ertl, Hildegund CJ. "Immunogenicity and toxicity of AAV gene therapy." *Frontiers in Immunology* 13 (2022): 975803.
92. Paulk, Nicole. "Gene Therapy: It Is Time to Talk about High-Dose AAV: The deaths of two children with X-linked myotubular myopathy in the ASPIRO trial prompts a reexamination of vector safety." *Genetic Engineering & Biotechnology News* 40.9 (2020): 14-16.
93. Duan, Dongsheng, *et al*. "A new dual-vector approach to enhance recombinant adeno-associated virus-mediated gene expression through intermolecular cis activation." *Nature medicine* 6.5 (2000): 595-598.
94. Nakai, Hiroyuki, Theresa A. Storm, and Mark A. Kay. "Increasing the size of rAAV-mediated expression cassettes in vivo by intermolecular joining of two complementary vectors." *Nature biotechnology* 18.5 (2000): 527-532.
95. Duan, Dongsheng, Yongping Yue, and John F. Engelhardt. "Expanding AAV packaging capacity with trans-splicing or overlapping vectors: a quantitative comparison." *Molecular therapy* 4.4 (2001): 383-391.
96. Lopes, Vanda S., *et al*. "Retinal gene therapy with a large MYO7A cDNA using adeno-associated virus." *Gene therapy* 20.8 (2013): 824-833.
97. Trapani, Ivana, *et al*. "Improved dual AAV vectors with reduced expression of truncated proteins are safe and effective in the retina of a mouse model of Stargardt disease." *Human molecular genetics* 24.23 (2015): 6811-6825.
98. Chen, Lingxia, *et al*. "The enhancing effects of the light chain on heavy chain secretion in split delivery of factor VIII gene." *Molecular therapy* 15.10 (2007): 1856-1862.
99. Tornabene, Patrizia, *et al*. "Intein-mediated protein trans-splicing expands adeno-associated virus transfer capacity in the retina." *Science translational medicine* 11.492 (2019): eaav4523.
100. Domenger, Claire, and Dirk Grimm. "Next-generation AAV vectors—do not judge a virus (only) by its cover." *Human molecular genetics* 28.R1 (2019): R3-R14.
101. Paterna, J. C., *et al*. "Influence of promoter and WHV post-transcriptional regulatory element on AAV-mediated transgene expression in the rat brain." *Gene therapy* 7.15 (2000): 1304-1311.
102. Senís, Elena, *et al*. "CRISPR/Cas9-mediated genome engineering: an adeno-associated viral (AAV) vector toolbox." *Biotechnology journal* 9.11 (2014): 1402-1412.
103. Patrício, Maria I., *et al*. "Inclusion of the woodchuck hepatitis virus posttranscriptional regulatory element enhances AAV2-driven transduction of mouse and human retina." *Molecular Therapy-Nucleic Acids* 6 (2017): 198-208.
104. Wang, Dan, *et al*. "Adeno-associated virus neutralizing antibodies in large animals and their impact on brain intraparenchymal gene transfer." *Molecular Therapy-Methods & Clinical Development* 11 (2018): 65-72.
105. Wang, Z., *et al*. "Rapid and highly efficient transduction by double-stranded adeno-associated virus vectors in vitro and in vivo." *Gene therapy* 10.26 (2003): 2105-2111.
106. McCarty, D. M., *et al*. "Adeno-associated virus terminal repeat (TR) mutant generates self-complementary vectors to overcome the rate-limiting step to transduction in vivo." *Gene therapy* 10.26 (2003): 2112-2118.
107. Wu, Zhijian, *et al*. "Optimization of self-complementary AAV vectors for liver-directed expression results in sustained correction of hemophilia B at low vector dose." *Molecular Therapy* 16.2 (2008): 280-289.
108. Girod, Anne, *et al*. "Genetic capsid modifications allow efficient re-targeting of adeno-associated virus type 2." *Nature medicine* 5.9 (1999): 1052-1056.
109. Grifman, Mirta, *et al*. "Incorporation of tumor-targeting peptides into recombinant adeno-associated virus capsids." *Molecular Therapy* 3.6 (2001): 964-975.

110. Shi, Wenfang, and Jeffrey S. Bartlett. "RGD inclusion in VP3 provides adeno-associated virus type 2 (AAV2)-based vectors with a heparan sulfate-independent cell entry mechanism." *Molecular Therapy* 7.4 (2003): 515-525.
111. Yu, Chi-Yi, *et al*. "A muscle-targeting peptide displayed on AAV2 improves muscle tropism on systemic delivery." *Gene therapy* 16.8 (2009): 953-962.
112. Yao, Yizheng, *et al*. "Variants of the adeno-associated virus serotype 9 with enhanced penetration of the blood–brain barrier in rodents and primates." *Nature biomedical engineering* 6.11 (2022): 1257-1271.
113. Yang, Qicheng, *et al*. "Development of novel cell surface CD34-targeted recombinant adenoassociated virus vectors for gene therapy." *Human gene therapy* 9.13 (1998): 1929-1937.
114. Münch, Robert C., *et al*. "Displaying high-affinity ligands on adeno-associated viral vectors enables tumor cell-specific and safe gene transfer." Molecular therapy 21.1 (2013): 109-118.
115. Eichhoff, Anna Marei, *et al*. "Nanobody-enhanced targeting of AAV gene therapy vectors." *Molecular Therapy-Methods & Clinical Development* 15 (2019): 211-220.
116. Warrington Jr, Kenneth H., *et al*. "Adeno-associated virus type 2 VP2 capsid protein is nonessential and can tolerate large peptide insertions at its N terminus." *Journal of virology* 78.12 (2004): 6595-6609.
117. Judd, Justin, *et al*. "Random insertion of mCherry into VP3 domain of adeno-associated virus yields fluorescent capsids with no loss of infectivity." *Molecular Therapy-Nucleic Acids* 1 (2012).
118. Michels, Alexander, *et al*. "Lentiviral and adeno-associated vectors efficiently transduce mouse T lymphocytes when targeted to murine CD8." *Molecular Therapy-Methods & Clinical Development* 23 (2021): 334-347.
119. Asokan, Aravind, *et al*. "Reengineering a receptor footprint of adeno-associated virus enables selective and systemic gene transfer to muscle." *Nature biotechnology* 28.1 (2010): 79-82.
120. Shen, Shen, *et al*. "Engraftment of a galactose receptor footprint onto adeno-associated viral capsids improves transduction efficiency." *Journal of Biological Chemistry* 288.40 (2013): 28814-28823.
121. Zhong, L. I., *et al*. "Tyrosine-phosphorylation of AAV2 vectors and its consequences on viral intracellular trafficking and transgene expression." *Virology* 381.2 (2008): 194-202.
122. Zhong, Li, *et al*. "Next generation of adeno-associated virus 2 vectors: point mutations in tyrosines lead to high-efficiency transduction at lower doses." *Proceedings of the National Academy of Sciences* 105.22 (2008): 7827-7832.
123. Markusic, David M., *et al*. "High-efficiency transduction and correction of murine hemophilia B using AAV2 vectors devoid of multiple surface-exposed tyrosines." *Molecular Therapy* 18.12 (2010): 2048-2056.
124. Kern, A. S. C. H. M. I. D. T., *et al*. "Identification of a heparin-binding motif on adeno-associated virus type 2 capsids." *Journal of virology* 77.20 (2003): 11072-11081.
125. Bell, Christie L., *et al*. "Identification of the galactose binding domain of the adeno-associated virus serotype 9 capsid." *Journal of virology* 86.13 (2012): 7326-7333.
126. Hoffman, Jacob A., *et al*. "Modulation of AAV9 Galactose Binding Yields Novel Gene Therapy Vectors and Predicts Cross-Species Differences in Glycan Avidity." *Human Gene Therapy* 35.17-18 (2024): 734-753.
127. Boucas, Jorge, *et al*. "Engineering adeno-associated virus serotype 2-based targeting vectors using a new insertion site-position 453-and single point mutations." *The Journal of Gene Medicine: A cross-disciplinary journal for research on the science of gene transfer and its clinical applications* 11.12 (2009): 1103-1113.
128. Giannelli, Serena Gea, *et al*. "New AAV9 engineered variants with enhanced neurotropism and reduced liver off-targeting in mice and marmosets." *Iscience* 27.5 (2024).

129. Li, Chengwen, *et al*. "Single amino acid modification of adeno-associated virus capsid changes transduction and humoral immune profiles." *Journal of virology* 86.15 (2012): 7752-7759.
130. Selot, Ruchita, *et al*. "Optimized AAV rh. 10 vectors that partially evade neutralizing antibodies during hepatic gene transfer." *Frontiers in Pharmacology* 8 (2017): 441.
131. Perabo, Luca, *et al*. "In vitro selection of viral vectors with modified tropism: the adeno-associated virus display." *Molecular therapy* 8.1 (2003): 151-157.
132. Müller, Oliver J., *et al*. "Random peptide libraries displayed on adeno-associated virus to select for targeted gene therapy vectors." *Nature biotechnology* 21.9 (2003): 1040-1046.
1st two papers
133. Michelfelder, Stefan, *et al*. "Successful expansion but not complete restriction of tropism of adeno-associated virus by in vivo biopanning of random virus display peptide libraries." *PloS one* 4.4 (2009): e5122.
134. Körbelin, Jakob, *et al*. "Pulmonary targeting of adeno-associated viral vectors by next-generation sequencing-guided screening of random capsid displayed peptide libraries." *Molecular therapy* 24.6 (2016): 1050-1061.
135. Deverman, Benjamin E., *et al*. "Cre-dependent selection yields AAV variants for widespread gene transfer to the adult brain." *Nature biotechnology* 34.2 (2016): 204-209.
136. Tabebordbar, Mohammadsharif, *et al*. "Directed evolution of a family of AAV capsid variants enabling potent muscle-directed gene delivery across species." *Cell* 184.19 (2021): 4919-4938.
137. Grimm, Dirk, *et al*. "In vitro and in vivo gene therapy vector evolution via multispecies interbreeding and retargeting of adeno-associated viruses." *Journal of virology* 82.12 (2008): 5887-5911.
138. Tse, Longping Victor, *et al*. "Structure-guided evolution of antigenically distinct adeno-associated virus variants for immune evasion." *Proceedings of the National Academy of Sciences* 114.24 (2017): E4812-E4821.
139. Paulk, Nicole K., *et al*. "Bioengineered AAV capsids with combined high human liver transduction in vivo and unique humoral seroreactivity." *Molecular Therapy* 26.1 (2018): 289-303.
140. El Andari, Jihad, *et al*. "Semirational bioengineering of AAV vectors with increased potency and specificity for systemic gene therapy of muscle disorders." *Science advances* 8.38 (2022): eabn4704.
141. Perabo, Luca, *et al*. "Combinatorial engineering of a gene therapy vector: directed evolution of adeno-associated virus." The Journal of Gene Medicine: A cross-disciplinary journal for research on the science of gene transfer and its clinical applications 8.2 (2006): 155-162.
142. Qian, Randolph, *et al*. "Directed evolution of AAV serotype 5 for increased hepatocyte transduction and retained low humoral seroreactivity." *Molecular Therapy-Methods & Clinical Development* 20 (2021): 122-132.
143. Zinn, Eric, et al. "In silico reconstruction of the viral evolutionary lineage yields a potent gene therapy vector." *Cell reports* 12.6 (2015): 1056-1068.
144. Santiago-Ortiz, Jorge, et al. "AAV ancestral reconstruction library enables selection of broadly infectious viral variants." *Gene therapy* 22.12 (2015): 934-946.
145. Bryant, Drew H., et al. "Deep diversification of an AAV capsid protein by machine learning." *Nature Biotechnology* 39.6 (2021): 691-696.
146. Marques, Andrew D., et al. "Applying machine learning to predict viral assembly for adeno-associated virus capsid libraries." *Molecular Therapy-Methods & Clinical Development* 20 (2021): 276-286.
147. Zhu, Danqing, et al. "Optimal trade-off control in machine learning–based library design, with application to adeno-associated virus (AAV) for gene therapy." *Science Advances* 10.4 (2024): eadj3786.

148. Lee, Gary K., *et al*. "PEG conjugation moderately protects adeno-associated viral vectors against antibody neutralization." *Biotechnology and bioengineering* 92.1 (2005): 24-34.
149. Le, Hong T., *et al*. "Utility of PEGylated recombinant adeno-associated viruses for gene transfer." Journal of controlled release 108.1 (2005): 161-177
150. Mével, Mathieu, *et al*. "Chemical modification of the adeno-associated virus capsid to improve gene delivery." *Chemical science* 11.4 (2020): 1122-1131.
151. Yuan, Zhefan, *et al*. "Mitigating the immunogenicity of AAV-mediated gene therapy with an immunosuppressive phosphoserine-containing zwitterionic peptide." *Journal of the American Chemical Society* 144.44 (2022): 20507-20513.
152. Mulcrone, Patrick L., *et al*. "Chemical modification of AAV9 capsid with N-ethyl maleimide alters vector tissue tropism." *Scientific Reports* 13.1 (2023): 8436.
153. Yoo, Seungju, *et al*. "A versatile adeno-associated viral vector cross-linking platform capable of tuning cellular tropisms and simultaneously inducing solid-phase gene delivery." *ACS Applied Bio Materials* 3.8 (2020): 4847-4857.
154. Horowitz, Eric D., Marc S. Weinberg, and Aravind Asokan. "Glycated AAV vectors: chemical redirection of viral tissue tropism." *Bioconjugate chemistry* 22.4 (2011): 529-532.
155. Leray, Aurélien, *et al*. "Novel chemical tyrosine functionalization of adeno-associated virus improves gene transfer efficiency in liver and retina." *Biomedicine & Pharmacotherapy* 171 (2024): 116148.
156. Kelemen, Rachel E., *et al*. "A precise chemical strategy to alter the receptor specificity of the adeno-associated virus." *Angewandte Chemie International Edition* 55.36 (2016): 10645-10649.
157. Zhang, Chuanling, *et al*. "Development of next generation adeno-associated viral vectors capable of selective tropism and efficient gene delivery." *Biomaterials* 80 (2016): 134-145.
158. Puzzo, Francesco, *et al*. "Aptamer-programmable adeno-associated viral vectors as a novel platform for cell-specific gene transfer." *Molecular Therapy-Nucleic Acids* 31 (2023): 383-397.
159. Pham, Quan, *et al*. "A facile chemical strategy to synthesize precise AAV-protein conjugates for targeted gene delivery." *bioRxiv* (2024): 2024-07.
160. Chang, Hao, *et al*. "Non-canonical amino acid incorporation into AAV5 capsid enhances lung transduction in mice." Molecular Therapy Methods & Clinical Development 31 (2023).
161. Bartlett, Jeffrey S., *et al*. "Targeted adeno-associated virus vector transduction of nonpermissive cells mediated by a bispecific F (ab'γ) 2 antibody." Nature biotechnology 17.2 (1999): 181-186.
162. Zhang, Xintao, *et al*. "Blood-brain barrier shuttle peptides enhance AAV transduction in the brain after systemic administration." Biomaterials 176 (2018): 71-83.
163. Meng, Yuan, *et al*. "Cell-penetrating peptides enhance the transduction of adeno-associated virus serotype 9 in the central nervous system." Molecular Therapy-Methods & Clinical Development 21 (2021): 28-41.
164. Hauck, Bernd, Ling Chen, and Weidong Xiao. "Generation and characterization of chimeric recombinant AAV vectors." *Molecular Therapy* 7.3 (2003): 419-425.
165. Rabinowitz, Joseph E., *et al*. "Cross-dressing the virion: the transcapsidation of adeno-associated virus serotypes functionally defines subgroups." *Journal of virology* 78.9 (2004): 4421-4432.
166. Chai, Zheng, et al. "Application of polyploid adeno-associated virus vectors for transduction enhancement and neutralizing antibody evasion." Journal of Controlled Release 262 (2017): 348-356.
167. Adachi, Kei, *et al*. "Drawing a high-resolution functional map of adeno-associated virus capsid by massively parallel sequencing." *Nature communications* 5.1 (2014): 1-14.
168. Marsic, Damien, *et al*. "Vector design Tour de Force: integrating combinatorial and rational approaches to derive novel adeno-associated virus variants." *Molecular Therapy* 22.11 (2014): 1900-1909.

169. Weinmann, Jonas, *et al*. "Identification of a myotropic AAV by massively parallel in vivo evaluation of barcoded capsid variants." *Nature communications* 11.1 (2020): 5432.
170. Scialo, Filippo, *et al*. "ACE2: the major cell entry receptor for SARS-CoV-2." *Lung* 198 (2020): 867-877.
171. Lan, Jun, *et al*. "Structure of the SARS-CoV-2 spike receptor-binding domain bound to the ACE2 receptor." *nature* 581.7807 (2020): 215-220.
172. Zhang, Haibo, *et al*. "Angiotensin-converting enzyme 2 (ACE2) as a SARS-CoV-2 receptor: molecular mechanisms and potential therapeutic target." *Intensive care medicine* 46 (2020): 586-590.
173. Jackson, Cody B., *et al*. "Mechanisms of SARS-CoV-2 entry into cells." *Nature reviews Molecular cell biology* 23.1 (2022): 3-20.
174. Lukassen, Soeren, *et al*. "SARS-CoV-2 receptor ACE 2 and TMPRSS 2 are primarily expressed in bronchial transient secretory cells." *The EMBO journal* 39.10 (2020): e105114.
175. Hikmet, Feria, *et al*. "The protein expression profile of ACE2 in human tissues." *Molecular systems biology* 16.7 (2020): e9610.
176. Polack, Fernando P., *et al*. "Safety and efficacy of the BNT162b2 mRNA Covid-19 vaccine." *New England journal of medicine* 383.27 (2020): 2603-2615.
177. Mahase, Elisabeth. "Covid-19: Moderna vaccine is nearly 95% effective, trial involving high risk and elderly people shows." *BMJ: British Medical Journal (Online)* 371 (2020): m4471.
178. Lamb, Yvette N. "Remdesivir: first approval." *Drugs* 80 (2020): 1355-1363.
179. Syed, Yahiya Y. "Molnupiravir: first approval." *Drugs* 82.4 (2022): 455-460.
180. Lamb, Yvette N. "Nirmatrelvir plus ritonavir: first approval." *Drugs* 82.5 (2022): 585-591.
181. Taylor, Peter C., *et al*. "Neutralizing monoclonal antibodies for treatment of COVID-19." *Nature Reviews Immunology* 21.6 (2021): 382-393.
182. Chaqroun, Ahlam, Cédric Hartard, and Evelyne Schvoerer. "Anti-SARS-CoV-2 vaccines and monoclonal antibodies facing viral variants." Viruses 13.6 (2021): 1171.
183. Hannon, Gregory J. "RNA interference." *nature* 418.6894 (2002): 244-251.
184. Lee, Ying-Ray, *et al*. "RNA Interference approach is a good strategy against SARS-CoV-2." *Viruses* 15.1 (2022): 100.
185. Chowdhury, Umar Faruq, *et al*. "A computational approach to design potential siRNA molecules as a prospective tool for silencing nucleocapsid phosphoprotein and surface glycoprotein gene of SARS-CoV-2." *Genomics* 113.1 (2021): 331-343.
186. Medeiros, Inácio Gomes, *et al*. "A small interfering RNA (siRNA) database for SARS-CoV-2." *Scientific reports* 11.1 (2021): 8849.
187. Shawan, Mohammad Mahfuz Ali Khan, *et al*. "Designing an effective therapeutic siRNA to silence RdRp gene of SARS-CoV-2." *Infection, Genetics and Evolution* 93 (2021): 104951.
188. Abbaszadeh-Goudarzi, Kazem, *et al*. "Targeted delivery of CRISPR/Cas13 as a promising therapeutic approach to treat SARS-CoV-2." *Current pharmaceutical biotechnology* 22.9 (2021): 1149-1155.
189. Blanchard, Emmeline L., *et al*. "Treatment of influenza and SARS-CoV-2 infections via mRNA-encoded Cas13a in rodents." Nature biotechnology 39.6 (2021): 717-726.
190. Idris, Adi, *et al*. "A SARS-CoV-2 targeted siRNA-nanoparticle therapy for COVID-19." *Molecular Therapy* 29.7 (2021): 2219-2226.
191. Saify Nabiabad, Haidar, Massoume Amini, and Serwet Demirdas. "Specific delivering of RNAi using Spike's aptamer-functionalized lipid nanoparticles for targeting SARS-CoV-2: A strong anti-Covid drug in a clinical case study." Chemical biology & drug design 99.2 (2022): 233-246.
192. Khaitov, Musa, *et al*. "Silencing of SARS-CoV-2 with modified siRNA-peptide dendrimer formulation." Allergy 76.9 (2021): 2840-2854.
193. Baldassi, Domizia, *et al*. "Inhibition of SARS-CoV-2 replication in the lung with siRNA/VIPER polyplexes." Journal of Controlled Release 345 (2022): 661-674.

194. Becker, Jonas, *et al*. "Ex vivo and in vivo suppression of SARS-CoV-2 with combinatorial AAV/RNAi expression vectors." *Molecular Therapy* 30.5 (2022): 2005-2023.
195. Aldape, Kenneth, *et al*. "Glioblastoma: pathology, molecular mechanisms and markers." *Acta neuropathologica* 129 (2015): 829-848.
196. Yabo, Yahaya A., and Dieter Henrik Heiland. "Understanding glioblastoma at the single-cell level: Recent advances and future challenges." *PLoS biology* 22.5 (2024): e3002640.
197. Stupp, Roger, *et al*. "Radiotherapy plus concomitant and adjuvant temozolomide for glioblastoma." *New England journal of medicine* 352.10 (2005): 987-996.
198. Wirsching, Hans-Georg, and Michael Weller. "Glioblastoma." *Malignant Brain Tumors: State-of-the-Art Treatment* (2017): 265-288.
199. Ginn, Samantha L., *et al*. "Gene therapy clinical trials worldwide to 2023—an update." *The Journal of Gene Medicine* 26.8 (2024): e3721.
200. Santiago-Ortiz, Jorge L., and David V. Schaffer. "Adeno-associated virus (AAV) vectors in cancer gene therapy." *Journal of Controlled Release* 240 (2016): 287-301.
201. Hacker, Ulrich T., *et al*. "Towards clinical implementation of adeno-associated virus (AAV) vectors for cancer gene therapy: current status and future perspectives." *Cancers* 12.7 (2020): 1889.
202. Xu, Xin, *et al*. "Adeno-associated virus (AAV)-based gene therapy for glioblastoma." *Cancer Cell International* 21 (2021): 1-10.
203. Ma, H. I., *et al*. "Intratumoral gene therapy of malignant brain tumor in a rat model with angiostatin delivered by adeno-associated viral (AAV) vector." *Gene Therapy* 9.1 (2002): 2-11
204. Ng, S. S. M., *et al*. "A novel glioblastoma cancer gene therapy using AAV-mediated long-term expression of human TERT C-terminal polypeptide." *Cancer gene therapy* 14.6 (2007): 561-572.
205. Meijer, Dimphna H., *et al*. "Controlling brain tumor growth by intraventricular administration of an AAV vector encoding IFN-β." *Cancer gene therapy* 16.8 (2009): 664-671.
206. Hammond, Sean L., *et al*. "Cellular selectivity of AAV serotypes for gene delivery in neurons and astrocytes by neonatal intracerebroventricular injection." *PloS one* 12.12 (2017): e0188830.
207. Samaranch, Lluis, *et al*. "Adeno-associated virus serotype 9 transduction in the central nervous system of nonhuman primates." *Human gene therapy* 23.4 (2012): 382-389.
208. Crommentuijn, Matheus HW, *et al*. "Systemically administered AAV9-sTRAIL combats invasive glioblastoma in a patient-derived orthotopic xenograft model." *Molecular Therapy-Oncolytics* 3 (2016).
209. Abbott, N. Joan, *et al*. "Structure and function of the blood–brain barrier." *Neurobiology of disease* 37.1 (2010): 13-25.
210. Hajal, Cynthia, *et al*. "Biology and models of the blood–brain barrier." *Annual review of biomedical engineering* 23.1 (2021): 359-384.
211. Kadry, Hossam, Behnam Noorani, and Luca Cucullo. "A blood–brain barrier overview on structure, function, impairment, and biomarkers of integrity." *Fluids and Barriers of the CNS* 17 (2020): 1-24.
212. Pandit, Rucha, Liyu Chen, and Jürgen Götz. "The blood-brain barrier: Physiology and strategies for drug delivery." *Advanced drug delivery reviews* 165 (2020): 1-14.
213. Merkel, Steven F., *et al*. "Trafficking of AAV vectors across a model of the blood-brain barrier; a comparative study of transcytosis and transduction using primary human brain endothelial cells." *Journal of neurochemistry* 140.2 (2017): 216.
214. Yang, Bin, *et al*. "Global CNS transduction of adult mice by intravenously delivered rAAVrh. 8 and rAAVrh. 10 and nonhuman primates by rAAVrh. 10." *Molecular Therapy* 22.7 (2014): 1299-1309.
215. Liu, Dan, *et al*. "Crossing the blood-brain barrier with AAV vectors." *Metabolic Brain Disease* 36 (2021): 45-52.

216. Chan, Ken Y., *et al*. "Engineered AAVs for efficient noninvasive gene delivery to the central and peripheral nervous systems." *Nature neuroscience* 20.8 (2017): 1172-1179.
217. Huang, Qin, *et al*. "Delivering genes across the blood-brain barrier: LY6A, a novel cellular receptor for AAV-PHP. B capsids." *PloS one* 14.11 (2019): e0225206.
218. Hordeaux, Juliette, *et al*. "The GPI-linked protein LY6A drives AAV-PHP. B transport across the blood-brain barrier." *Molecular Therapy* 27.5 (2019): 912-921.
219. Batista, Ana Rita, *et al*. "Ly6a differential expression in blood–brain barrier is responsible for strain specific central nervous system transduction profile of AAV-PHP. B." *Human gene therapy* 31.1-2 (2020): 90-102.
220. Rapti, Kleopatra, *et al*. "Isolation of Next-Generation Gene Therapy Vectors through Engineering, Barcoding, and Screening of Adeno-Associated Virus (AAV) Capsid Variants." *JoVE (Journal of Visualized Experiments)* 188 (2022): e64389.
221. Gladson, Candece L. "Expression of integrin αvβ3 in small blood vessels of glioblastoma tumors." *Journal of Neuropathology & Experimental Neurology* 55.11 (1996): 1143-1149.
222. Mattern, Ralph-Heiko, *et al*. "Glioma cell integrin expression and their interactions with integrin antagonists." *Cancer therapy* 3 (2005): 325.
223. Reardon, David A., *et al*. "Cilengitide: an RGD pentapeptide αvβ3 and αvβ5 integrin inhibitor in development for glioblastoma and other malignancies." *Future oncology* 7.3 (2011): 339-354.
224. Danhier, Fabienne, Aude Le Breton, and Véronique Préat. "RGD-based strategies to targ*et al*pha (v) beta (3) integrin in cancer therapy and diagnosis." *Molecular pharmaceutics* 9.11 (2012): 2961-2973.
225. Temming, Kai, *et al*. "RGD-based strategies for selective delivery of therapeutics and imaging agents to the tumour vasculature." *Drug resistance updates* 8.6 (2005): 381-402.
226. Koivunen, Erkki, Bingcheng Wang, and Erkki Ruoslahti. "Phage libraries displaying cyclic peptides with different ring sizes: ligand specificities of the RGD-directed integrins." *Bio/technology* 13.3 (1995): 265-270.
Discovery
227. Arap, Wadih, Renata Pasqualini, and Erkki Ruoslahti. "Cancer treatment by targeted drug delivery to tumor vasculature in a mouse model." *Science* 279.5349 (1998): 377-380.
228. Kim, Jin-Wook, and Hyo-Suk Lee. "Tumor targeting by doxorubicin-RGD-4C peptide conjugate in an orthotopic mouse hepatoma model." *International journal of molecular medicine* 14.4 (2004): 529-564.
229. Zuppone, Stefania, *et al*. "A novel RGD-4C-saporin conjugate inhibits tumor growth in mouse models of bladder cancer." *Frontiers in Oncology* 12 (2022): 846958.
230. Ellerby, H. Michael, *et al*. "Anti-cancer activity of targeted pro-apoptotic peptides." *Nature medicine* 5.9 (1999): 1032-1038.
231. Zarovni, Natasa, Lucia Monaco, and Angelo Corti. "Inhibition of tumor growth by intramuscular injection of cDNA encoding tumor necrosis factor α coupled to NGR and RGD tumor-homing peptides." *Human gene therapy* 15.4 (2004): 373-382.
232. Li, Jinhua, *et al*. "Fusion protein from RGD peptide and Fc fragment of mouse immunoglobulin G inhibits angiogenesis in tumor." *Cancer gene therapy* 11.5 (2004): 363-370.
233. Xiao, Bin, *et al*. "RGD-IL-24, a novel tumor-targeted fusion cytokine: expression, purification and functional evaluation." *Molecular biotechnology* 41 (2009): 138-144.
234. Thompson, B., *et al*. "Neutral postgrafted colloidal particles for gene delivery." *Bioconjugate chemistry* 16.3 (2005): 608-614.
235. Zhen, Zipeng, *et al*. "RGD-modified apoferritin nanoparticles for efficient drug delivery to tumors." *ACS nano* 7.6 (2013): 4830-4837.
236. Wu, Ping-Ching, *et al*. "Modularly assembled magnetite nanoparticles enhance in vivo targeting for magnetic resonance cancer imaging." *Bioconjugate chemistry* 19.10 (2008): 1972-1979.

237. Hölig, Peter, *et al*. "Novel RGD lipopeptides for the targeting of liposomes to integrin-expressing endothelial and melanoma cells." *Protein Engineering Design and Selection* 17.5 (2004): 433-441.
238. Li, Wei, *et al*. "RGD-targeted paramagnetic liposomes for early detection of tumor: in vitro and in vivo studies." *European journal of radiology* 80.2 (2011): 598-606.
239. Wickham, Thomas J., *et al*. "Increased in vitro and in vivo gene transfer by adenovirus vectors containing chimeric fiber proteins." *Journal of virology* 71.11 (1997): 8221-8229.
240. Nagel, Herbert, *et al*. "The αvβ5 integrin of hematopoietic and nonhematopoietic cells is a transduction receptor of RGD-4C fiber-modified adenoviruses." *Gene therapy* 10.19 (2003): 1643-1653.
241. Majhen, Dragomira, *et al*. "Differential role of αvβ3 and αvβ5 integrins in internalization and transduction efficacies of wild type and RGD4C fiber-modified adenoviruses." *Virus research* 139.1 (2009): 64-73.
242. Majhen, Dragomira, *et al*. "The disulfide bond of an RGD4C motif inserted within the Hi loop of the adenovirus type 5 fiber protein is critical for retargeting to αv-integrins." *The Journal of Gene Medicine* 14.12 (2012): 788-797.
243. Shi, Wenfang, Akseli Hemminki, and Jeffrey S. Bartlett. "Capsid modifications overcome low heterogeneous expression of heparan sulfate proteoglycan that limits AAV2-mediated gene transfer and therapeutic efficacy in human ovarian carcinoma." *Gynecologic oncology* 103.3 (2006): 1054-1062.
244. Stachler, M. D., and J. S. Bartlett. "Mosaic vectors comprised of modified AAV1 capsid proteins for efficient vector purification and targeting to vascular endothelial cells." *Gene therapy* 13.11 (2006): 926-931.
245. Sayroo, R., *et al*. "Development of novel AAV serotype 6 based vectors with selective tropism for human cancer cells." *Gene Therapy* 23.1 (2016): 18-25.
246. Börner, Kathleen, *et al*. "Pre-arrayed pan-AAV peptide display libraries for rapid single-round screening." *Molecular therapy* 28.4 (2020): 1016-1032.
247. Grieger, Joshua C., Stephen M. Soltys, and Richard Jude Samulski. "Production of recombinant adeno-associated virus vectors using suspension HEK293 cells and continuous harvest of vector from the culture media for GMP FIX and FLT1 clinical vector." *Molecular Therapy* 24.2 (2016): 287-297.
248. Barker II, Fred G., *et al*. "EGFR overexpression and radiation response in glioblastoma multiforme." *International Journal of Radiation Oncology* Biology* Physics* 51.2 (2001): 410-418.
249. E Taylor, T., F. B Furnari, and W. K Cavenee. "Targeting EGFR for treatment of glioblastoma: molecular basis to overcome resistance." *Current cancer drug targets* 12.3 (2012): 197-209.
250. Zahonero, Cristina, and Pilar Sánchez-Gómez. "EGFR-dependent mechanisms in glioblastoma: towards a better therapeutic strategy." *Cellular and Molecular Life Sciences* 71 (2014): 3465-3488.
251. Xu, Hongsheng, *et al*. "Epidermal growth factor receptor in glioblastoma." *Oncology letters* 14.1 (2017): 512-516.
252. Saadeh, Fadi S., Rami Mahfouz, and Hazem I. Assi. "EGFR as a clinical marker in glioblastomas and other gliomas." *The International journal of biological markers* 33.1 (2018): 22-32.
253. Heimberger, Amy B., *et al*. "The natural history of EGFR and EGFRvIII in glioblastoma patients." *Journal of translational medicine* 3 (2005): 1-6.
254. Montano, Nicola, *et al*. "Expression of EGFRvIII in glioblastoma: prognostic significance revisited." *Neoplasia* 13.12 (2011): 1113-IN6.
255. An, Zhenyi, *et al*. "Epidermal growth factor receptor and EGFRvIII in glioblastoma: signaling pathways and targeted therapies." *Oncogene* 37.12 (2018): 1561-1575.

256. Li, Zonghai, *et al*. "Identification and characterization of a novel peptide ligand of epidermal growth factor receptor for targeted delivery of therapeutics." *The FASEB journal* 19.14 (2005): 1978-1985.
257. Cheng, Liang, *et al*. "GE11-modified liposomes for non-small cell lung cancer targeting: preparation, ex vitro and in vivo evaluation." *International journal of nanomedicine* (2014): 921-935.
258. Xu, Wei-Wei, *et al*. "GE11 peptide-conjugated nanoliposomes to enhance the combinational therapeutic efficacy of docetaxel and siRNA in laryngeal cancers." *International Journal of Nanomedicine* (2017): 6461-6470.
259. Zhou, Cheng, *et al*. "GE11 peptide-installed chimaeric polymersomes tailor-made for high-efficiency EGFR-targeted protein therapy of orthotopic hepatocellular carcinoma." *Acta biomaterialia* 113 (2020): 512-521.
260. Huang, Xueqin, *et al*. "GE11 Peptide Conjugated Liposomes for EGFR-Targeted and Chemophotothermal Combined Anticancer Therapy." *Bioinorganic Chemistry and Applications* 2021.1 (2021): 5534870.
261. Spellerberg, Rebekka, *et al*. "Dual EGFR-and TfR-targeted gene transfer for sodium iodide symporter gene therapy of glioblastoma." *Molecular Therapy-Oncolytics* 27 (2022): 272-287.
262. Hailing, Tang, *et al*. "Challenges for the application of EGFR-targeting peptide GE11 in tumor diagnosis and treatment." *Journal of Controlled Release* 349 (2022): 592-605.
263. Denholt, Charlotte Lund, *et al*. "Identification of novel peptide ligands for the cancer-specific receptor mutation EFGRvIII using a mixture-based synthetic combinatorial library." *Biopolymers: Original Research on Biomolecules* 91.3 (2009): 201-206.
264. Denholt, Charlotte Lund, *et al*. "Evaluation of 4-[18F] fluorobenzoyl-FALGEA-NH2 as a positron emission tomography tracer for epidermal growth factor receptor mutation variant III imaging in cancer." *Nuclear medicine and biology* 38.4 (2011): 509-515.
265. Mao, Jiani, *et al*. "EGFR/EGFRvIII dual-targeting peptide-mediated drug delivery for enhanced glioma therapy." *ACS applied materials & interfaces* 9.29 (2017): 24462-24475.
266. Ratajczyk, Tomasz, *et al*. "Magnetic resonance signal amplification by reversible exchange of selective PyFALGEA oligopeptide ligands towards epidermal growth factor receptors." *ChemBioChem* 22.5 (2021): 855-860.
267. Mansour, Sourour, *et al*. "Identification of a novel peptide ligand for the cancer-specific receptor mutation EGFRvIII using high-throughput sequencing of phage-selected peptides." *Scientific Reports* 12.1 (2022): 20725.
268. Haynik, Denise M., Andres A. Roma, and Richard A. Prayson. "HER-2/neu expression in glioblastoma multiforme." *Applied Immunohistochemistry & Molecular Morphology* 15.1 (2007): 56-58.
269. Koka, Vijay, *et al*. "Role of Her-2/neu overexpression and clinical determinants of early mortality in glioblastoma multiforme." *American journal of clinical oncology* 26.4 (2003): 332-335.
270. Shadidi, Mohsen, and Mouldy Sioud. "Identification of novel carrier peptides for the specific delivery of therapeutics into cancer cells." *The FASEB Journal* 17.2 (2003): 256-258.
271. Jie, Li-Yong, *et al*. "Actively-targeted LTVSPWY peptide-modified magnetic nanoparticles for tumor imaging." *International Journal of Nanomedicine* (2012): 3981-3989.
272. Bayram, Nazende Nur, *et al*. "HER2-specific peptide (LTVSPWY) and antibody (herceptin) targeted core cross-linked micelles for breast cancer: A Comparative study." *Pharmaceutics* 15.3 (2023): 733.
273. Paasonen, Lauri, *et al*. "New p32/gC1qR ligands for targeted tumor drug delivery." *ChemBioChem* 17.7 (2016): 570-575.
274. Hunt, Hedi, *et al*. "Targeting of p32 in peritoneal carcinomatosis with intraperitoneal linTT1 peptide-guided pro-apoptotic nanoparticles." *Journal of Controlled Release* 260 (2017): 142-153.

275. Säälik, Pille, *et al*. "P32-targeting TT1 peptide delivers nanoparticles to intracranial glioblastomas." *Cancer Research* 76.14_Supplement (2016): 1343-1343.
276. Säälik, Pille, *et al*. "Peptide-guided nanoparticles for glioblastoma targeting." *Journal of Controlled Release* 308 (2019): 109-118.
277. Teesalu, Tambet, *et al*. "C-end rule peptides mediate neuropilin-1-dependent cell, vascular, and tissue penetration." *Proceedings of the National Academy of Sciences* 106.38 (2009): 16157-16162.
278. Wang, Jing, *et al*. "Targeted gene delivery to glioblastoma using a C-end rule RGERPPR peptide-functionalised polyethylenimine complex." *International journal of pharmaceutics* 458.1 (2013): 48-56.
279. Paolillo, Mayra, Massimo Serra, and Sergio Schinelli. "Integrins in glioblastoma: Still an attractive target?." *Pharmacological Research* 113 (2016): 55-61.
280. Pierschbacher, Michael D., and Erkki Ruoslahti. "Cell attachment activity of fibronectin can be duplicated by small synthetic fragments of the molecule." *Nature* 309.5963 (1984): 30-33.
281. Kapp, Tobias G., *et al*. "A comprehensive evaluation of the activity and selectivity profile of ligands for RGD-binding integrins." *Scientific reports* 7.1 (2017): 1-13.
282. Kraft, Sabine, *et al*. "Definition of an unexpected ligand recognition motif for αvβ6 integrin." *Journal of Biological Chemistry* 274.4 (1999): 1979-1985.
283. Demeule, Michel, *et al*. "Identification and design of peptides as a new drug delivery system for the brain." *Journal of Pharmacology and Experimental Therapeutics* 324.3 (2008): 1064-1072.
284. Habib, Saffiya, and Moganavelli Singh. "Angiopep-2-modified nanoparticles for brain-directed delivery of therapeutics: A review." *Polymers* 14.4 (2022): 712.
285. Ke, Weilun, *et al*. "Gene delivery targeted to the brain using an Angiopep-conjugated polyethyleneglycol-modified polyamidoamine dendrimer." *Biomaterials* 30.36 (2009): 6976-6985.
286. Huang, Shixian, *et al*. "Dual targeting effect of Angiopep-2-modified, DNA-loaded nanoparticles for glioma." *Biomaterials* 32.28 (2011): 6832-6838.
287. Gao, Shiqian, *et al*. "A non-viral suicide gene delivery system traversing the blood brain barrier for non-invasive glioma targeting treatment." *Journal of Controlled Release* 243 (2016): 357-369.
288. Anami, Yasuaki, *et al*. "Homogeneous antibody–angiopep 2 conjugates for effective brain targeting." *RSC advances* 12.6 (2022): 3359-3364.
289. di Polidoro, Angela Costagliola, *et al*. "Revealing angiopep-2/LRP1 molecular interaction for optimal delivery to glioblastoma (GBM)." *Molecules* 27.19 (2022): 6696.
290. Ruan, Huitong, *et al*. "A novel peptide ligand RAP12 of LRP1 for glioma targeted drug delivery." *Journal of controlled release* 279 (2018): 306-315.
291. Sun, Xiaoru, *et al*. "Targeted regulation of neuroinflammation via nanobiosignaler for repairing the central nerve system injuries." *Nano Research* 16.2 (2023): 2938-2948.
292. Branco, Francisco, *et al*. "Peptide-Hitchhiking for the Development of Nanosystems in Glioblastoma." *ACS nano* (2024).
293. Lee, Jae H., *et al*. "Receptor mediated uptake of peptides that bind the human transferrin receptor." *European journal of biochemistry* 268.7 (2001): 2004-2012.
294. Prades, Roger, *et al*. "Delivery of gold nanoparticles to the brain by conjugation with a peptide that recognizes the transferrin receptor." *Biomaterials* 33.29 (2012): 7194-7205.
295. Li, Yutao, *et al*. "Neutrophil affinity for PGP and HAIYPRH (T7) peptide dual-ligand functionalized nanoformulation enhances the brain delivery of tanshinone IIA and exerts neuroprotective effects against ischemic stroke by inhibiting proinflammatory signaling pathways." *New Journal of Chemistry* 42.23 (2018): 19043-19061.
296. Lai, Yi, *et al*. "Design of an activatable NIR-II nanoprobe for the in vivo elucidation of Alzheimer's disease-related variations in methylglyoxal concentrations." Chemical Science 13.42 (2022): 12511-12518.

297. Staquicini, Fernanda I., *et al*. "Systemic combinatorial peptide selection yields a non-canonical iron-mimicry mechanism for targeting tumors in a mouse model of human glioblastoma." *The Journal of clinical investigation* 121.1 (2011): 161-173.
298. Kang, Ting, *et al*. "Enhancing glioblastoma-specific penetration by functionalization of nanoparticles with an iron-mimic peptide targeting transferrin/transferrin receptor complex." *Molecular pharmaceutics* 12.8 (2015): 2947-2961.
299. Zhang, Chi, *et al*. "Phage-displayed peptide-conjugated biodegradable nanoparticles enhanced brain drug delivery." *Materials Letters* 167 (2016): 213-217.
300. Huang, Na, *et al*. "PLGA nanoparticles modified with a BBB-penetrating peptide co-delivering Aβ generation inhibitor and curcumin attenuate memory deficits and neuropathology in Alzheimer's disease mice." *Oncotarget* 8.46 (2017): 81001.
301. Ni, Xiang-Rong, *et al*. "Transferrin receptor 1 targeted optical imaging for identifying glioma margin in mouse models." *Journal of Neuro-Oncology* 148 (2020): 245-258.
302. De Capua, Alberta, *et al*. "Peptide Functionalization of Emulsion-Based Nanocarrier to Improve Uptake across Blood–Brain Barrier." *Pharmaceutics* 16.8 (2024): 1010.
303. Li, Jingwei, *et al*. "Targeting the brain with PEG–PLGA nanoparticles modified with phage-displayed peptides." *Biomaterials* 32.21 (2011): 4943-4950.
304. Zhang, Xintao, *et al*. "Customized blood-brain barrier shuttle peptide to increase AAV9 vector crossing the BBB and augment transduction in the brain." *Biomaterials* 281 (2022): 121340.
305. Zhou, Yu, Sonal Priya, and Joseph Y. Ong. "Characterizing Glycosylation of Adeno-Associated Virus Serotype 9 Capsid Proteins Generated from HEK293 Cells through Glycopeptide Mapping and Released Glycan Analysis." Microorganisms 12.5 (2024): 946.
Glycosylation
306. Xie, Yongjing, and Michael Butler. "N-glycomic profiling of capsid proteins from Adeno-Associated Virus serotypes." Glycobiology 34.1 (2024): cwad074.
307. Hong, Ai Vu, *et al*. "An integrin-targeting AAV developed using a novel computational rational design methodology presents improved targeting of the skeletal muscle and reduced liver tropism." (2023).
TGF
308. Stepanenko, Aleksei A., *et al*. "A new insight into aggregation of oncolytic adenovirus Ad5-delta-24-RGD during CsCl gradient ultracentrifugation." *Scientific Reports* 11.1 (2021): 16088.
309. Pulicherla, Nagesh, *et al*. "Intra-and inter-subunit disulfide bond formation is nonessential in adeno-associated viral capsids." *PLoS One* 7.2 (2012): e32163.
310. Sevier, Carolyn S., and Chris A. Kaiser. "Formation and transfer of disulphide bonds in living cells." *Nature reviews Molecular cell biology* 3.11 (2002): 836-847.
311. Bulleid, Neil J. "Disulfide bond formation in the mammalian endoplasmic reticulum." *Cold Spring Harbor perspectives in biology* 4.11 (2012): a013219.
312. Saaranen, Mirva J., and Lloyd W. Ruddock. "Disulfide bond formation in the cytoplasm." *Antioxidants & redox signaling* 19.1 (2013): 46-53.
313. Hakim, Motti, and Deborah Fass. "Cytosolic disulfide bond formation in cells infected with large nucleocytoplasmic DNA viruses." *Antioxidants & Redox Signaling* 13.8 (2010): 1261-1271.
314. Naumer, Matthias, *et al*. "Development and validation of novel AAV2 random libraries displaying peptides of diverse lengths and at diverse capsid positions." *Human gene therapy* 23.5 (2012): 492-507.
315. Varadi, Karl, *et al*. "Novel random peptide libraries displayed on AAV serotype 9 for selection of endothelial cell-directed gene transfer vectors." *Gene therapy* 19.8 (2012): 800-809.
316. Huang, Qin, *et al*. "Targeting AAV vectors to the central nervous system by engineering capsid–receptor interactions that enable crossing of the blood–brain barrier." *PLoS Biology* 21.7 (2023): e3002112.

317. Eid, Fatma-Elzahraa, *et al*. "Systematic multi-trait AAV capsid engineering for efficient gene delivery." *Nature Communications* 15.1 (2024): 6602.
318. Berrow, Nick, *et al*. "Quality control of purified proteins to improve data quality and reproducibility: results from a large-scale survey." *European Biophysics Journal* 50.3 (2021): 453-460.
319. Grishin, Andrey M., *et al*. "Disulfide bonds play a critical role in the structure and function of the receptor-binding domain of the SARS-CoV-2 spike antigen." *Journal of Molecular Biology* 434.2 (2022): 167357.
320. Yang, Qicheng, *et al*. "Development of novel cell surface CD34-targeted recombinant adenoassociated virus vectors for gene therapy." *Human gene therapy* 9.13 (1998): 1929-1937.
321. Büning, Hildegard, and Arun Srivastava. "Capsid modifications for targeting and improving the efficacy of AAV vectors." *Molecular therapy Methods & clinical development* 12 (2019): 248-265.
322. Münch, Robert C., *et al*. "Off-target-free gene delivery by affinity-purified receptor-targeted viral vectors." *Nature communications* 6.1 (2015): 6246.
323. Reul, Johanna, *et al*. "Tumor-specific delivery of immune checkpoint inhibitors by engineered AAV vectors." *Frontiers in oncology* 9 (2019): 52.
324. Hartmann, Jessica, *et al*. "A library-based screening strategy for the identification of DARPins as ligands for receptor-targeted AAV and lentiviral vectors." *Molecular Therapy Methods & Clinical Development* 10 (2018): 128-143.
325. Hartmann, Jessica, *et al*. "GluA4-Targeted AAV vectors deliver genes selectively to interneurons while relying on the AAV receptor for entry." *Molecular Therapy Methods & Clinical Development* 14 (2019): 252-260
326. Günther, D. M., *et al*. "Substantially improved gene transfer to interneurons with second-generation glutamate receptor-targeted DART-AAV vectors." *Journal of Neuroscience Methods* 399 (2023): 109981.
327. Theuerkauf, Samuel A., *et al*. "AAV vectors displaying bispecific DARPins enable dual-control targeted gene delivery." *Biomaterials* 303 (2023): 122399.
328. Lv, Ya-feng, *et al*. "Gene delivery to breast cancer by incorporated EpCAM targeted DARPins into AAV2." *BMC cancer* 23.1 (2023): 1220.
329. Hagen, Sven, *et al*. "Modular adeno-associated virus (rAAV) vectors used for cellular virus-directed enzyme prodrug therapy." *Scientific reports* 4.1 (2014): 3759.
330. Lux, Kerstin, *et al*. "Green fluorescent protein-tagged adeno-associated virus particles allow the study of cytosolic and nuclear trafficking." *Journal of virology* 79.18 (2005): 11776-11787.
331. Asokan, Aravind, *et al*. "Bioluminescent virion shells: new tools for quantitation of AAV vector dynamics in cells and live animals." *Gene therapy* 15.24 (2008): 1618-1622.
332. Hamann, Martin V., *et al*. "Improved targeting of human CD4+ T cells by nanobody-modified AAV2 gene therapy vectors." *PLoS One* 16.12 (2021): e0261269.
333. Akazawa-Ogawa, Yoko, Koichi Uegaki, and Yoshihisa Hagihara. "The role of intra-domain disulfide bonds in heat-induced irreversible denaturation of camelid single domain VHH antibodies." *The journal of biochemistry* 159.1 (2016): 111-121.
334. Liu, Haipei, Valentin Schittny, and Michael A. Nash. "Removal of a conserved disulfide bond does not compromise mechanical stability of a VHH antibody complex." *Nano letters* 19.8 (2019): 5524-5529.
335. Körbelin, J., *et al*. "Optimization of design and production strategies for novel adeno-associated viral display peptide libraries." *Gene therapy* 24.8 (2017): 470-481.
336. Camilloni, Carlo, *et al*. "Towards a structural biology of the hydrophobic effect in protein folding." *Scientific reports* 6.1 (2016): 1-9.
337. Jacak, Ron, Andrew Leaver-Fay, and Brian Kuhlman. "Computational protein design with explicit consideration of surface hydrophobic patches." *Proteins: Structure, Function, and Bioinformatics* 80.3 (2012): 825-838.

338. Jackson, Cody B., *et al*. "AAV vectors engineered to target insulin receptor greatly enhance intramuscular gene delivery." *Molecular Therapy-Methods & Clinical Development* 19 (2020): 496-506.
339. Boucas, Jorge, *et al*. "Engineering adeno-associated virus serotype 2-based targeting vectors using a new insertion site-position 453-and single point mutations." *The Journal of Gene Medicine: A cross-disciplinary journal for research on the science of gene transfer and its clinical applications* 11.12 (2009): 1103-1113.
340. Xu, Guangxue, *et al*. "Structural basis for the neurotropic AAV9 and the engineered AAVPHP. eB recognition with cellular receptors." *Molecular Therapy Methods & Clinical Development* 26 (2022): 52-60.
341. Kimura, Kei, *et al*. "A mosaic adeno-associated virus vector as a versatile tool that exhibits high levels of transgene expression and neuron specificity in primate brain." *Nature Communications* 14.1 (2023): 4762.
342. Goertsen, David, *et al*. "AAV capsid variants with brain-wide transgene expression and decreased liver targeting after intravenous delivery in mouse and marmoset." *Nature neuroscience* 25.1 (2022): 106-115.
343. Erickson, Sarah B., et al. "Precise Manipulation of the Site and Stoichiometry of Capsid Modification Enables Optimization of Functional Adeno-Associated Virus Conjugates." *Bioconjugate Chemistry* 35.1 (2023): 64-71.
344. Bartlett, Jeffrey S., R. Jude Samulski, and Thomas J. Mccown. "Selective and rapid uptake of adeno-associated virus type 2 in brain." *Human gene therapy* 9.8 (1998): 1181-1186.
345. Stanton, Alexandra C., et al. "Systemic administration of novel engineered AAV capsids facilitates enhanced transgene expression in the macaque CNS." *Med* 4.1 (2023): 31-50.
346. Chuapoco, Miguel R., et al. "Adeno-associated viral vectors for functional intravenous gene transfer throughout the non-human primate brain." *Nature nanotechnology* 18.10 (2023): 1241-1251.
347. Huang, Qin, et al. "An AAV capsid reprogrammed to bind human Transferrin Receptor mediates brain-wide gene delivery." *Science* 384.6701 (2024): 1220-1227.
348. Feiner, Rebecca C., et al. "EGFR-binding peptides: From computational design towards tumor-targeting of adeno-associated virus capsids." *International journal of molecular sciences* 21.24 (2020): 9535.
349. Strecker, M. I., et al. "AAV-mediated gene transfer of a checkpoint inhibitor in combination with HER2-targeted CAR-NK cells as experimental therapy for glioblastoma." *Oncoimmunology* 11.1 (2022): 2127508.
350. Freeman, Scott M., et al. "The “bystander effect”: tumor regression when a fraction of the tumor mass is genetically modified." Cancer research 53.21 (1993): 5274-5283.
351. van Dillen, Ingrid J., et al. "Influence of the bystander effect on HSV-tk/GCV gene therapy. A review." *Current gene therapy* 2.3 (2002): 307-322.
352. Duarte, Sónia, et al. "Suicide gene therapy in cancer: where do we stand now?." *Cancer letters* 324.2 (2012): 160-170.
353. Robson, Tracy, and David G. Hirst. "Transcriptional targeting in cancer gene therapy." *BioMed Research International* 2003.2 (2003): 110-137.
354. Montaño-Samaniego, Mariela, et al. "Strategies for targeting gene therapy in cancer cells with tumor-specific promoters." *Frontiers in oncology* 10 (2020): 605380.
355. Van Hove, Inge, et al. "Targeting RGD-binding integrins as an integrative therapy for diabetic retinopathy and neovascular age-related macular degeneration." *Progress in retinal and eye research* 85 (2021): 100966.
356. Cabanes-Creus, Marti, et al. "Restoring the natural tropism of AAV2 vectors for human liver." Science Translational Medicine 12.560 (2020): eaba3312.
357. Nonnenmacher, Mathieu, et al. "Rapid evolution of blood-brain-barrier-penetrating AAV capsids by RNA-driven biopanning." Molecular Therapy-Methods & Clinical Development 20 (2021): 366-378.

358. Shay, Timothy F., *et al*. "Primate-conserved carbonic anhydrase IV and murine-restricted LY6C1 enable blood-brain barrier crossing by engineered viral vectors." *Science advances* 9.16 (2023): eadg6618.
359. Shay, Timothy F., *et al*. "Human cell surface-AAV interactomes identify LRP6 as blood-brain barrier transcytosis receptor and immune cytokine IL3 as AAV9 binder." *Nature Communications* 15.1 (2024): 7853.

Acknowledgements

I would like to express my sincere appreciation to all the people who supported me during my doctoral study. First and foremost, I would like to thank my supervisor Prof. Dr. Dirk Grimm for accepting me in his research group and giving me the opportunity to work in the field of AAV-mediated gene therapy. I am truly grateful for all of his inspiring and valuable advices and suggestions which make my doctoral thesis possible. Many thanks to his supervising, supporting and encouraging in all aspects during the past years.

I would like to also thank Prof. Dr. Ursula Klingmüller for her support as the first reviewer of my doctoral thesis and Prof. Dr. Stephan Urban for his support as the member of my TAC meeting. Thank them for attending my yearly reports and giving me precious advices every time. Thank Prof. Dr. Ana Martín-Villalba for her willingness to be the chairman and examiner of my examination committee and Prof. Dr. Nina Papavasiliou for her willingness to be the examiner of my examination committee. Thank the HBIGS team, especially Dr. Rolf Lutz and Ms. Martina Galvan for the administrative support. And many thanks to the SFB1109 program for funding my work, and organizing seminar series and annual conferences.

I would like to thank all my collaborators. Thank Prof. Dr. Michael Platten, Dr. Khwab Sanghvi and Dr. Dennis Alexander Agardy for collaborating on the GBM-targeting project. Thank them for doing the mouse experiments and offering U-87 and GL261 cell lines. Thank Prof. Dr. Friedrich Koch-Nolte and Dr. Anna Marei Mann for collaborating on the hACE2-targeting project. Thank them for offering me the RBD-antibodies and hACE2-expressing HEK293 cells. Thank Dr. Ivana Nikic-Spiege and Dr. Nevena Stajkovic for collaborating on an AAV-mediated click labeling of ion channels project and including me as a co-author in their manuscript. Thank Prof. Dr. Elisabetta Ada Cavalcanti-Adam, Jonah Voigt and Dr. Joel Christian on collaborating on a AAV cellular uptake project and including me as a co-author in their manuscript. Thank Dr. Vojtech Zila for teaching and helping me to use EM. Thank Jonah Voigt for doing the DLS measurement, and thank Angga Prawira for doing the FPLC. Also, thank Prof. Dr. Rob Russel for giving me advices about the protein folding, and Prof. Dr. Ben Davis and Dr. Chao Guo for giving me advices about the chemical conjugation.

I would like to thank all my former and current colleagues in the Grimm group for their help and for the pleasant and friendly working atmosphere. I would particularly thank Dr.

Kleopatra Rapti, who taught, helped and discussed with me all the time. Thank Dr. Jonas Becker and Ellen Wiedtke, who introduced me into the group at the beginning and helped me whenever I need. Thank Nico Fisher, who sat next to me and often cheered me up. Thank Jixin Liu and Man Xu, who also spent time with me during weekends and holidays.

Many thanks to my dearest parents. Without your unconditional love, care, support and encouragement, I would not be able to stand here. Thank you very much for everything.